Renewable Power Systems for Microgrids in Public Buildings

Miguel Quitério Simão Coelho

Thesis to obtain the Master of Science Degree in

Mechanical Engineering

Supervisors: Prof. Carlos Augusto Santos Silva
Dr. Ana Isabel Lopes Estanqueiro

Examination Committee

Chairperson: Prof. Edgar Caetano Fernandes
Supervisor: Prof. Carlos Augusto Santos Silva
Member of the Committee: Prof. Duarte de Mesquita e Sousa

December 2021

ACKNOWLEDGEMENTS

First and foremost, I would like to thank both my supervisors, Professor Carlos Santos Silva and Professor Ana Estanqueiro, for giving me this opportunity, guidance, and encouragement.

I would also like to thank CQS and all its members for giving me their full support and technical guidance.

Over the course of this degree, I had the chance of working with wonderful colleagues and professors who motivated me and pushed me to the limit, making my journey so much more enjoyable. To all of them, I show my deep appreciation.

Last but not least, I would like to thank my girlfriend and my family. You have given me unconditional support, unconditional love and have always encouraged me to follow the path that I thought better. Without all of you, none of this would make sense.

ABSTRACT

With climate change and environmental problems being one of the biggest concerns in Europe, efforts have been made to redesign the power system, enabling higher penetration of renewable energy. Energy systems, like microgrids, that allow the local integration of renewable energy generation technologies with energy storage and energy demand, will play an important role in the future power system. Due to the uncertainty in the energy generation of dispatchable generation technologies (namely photovoltaic and wind power systems), there is a need to develop modeling tools to assist energy planners in sizing and predicting the operation of energy systems like microgrids. In this work, an energy model tool capable of modeling the interaction between energy generation, using photovoltaic and wind power systems, energy storage, using lithium-ion batteries, and energy demand, has been developed in MATLAB-Simulink. The tool was developed to model the specific case of a microgrid implemented in a pilot office located in Laboratório Nacional de Energia e Geologia, and, to enhance its capabilities while evaluating and validating its performance, the developed model was compared to a commercially available software, POLYSUN, presenting a mean absolute percentage error always inferior to 5%, while guaranteeing power quality at every instant. Furthermore, the results of the tests carried out revealed the environmental and economical potential of increasing the size of the generation and storage technologies implemented in the microgrid under analysis.

Keywords: Distributed Energy; Energy Model Tool; Energy Storage; Microgrid; Power Quality; Renewable Energy Sources.

RESUMO

As alterações climáticas e os problemas ambientais associados às emissões de gases com efeito de estufa são uma das principais preocupações na Europa. Estas adversidades têm despertado o interesse de uma reformulação do sistema energético, permitindo uma maior integração de fontes de energia renováveis. Sistemas como micro-redes, que permitem a integração local de tecnologias de geração e armazenamento de energia proveniente de fontes renováveis, associadas a consumo local, desempenharão um papel importante no sistema energético futuro. Contudo, devido à intermitência na geração associada às tecnologias utilizadas (nomeadamente sistemas fotovoltaicos e eólicos), existe a necessidade de desenvolver ferramentas capazes de auxiliar não só na planificação e dimensionamento, mas também na previsão do desempenho de sistemas como as micro-redes. Neste trabalho, uma ferramenta capaz de modelar a interação entre geração, utilizando sistemas fotovoltaicos e eólicos, armazenamento, utilizando baterias de *lithium-ion*, e consumo de energia, foi desenvolvida utilizando o software MATLAB-Simulink. A ferramenta foi desenvolvida para modelar o caso específico de uma micro-rede implementada num escritório piloto localizado no Laboratório Nacional de Energia e Geologia, tendo primeiro sido sujeita a um processo de avaliação e validação do seu desempenho, através da comparação com um modelo idêntico desenvolvido num software comercialmente disponível, POLYSUN, apresentando um erro percentual absoluto médio sempre inferior a 5% e garantindo o cumprimento dos parâmetros de qualidade de energia. Os resultados dos testes realizados revelaram também o potencial ambiental e econômico de redimensionar as tecnologias de geração e armazenamento implementadas na micro-rede em análise.

Palavras-chave: Armazenamento De Energia; Fontes de Energia Renováveis**;** Micro-Rede; Modelação Energética; Parâmetros de Qualidade de Energia; Produção De Energia Descentralizada.

TABLE OF CONTENTS

LIST OF TABLES

LIST OF FIGURES

LIST OF ACRONYMS

AC - Alternative current
CC - Constant Current
CERTS - Consortium for Electric Reliability Technology Solutions
CV - Constant Voltage
DC - Direct Current
DER - Distributed Energy Resource
DG - Distributed generation
DOD - Depth of Discharge
DR - Demand Response
DSM - Demand Side Management
ESS - Energy Storage System
EU - European Union
IN+ - Center for Innovation, Technology and Policy Research
LNEG - Laboratório Nacional de Energia e Geologia
MAPE - Mean Absolute Percentage Error
MCC - Multi-Step Constant Current
MPC - Model Predictive Control
MPP - Maximum Power Point
MPPT - Maximum Power Point Tracking
NPV - Net Present Value
nZEB - net Zero Energy Buildings
PCU - Power Conditioning Unit
PI - Proportional Integral
PMSG - Permanent Magnet Synchronous Generator
PSO - Particle Swarm Optimization
PV - Photovoltaic
PVT - Photovoltaic-Thermal System
PWM - Pulse Width Modulation
P&O - Perturb and Observe
RMS - Root Mean Square
SOC - State of Charge
STC - Standard Test Conditions
THD - Total Harmonic Distribution
USA - United States of America

LIST OF SYMBOLS

A - Wind Turbine Swept Area $[m^2]$

C - Capacitance [F]

C_{Boost} - DC-DC Boost Converter Capacitance [F]

Cf - Cash Flow [€]

C_{filter} - Filter Capacitance [F]

C_p - Performance Coefficient

c_t - Electricity Hourly Cost [€]

$c1_i^n$ - Particle Swarm Optimization Cognitive Learning Acceleration Coefficient

$c2_i^n$ - Particle Swarm Optimization Global Learning Acceleration Coefficient

D - DC-DC Boost Converter Duty Signal

D_{space} - Particle Swarm Optimization Search Space Dimension

E_{annual} - Annual Energy Generation [kWh]

$E_{battery}^{Capacity}$ - Battery Energy Capacity [kWh]

f - Demand Side Management Optimization Function

f_{Grid} - Grid Frequency $[Hz]$

f_{ws} - DC-DC Boost Converter Switching Frequency $[Hz]$

f' - Particle Swarm Optimization Penalization Function

G - Irradiance $[W/m^2]$

G^r - Irradiance at STC $[W/m^2]$

h_a - Utilization of Peak Power $[Hz]$

I_{nv} - Investment [€]

I - Current $[A]$

i - Current $[A]$

I_D - Photovoltaic Diode Current $[A]$

i_d - Wind Power System Generator d axis current $[A]$

I_{nv_0} - Initial Investment [€]

i_q - Wind Power System Generator q axis current $[A]$

I_s - Current Generated by The Radiation Photons $[A]$

I_{sc} - Photovoltaic Short-Circuit Current $[A]$

I_{sh} - Photovoltaic Leakage-Current $[A]$

I_0 - Photovoltaic Diodes Inverse Saturation Current $[A]$

K - Boltzmann Constant $[J/K]$

L - Inductance $[H]$

L_{filter} - Filter Inductance $[H]$

L_{Boost} - DC-DC Boost Converter Inductance $[H]$

L_q - Wind Power System Generator q axis inductances $[H]$

L_d - Wind Power System Generator d axis inductances $[H]$

m - Photovoltaic Ideality Factor

N - Particle Swarm Optimization Total Number of Particles

N_s - Photovoltaic Modules' Cell Number

P - Power $[kW]$

P_{bat_Chg} - Battery Charge Power $[kW]$

$P_{bat_{Dchg}}$ - Battery Discharge Power $[kW]$

P_{Best} - Particle Swarm Optimization Particle Best Position

$P_{Flexible}$ - Flexible Load Nominal Power $[kW]$

$P_{GlobalBest}$ - Particle Swarm Optimization Swarm Best Position

P_m - Mechanical Power $[W]$

P_P - Peak Power $[W]$

P_{rated} - Rated Power $[W]$

P_s - Wind Power System Generator Stator Active Power $[W]$

$P_{t\ battery}$ - Hourly Battery Power $[kW]$

$P_{t\ Fixed}$ - Hourly Fixed Loads Power $[kW]$

$P_{t\ generation}$ - Hourly Generation Power $[kW]$

$P_{t\ grid}$ - Hourly Grid Power Value $[kW]$

$P_{t\ Load}$ - Hourly Load Power $[kW]$

q - Electron's Electric Charge $[C]$

Q_s - Wind Power System Generator Stator Reactive Power $[VAR]$

R_s - Photovoltaic Metal Electrodes and Contact's Resistance $[\Omega]$

R_{sh} - Photovoltaic Shunt Resistance $[\Omega]$

S - Energy Savings $[kWh]$

T - Temperature $[°C]$

T_{amb} - Ambient Temperature $[°C]$

T_{cell} - Photovoltaic Module Cell Temperature $[°C]$

T_e - Electromagnetic Torque

T^r - Ambient Temperature at STC $[°C]$

u - Wind Speed $[m/s]$

V - Voltage $[V]$

v - Voltage $[V]$

v_d - Wind Power System Generator d Axis Voltage $[V]$

V_i^n - Particle Swarm Optimization Velocity Matrix

$\vec{v}_i^{\,n}$ - Particle Swarm Optimization Velocity Vector

V_{in} - Input Voltage $[V]$

V_{MP} - Maximum Power Voltage $[V]$

V_{out} - Output Voltage $[V]$

v_q - Wind Power System Generator q Axis Voltage $[V]$

V_T - Thermal Voltage $[V]$

w_i - Particle Swarm Optimization Inertia Weight

$\vec{x}_i^{\,n}$ - Particle Swarm Optimization Position Vector

X_i^n - Particle Swarm Optimization Position Matrix

x_t - Load Hourly Decision Variable

$x_{t,chg}$ - Battery Charging Process Hourly Decision Variable

$x_{t,dchg}$ - Battery Discharging Process Hourly Decision Variable

β - Pitch Angle [°]

γ - PV rear ventilation coefficient $[1/°C]$

λ - Tip Speed Ratio $[rad]$

μ_{Pp} - Temperature Coefficient $[\%/°C]$

ρ - Air Density $[Kg/m^3]$

ω_T - Wind Power System Angular Rotor Speed $[rad/s]$

1 INTRODUCTION

1.1 Motivation

Climate change and environmental problems are one of Europe's biggest concerns. To overcome these challenges, the European Unit (EU) has set ambitious environmental and energy goals, with the objective of making EU climate-neutral by 2050. Designing a low-carbon energy system by the middle of the 21st century is one of the EU's priorities, and targets have been set to drive and foster this transition [1]. For 2030 a target of 40% reduction in greenhouse gas emission (from 1990 levels) was set, as well as a share of 32% renewable electricity and a 32.5 % improvement in energy efficiency.

The European Commission's Energy Roadmap 2050 shares the desire of developing energy systems that protect the environment, create affordable and market-orientated energy services while ensuring the security, resilience, and reliability of the energy supply. These energy systems are designed with the purpose of being integrated into infrastructures for all energy carriers, using the electrical system as support. These technologies will introduce a redesign in the power system, where most centralized individual producers will be replaced by decentralized and collective prosumers, who consume directly the energy generated.

Buildings will play an important role in this new power system, due to the diverse possibilities of on-site energy generation, and to the need of decreasing the energy consumption in this sector, which is responsible for a share of roughly 60% of the final electricity consumption in the EU [2]. In fact, renovating the building sector is one of the priorities to achieve EU's climate targets for 2030. Buildings are responsible for a share of 36% of greenhouse gas emissions resulting from the energy sector [3]. Measures have been taken concerning new buildings, from the beginning of 2021 all new buildings in the EU need to be nearly Zero Energy Buildings [4]. But, since 85% of EU's building stock was built before 2001, and since it is predicted that in 2050 more than 85% of the building stock refer to buildings that are already built at the moment [3], solutions need to be found to enable lower greenhouse gas emissions in the existing buildings, being one of those solutions their conversion to prosumers by introducing distributed renewable energy systems, such as microgrids.

The possibility of constructing and operating local small-scale power supply technologies and energy storage systems associated with energy consumption in buildings, offers environmental benefits, such as lowering the greenhouse gas emissions, by self-consuming the locally generated renewable energy, social benefits, such as a power system more reliable, resilient, and affordable, and economical benefits, because microgrids contribute to a higher energy self-sufficiency, which is also an important target of the EU, since, according to the European Commission, in 2018 EU's energy dependency rate was equal to 58% [5].

1.2 Objectives and contributions of the thesis

The main objective of the present thesis is to develop an energy model tool that aims at modeling the interaction between energy demand and energy generation of microgrids implemented in services and non-residential buildings. This work will focus on the study of a microgrid implemented on a pilot office building owned and managed by the Laboratório Nacional de Energia e Geologia (LNEG) and the results will be integrated into the project IMPROVEMENT [6].

The model, composed of two types of generation technologies, photovoltaic and micro wind turbine, one energy storage system, and the building consumption pattern, will be developed using MATLAB-Simulink. To guarantee the quality of the results obtained, the model will be compared to an identical model developed in a commercially available software, POLYSUN. After the modeling and respective validation, a control and demand-side management program will be produced to ensure the security of supply and power quality (signal with a low total harmonic distortion value, and steady supply voltage that stays within the prescribed range, steady frequency close to its rated value).

MATLAB-Simulink is a graphical block-programming scheme used to model and simulate the dynamic behavior of a system. To fully fulfill the objectives prosed, different blocks will be created and then integrated to produce the desired system. Some of these blocks will be fully developed from scratch, while others will be adapted from information found in the literature. The block used to model the PV array, will be extracted from MATLAB-Simulink library, the blocks used to model the power conditioning units implemented in the PV system and wind power system, will be developed based on equivalent circuits, and the block used to model the inverter controller will be adapted from a control scheme found in the literature. The block used to implement the MPPT technique was developed by the author based on what was found as the common practice across the literature. The blocks developed to model the wind power generation unit, the battery unit, the battery control unit, the building consumption, all blocks used to perform auxiliary calculations, and all blocks used to collect and process input data and to present the output of the program, will be fully developed by the author. The demand-side management program, developed in MATLAB, will be also developed by the author.

1.3 Structure of the thesis

This thesis is structured in seven chapters, containing the flowing information:

- Chapter one provides an introduction to the work, presenting the motivation behind this thesis and the objectives of the proposed work.
- In chapter two the concept of microgrid is explored, and a review of the state of the art on the technologies implemented in microgrids and on the modeling tools currently used is carried out. Different microgrid components and control techniques are studied and the concept of demand-side management is presented.

- Chapter three provides information about the case study of this thesis, while exploring the different methods available and commonly used to model the technologies implemented in the microgrid under study.
- In chapter four a detailed description of the developed energy model tool is carried out.
- In chapter five the advantages of integrating a demand side management program to the model previously developed are explored, and a demand response optimization program developed using particle swarm optimization is presented.
- Chapter six presents the results of the evaluation and validation prosses carried out for all components of the microgrid model developed. A study of the annual behavior of the microgrid understudy is conducted, and the investment possibilities to improve the performance of the microgrid are presented.
- Chapter seven closes the work by reviewing the main conclusions and by suggesting some paths that could be followed as future work.

2 Literature review

2.1 Microgrids

2.1.1 Definition

The concept of microgrid is used in the engineering vocabulary for more than a decade. Yet, in the existent literature, there is not a singular definition to describe it [7], since this concept covers a wide range of configurations [8].

The most used definition by researchers was proposed by the U.S. Department of Energy and states that a microgrid is ‘‘a group of interconnected loads and distributed energy resources within clearly defined electrical boundaries that acts as a single controllable entity with respect to the grid. A microgrid can connect and disconnect from the grid to enable it to operate in both grid-connected or island mode.’’[9]

Although numerous definitions can be found in the literature, there are four common characteristics to all of them which are essential to describe a microgrid [10]:
1 – It is an integrated platform for local energy generation, storage, and demand, all placed within a local distribution grid.
2 – It has the possibility to operate in grid-connected mode or islanded mode.
3 – It enables the control of a combination of distributed energy resources.
4 – It may operate on multiple scales, from a single house to an entire neighborhood.

2.1.2 Background

In the end of the 19th century the first power networks were implemented. At that time, those networks were manly design to supply lighting applications, generating electricity in small power plants consisting of motor driven generators. This trend remained until the beginning of the 20th century [11]. Due to the increase of electricity demand, from the 1920s to the 1970s, these small-scale distributed power plants were replaced by larger power plants, which were connected to each other and to diverse loads, creating the utility grid. The conversion to a centralized power system enabled to decrease the electricity cost and to draw power from generating resources located in distant sites [12].

Although these centralized power system showed numerous advantages, mainly during the 20th century, economic and environmental concerns have been promoting a redesign of the centralized power system to a decentralized one, where large scale power plants would be replaced by decentralized units [13], with numerous benefits studied in detail in [14]. Microgrids research and development programs began almost simultaneously in Europe, with the project MICROGRIDS [15] in 2003, and in the United States of America (USA), with the Consortium for Electric Reliability Technology

Solutions (CERTS) publishing the first report related to microgrids on the end of 2003 [16]. The first goal of both projects was to find a solution to integrate distinct distributed energy resources in the utility grid, improving its reliability.

In the last years, the development and deployment of microgrids in Europe and in the USA have been driven by different factors that, according to [12], can be organized into three distinct categories: environmental benefits, economic benefits, and energy security. In the USA, the key drivers for the continuous bet on the development of microgrids are its potential to increase power resilience and reliability [17]. In Europe, the objective of integrating a large amount of renewable energy generation in the grid, in order to meet the environmental targets set for 2050, is the main driver in the continuous bet on microgrids.

2.2 Microgrid Architecture

According to [11] and [18], microgrids are composed of distributed energy resources (DERs), loads, distribution systems, control and communication systems. The loads can be divided into fixed loads, which cannot be changed and need to be satisfied in normal operating conditions, and flexible loads, which can be shifted from hours with high demand to hours with surplus generation, in order to facilitate matching the demand and supply sides [11]. The control system is responsible for ensuring the stability of the microgrid and by regulating voltage and frequency [18]. DERs are composed of distributed generation technologies and energy storage systems, connected to a local distribution system [11]. A more detailed study on these technologies is presented below.

2.2.1 Distributed generation

Distributed generation (DG) technologies can be divided into renewable and non-renewable, as it is presented in the figure 2.1. Reciprocating engines, gas turbines, and micro-turbines are the most widely used non-renewable DG technologies. Reciprocating engines offer a good efficiency, flexible control, and low cost. Due to these advantages, this used to be the most used technology [19], however, reciprocating engines have been replaced by environmentally friendly technologies. Going in the opposite direction, the importance of micro-turbines has increased in recent years, since this technology is seen as a way to overcome the reliability challenges created by the uncertainty of some renewable technologies [20]. In [21] the advantages of integrating renewable technologies with stable sources such as micro-turbines are presented, and [22] discusses the implementation of micro-turbines in microgrids for commercial buildings.

The most common renewable DG technologies are solar photovoltaic, wind turbines, hydro units, biomass, solar thermal, and geothermal [19], [23]. These technologies can be divided into two groups, dispatchable and non-dispatchable. Dispatchable technologies, like hydro and biomass, allow the control of the output power enabling more flexibility in meeting energy demands, non-dispatchable

technologies, like solar photovoltaic and wind turbines, cannot be controlled and generate in an intermittent way [24]. Yet, wind and solar are abundant in many locations, and adding to the fact that wind turbines can generate electricity throughout the whole day and solar photovoltaic units are easy to install or integrate into a building environment, the previous mention technologies are the most interesting when it comes to selection energy generation technologies for building-integrated microgrids [25]. In the literature, numerous examples of microgrids with renewable resources can be found, and a special focus has been given to overcoming the intermittence of non-dispatchable technologies in order to provide a more stable and reliable power generation. In [26], the author studied real data of weather variables and residential energy consumption and concluded that integrating diverse renewable generation technologies in microgrids is a way to overcome this limitation.

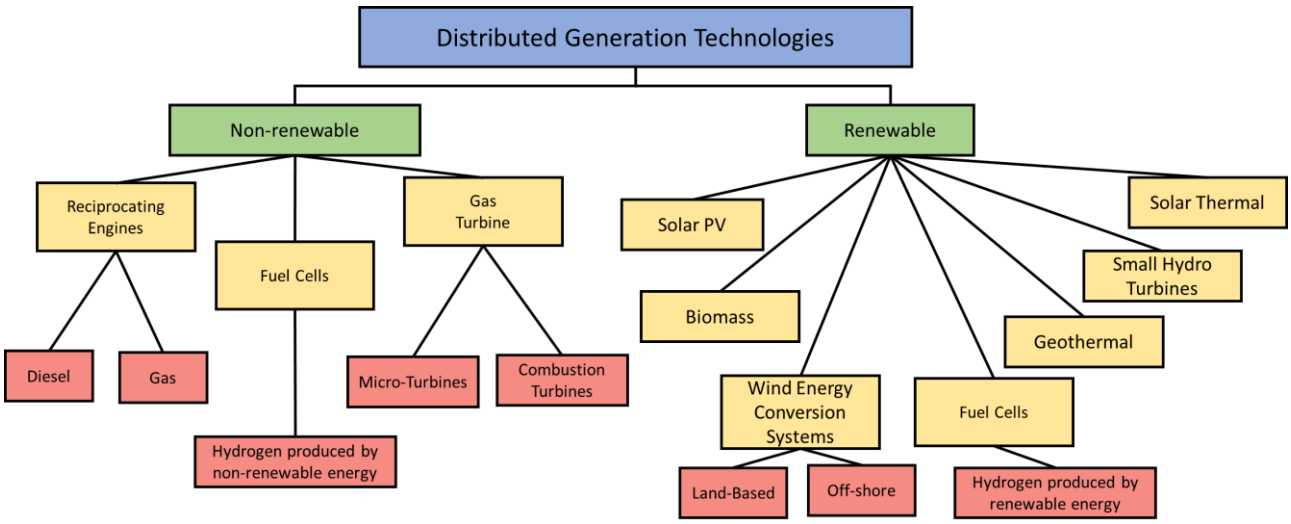

Figure 2.1 - Distributed Generation Technologies (adapted from [19]).

2.2.2 Energy Storage Systems

By converting electricity into a storable energy form during high generation periods, and converting the stored energy back to electricity during peak load, Energy Storage Systems (ESSs) play an important role in reducing the mismatch between the supply and demand side in microgrids [27]**.** Furthermore, these systems can also improve power quality, voltage and frequency stability, and power reliability [28]. According to [29] ESSs implemented in a microgrid can have two configurations, they can be aggregated or distributed. In the first configuration, all storage systems are aggregated and connected to the microgrid as one, in the second, ESS units are individually coupled to one Distributed Energy Resource.

ESSs can be divided into five groups, according to their primary source of energy, which are: electrical, mechanical, thermal, electrochemical, and magnetic [30], as it is presented in the figure 2.2. A more detailed study of energy storage technologies can be found in [31] and [32]. In the present work, a

special focus will be given to batteries since, due to their technological maturity and ease to design and install when compared to other energy storage technologies, batteries are the most used storage technology in microgrids [33].

Through an oxidation-reduction reaction, batteries are able to convert stored chemical energy into electricity. Different types of batteries and different applications of these technologies can be found in the literature. For microgrids, Lead-Acid and Lithium-Ion are the most suitable option [33]. Lead-acid stands out as the most mature and cheap battery technology, offering good charge retention and good tolerance to overcharging, however, these batteries have low cycle life, low energy density, and low efficiency when compared with other batteries, especially Lithium-Ion batteries [31]. Some examples of Lead-Acid batteries implemented in microgrids can be found in [34]. Lithium-Ion batteries are the fastest growing technology in recent years, according to [31], offering high efficiency and energy density, a good self-discharge rate, and rapid response time. Adding to these advantages, the continuous decrease of the acquisition cost, previously seen as the biggest drawback when compared to other alternatives such as Lead-Acid, has been one of the main drivers for increasing the implementation of Lithium-Ion batteries in microgrids [35].

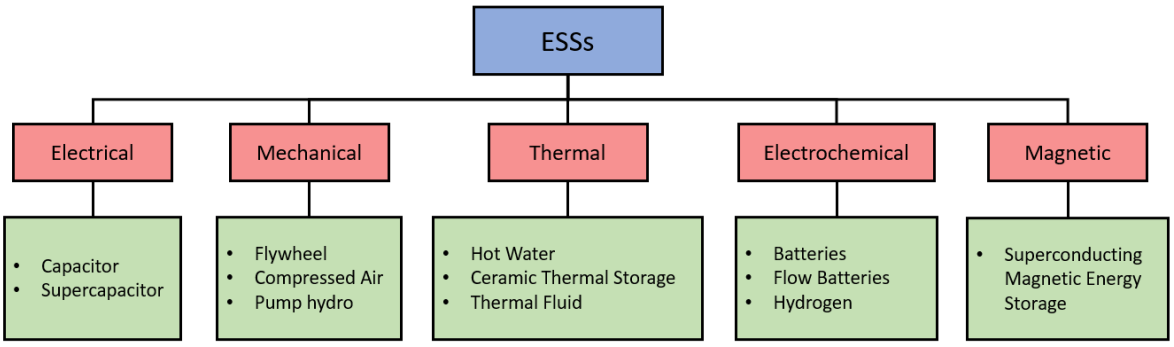

Figure 2.2 - Energy Storing System categories [32].

2.3 Modelling of Microgrids

Models play an important role in the energy system since they are a quick and cheap way to predict the performance of a system. Their role is particularly important when non-dispatchable distributed energy technologies are considered, as it is the case with most microgrids, due to the variability and unpredictability of power generation, which can reflect in mismatches between demand and generation. Models can forecast these problems and present solutions to overcome them. To model a microgrid two approaches can be taken: an existing modeling tool can be used, or a tailor-made model can be developed.

Different existing modeling tools for energy systems can be found in the literature, [36] presents 75 models and modeling tools that have been used in publications since 2012, so it is important to define parameters to distinguish between them and ease the selection of models that can be applied in the

study of microgrids. According to [36] models can be categorized based on three sets of parameters, which are the general logic, the spatiotemporal resolution, and the technological and economical parameters. The general logic contains information about the purpose of the study, the approach of the model, and the methodology taken. The spatiotemporal resolution sets limits to the dimension of the system under analysis and the time-step used. The technological and economical parameters contain information about the generation and storage technologies, demand characteristics, types of costs, and emissions that are available in the model. By evaluating all these categories, a model that fits the problem studied can be identified and selected. Figure 2.3 shows a flowchart of the selecting processes suggested in [36].

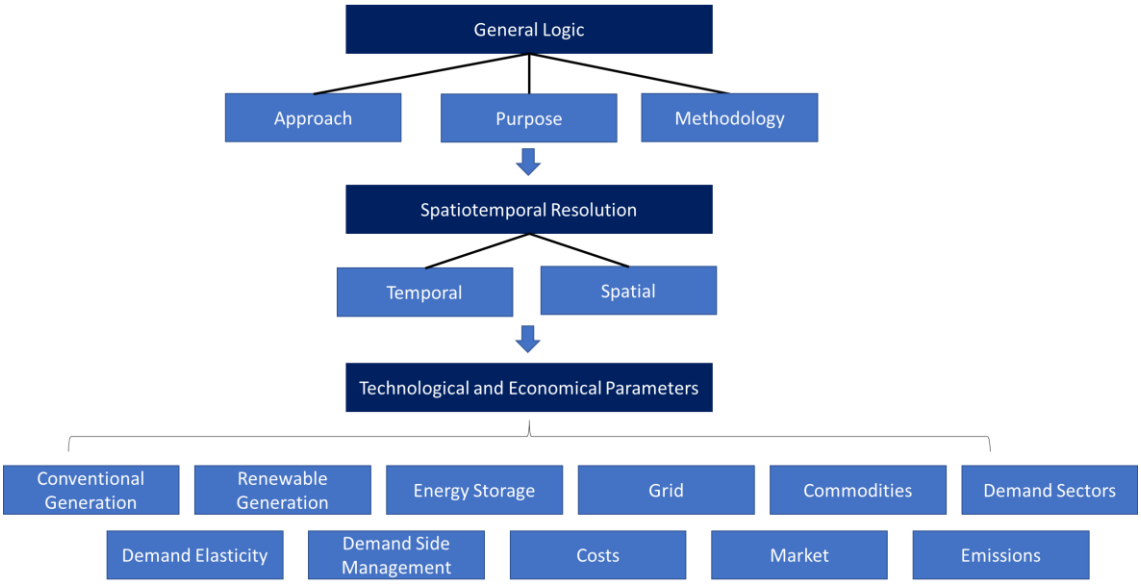

Figure 2.3 - representation of the modelling tools selection process [36].

HOMER [37] is one of the most widely used microgrid modeling software. It is used to simulate and optimize off-grid and grid-connected small-scale power systems for a one-year period, having the ability to simulate the system operation with a time-step from one minute to several hours. The software can model multiple distributed energy and energy storage technologies and has a good sensitivity analysis, allowing the comparison of thousands of possibilities in a single run, with the objective of minimizing investment and operation life-cycle costs [38]. HOMER offers two versions of the software, HOMER Pro, ideal for off-grid systems, and HOMER Grid, ideal for grid-connected systems, and an online tool, the HOMER QuickStart, to ease the introduction to any of the two versions of the software. After HOMER, RETScreen, iHOGA, HYBRID2, and TRNSYS are the most frequently used software tools found in the literature. A description of the analysis type offered by the previously mention tools as well as the types of energy sources available in each one of them, can be found in [39]. DER-CAM [40] is also an important software tool in the optimization of microgrids, as it can simulate the optimal configuration of integrating distributed energy resources and loads.

Although many microgrid modeling tools exist, such as the ones previously mentioned, tailor-made models are still the most frequent method, found in the literature, to model microgrids with

dispatchable energy technologies. This has to do with the higher flexibility, presented by the tailor-made models, in detailing the technical parameters of the generation technologies, and with the limitations felt by commercial tools when it comes to considering intra-hour variability and variations in the bus voltage, which is an important characteristic for networks with high PV power penetration since solar radiation can suffer high fluctuations in a short period of time [41]. From all modeling software that enable the development of tailor-made models, MATLAB-Simulink stands out as the most used tool in the literature to perform dynamic modeling and simulation of microgrids.

In 2010 [42] proposed a hybrid solar-wind system, modeled, and simulated with MATLAB-Simulink, to generate enough power to supply villages in the desert/rural areas of Iraq. In [43] the author studied the possibility of integrating energy sources, such as solar, wind, and fuel cell at the distribution level, by developing a dynamic model of a microgrid in MATLAB-Simulink, concluding that this integration produced satisfactory results, and suggesting the evaluation of a pilot scheme grid integration at a laboratory level. A renewable energy-based microgrid, composed of a solar-wind system, was proposed by [44] to supply a chosen sample number of houses at St. Martin's Island in Bangladesh, simulating the energy generation in a model developed using MATLAB-Simulink, and concluding that the microgrid could successfully supply a total of 200 houses, 20 shops and a hospital over a period of one year. In [45] the author presents a microgrid structure consisting of PV panels and a wind turbine modeled in MATLAB-Simulink and validated with real experimental data, designed to supply a household. More recently [46] modeled a building integrated hybrid microgrid, using MATLAB-Simulink, proposing an efficient power control scheme for the PV panels, wind turbine, and storage system and demonstrating an adequate output power quality with low Total Harmonic Distortion.

As it can be seen, different types of microgrids models, developed in MATLAB-Simulink, can be found in the literature, varying on the energy generation and storage technologies, on the generation scales, going from a single house to an entire city, and on the strategies used to control all the elements of the microgrid, which have been the main research topic in recent years.

2.4 Control strategies

To correctly develop a tailor-made model for a microgrid, especially when dispatchable energy sources such as photovoltaics and wind turbines are considered, one should start by having a good understanding of the dynamic nature of the energy sources, then, a robust control strategy should be adopted to guarantee the technical viability of the system.

The control system is responsible for guaranteeing maximum power conditions for the PV array and wind turbine, at different environmental conditions, for controlling the battery charging modes, and for ensuring power quality by guaranteeing that the output voltage and frequency of the inverter meet the required levels.

2.4.1 Maximum Power Point Tracker

Figure 2.4 presents the I-V curve for a PV array. As it can be seen, any point in this curve is a valid operating point, but only one corresponds to the maximum output power. In order to achieve maximum efficiency in operation, the PV array should always be operating at this point. Since the I-V curve of a PV array is influenced by the changes in weather conditions, mainly changes in irradiance and temperature, there is the need to adjust the operating conditions of the array so that the system is continuously operating at the maximum power point (MPP). The maximum power point tracker (MPPT) is responsible for finding the voltage (maximum power voltage) at which the PV array should operate to produce the maximum possible power at any irradiance and temperature conditions.

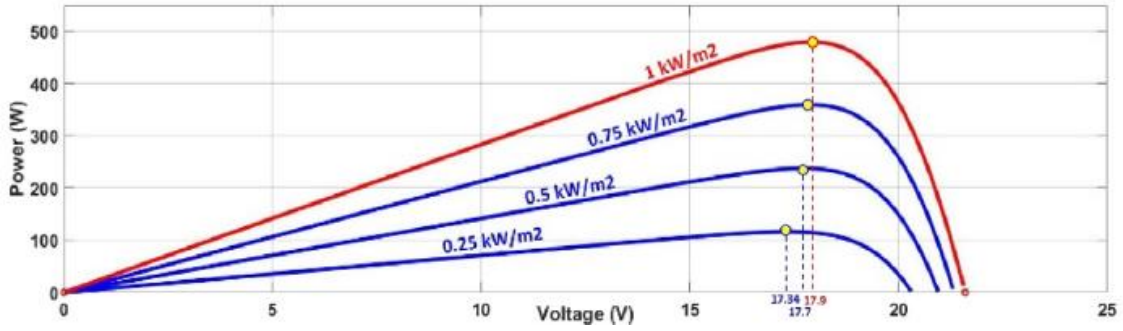

Figure 2.4 - I-V curve and MPP (yellow) of a PV array for different irradiance values [47].

Different techniques can be found in the literature to track the maximum power point of a PV array. These vary in the complexity of implementation, tracking speed, oscillation around the maximum power point, and efficiency. Fuzzy Logic and Neural Networks stand out as the most effective techniques [46]. These control techniques are used to deal with non-linear and complex systems, presenting a robust and fast response to atmospheric changes, being ideal to track the MPP under cloudy weather conditions. Despite the mentioned advantages, the high level of complexity of these techniques makes them less common than direct methods, which do not need radiation nor temperature sensing, such as Perturb and Observe (P&O) and Incremental Conductance. Since these two control techniques do not need any pre-knowledge of the system data, they can be used in any microgrid, which is the reason why these two methods are the most popular ones in the literature [46].

2.4.2 Battery Charging Control

When charging a Lithium-Ion battery three different methods could be used, the battery could be charged at constant current (CC) during the entire charging process, it could be charged with the maximum possible current level and switched to lower current values when needed, resulting in a multi-step constant current (MCC), or it could be charged at constant voltage (CV). The battery control

system will define how the current density varies during the charging process, being responsible for implementing a charging strategy based on the combination of previously mentioned charging methods. According to [47] numerous charging protocols and strategies have been proposed, in figure 2.5 the three most frequent strategies can be found. Standard Protocols is the most common charging protocol due to its simplicity and ease of implementation. It is composed of two phases, a CC charging phase where the voltage is increased to a certain limit, and a CV phase which is maintained until the current falls to a value close to zero.

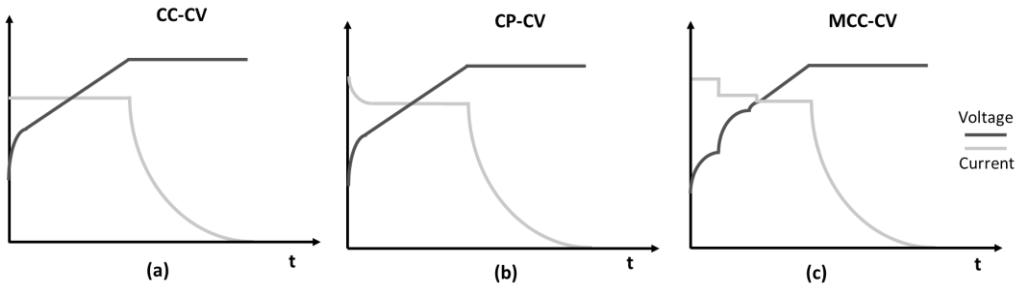

Figure 2.5 - Representation of the most common battery charging strategies: a) Standard Protocols, b) Constant Power - Constant Voltage, c) Multiple Constant Current Protocols (adapted from [48]).

2.5 Demand Side Management

By modeling the energy generation technologies, it is possible to predict the amount of energy generated by the microgrid, and its time distribution, enabling the determination of the generation pattern. As previously mentioned, the balance between demand and generation should be met at every instant, but, due to the uncertainty in power generation and the variability in demand patterns, this balance cannot be guaranteed only by the generation side, so two strategies should be adopted to guarantee the balance between generation and demand [48]. The first has been previously discussed in this chapter and is related to postponing the energy availability by storing the energy generated in periods where generation surpasses the demand and use the stored energy in periods when the opposite happens. The second is related to virtually creating energy availability without increasing the energy generation or changing the energy storing system, this can be accomplished by implementing management measures that help to reshape the load curve to better fit the generation pattern. The process of adjusting the load curve to the generation pattern, by reducing the demand quantity or changing the time of demand, is known as Demand Side Management (DSM).

DSM encourages consumers to modify their electricity usage behaviors, without compromising or trading off comfort, and to reduce the load at hours of peak demand instead of enlarging the generation capacity of the microgrid, resulting in financial savings for the consumer and environmental savings, since less energy is acquired from the grid. According to [48] DSM can be classified into two modalities: static and dynamic. Static DSM intends to reduce energy consumption by applying

techniques that improve the consumption pattern [49], such as Strategic Conservation, which has the goal of reducing the load to match the energy generation, and Flexible Load Shape, which aims at meeting the energy needs in periods of unpredicted low energy generation. Dynamic DSM intends to reduce the difference between the power consumption during peak and off-peak periods [49], for this purpose three mechanisms stand out: Peak-climbing, which aims at reducing the peak load, Valley Shifting, which intends at increasing the consumption during off-peak periods, and Load Shifting, which aims at shifting the load from peak to off-peak periods. Another commonly used dynamic DSM mechanism is known as Strategic Logic Growth, which intends to correct the profile load to improve the efficiency of the power system. A representation of all the previously mention techniques can be found in figure 2.6. The implementation of these methods enables to shape the load curve in order to fit the generation pattern as close as possible.

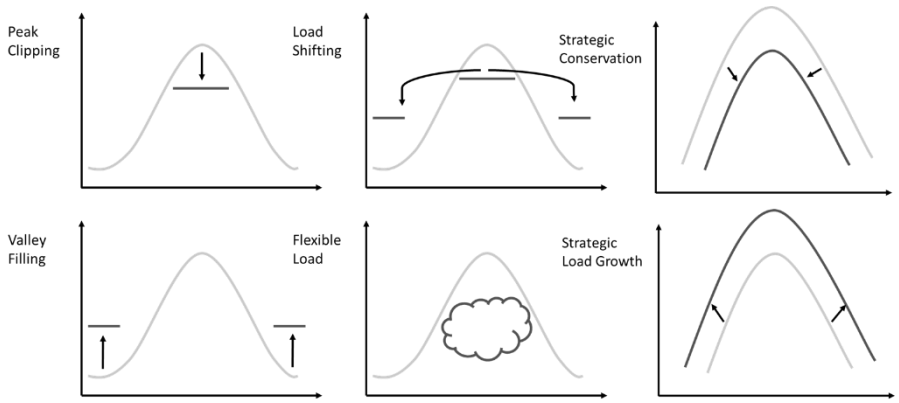

Figure 2.6 - Representation of the most common Demand-Side Management techniques.

Based on the incentive or actions that led to the implementation of the previously mentioned techniques, DSM can be divided into three main concepts: Demand Response, Energy Efficiency, and Energy Conservation. Demand Response (DR) refers to changing the consumption behavior, shifting loads from peak to off-peak hours, by implementing strategies of dynamic pricing, Energy Efficiency consists in reducing the total amount of energy demand by using appliances and equipment with higher efficiencies, and Energy Conservation lies on reducing the energy demand by changing the behavior of the consumer, encouraging this one to use passive solutions as much as possible, to reach comfort, for example, to use solar radiation during the winter, decreasing the heating needs, and natural ventilation in the summer to decrease the colling needs.

3 Methodology and technologies description

The work developed during this thesis is done in collaboration with the Center for Innovation, Technology and Policy Research (IN+) and with the “Laboratório Nacional de Engenharia e Geologia” (LNEG) and will be integrated into the project IMPROVEMENT [6].

IMPROVEMENT is a project co-financed by the Interreg SUDOE Program and the European Reginal Development Fund, which aims at converting existing buildings into net-zero energy buildings. To accomplish this goal, the IMPROVEMENT project will study the integration of combined cooling, heating, and power microgrids in public buildings, located in the SUDOE region, characterized by having high energy consumption in heating and colling, and in electrical appliances and equipment. With the objective of demonstrating, testing, and validating the systems developed during the project, two microgrid pilot plants were created, being one of them located in the LNEG main building. The LNEG microgrid can be divided into two separate systems: a thermal system and an electrical system, represented in figure 3.1, which is the object of study in this work.

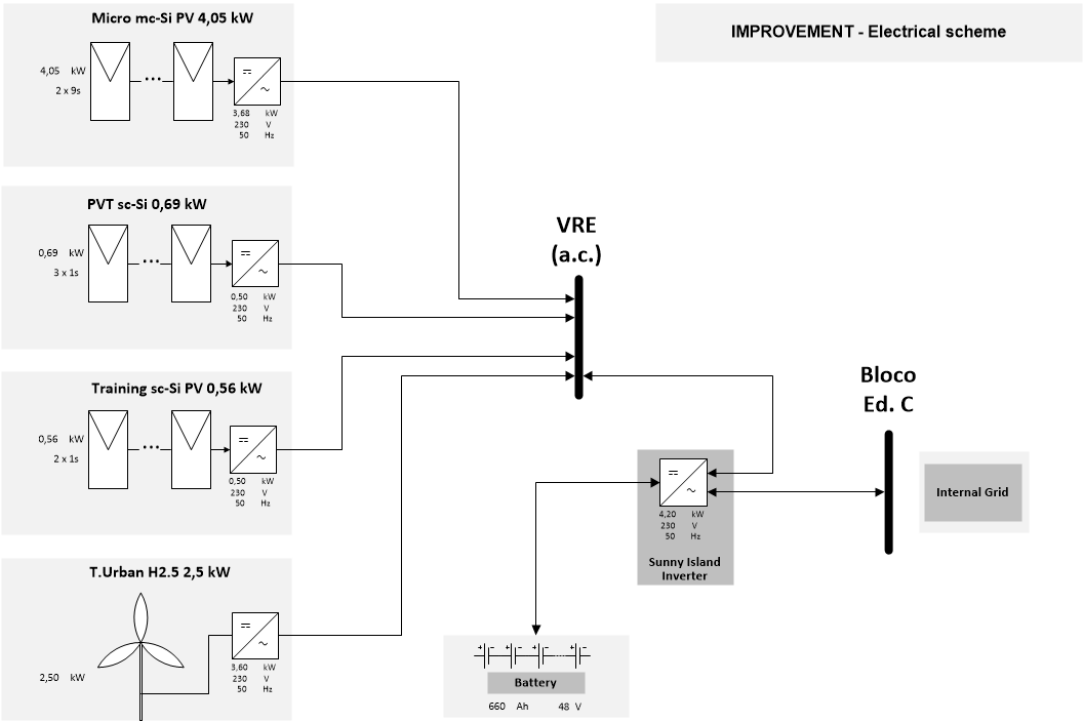

Figure 3.1 - LNEG pilot plant electrical microgrid.

The electric microgrid is composed of five systems: four energy generation systems, constituted by two PV systems, one with 4050 W and the other with a 560 W rated power, a PVT system with an electric rated power of 690 W and a 2500 W rated power wind power system, the fifth system consists in an energy storage system, composed by a 48V Lithium-Ion battery with 660 Ah energy capacity. These systems will be modeled and tested individually and then integrated to produce the desired

microgrid. The methodology used to model each one of these systems can be found in the following sections.

3.1 Photovoltaic System

A rooftop grid-connected photovoltaic system, such as the one in hands, is normally composed of a generation unit, the PV array, and a power conditioning unit (PCU) responsible for converting the DC power generated by the PV array into usable AC power. The PCU is connected to a distribution board, which transfers power to the building appliances or to the grid.

3.1.1 Photovoltaic performance models

With the objective of evaluating the performance of a PV module, and consequently a PV array, for any irradiance and temperature conditions, different models have been developed. Fast estimate [50] stands out as a simple model to evaluate the DC power generated by a PV module, equation 3.1. This model assumes that the output power depends linearly on the irradiance, and the peak power temperature coefficient introduces the temperature correction. Although simple, this model only gives information about the output power, so, if the objective is to evaluate other quantities such as the maximum power voltage or the maximum power current, other models should be adopted.

$$P(G,T) = \frac{G}{G^r} P_P\left[1 + \mu_{Pp}(T - T^r)\right] \tag{3.1}$$

A more precise model, which allows the evaluation of the previously mention quantities, is known as 1 Diode and 3 Parameters (1D+3P) [50]. This model describes the behavior of a PV module by an equivalent circuit, represented in figure 3.2. The current I_s is the current generated by the radiation photons, the *pn* junction [50] acts as a diode, only allowing the flow of the current through itself when the voltage is positive and greater than a certain minimum value and I_D is the current across the diode, given by equation 3.2, where V is the terminal voltage, *m* the diode's ideality factor, I_0 the diode's inverse saturation current, and V_T the thermal voltage given by equation 3.3.

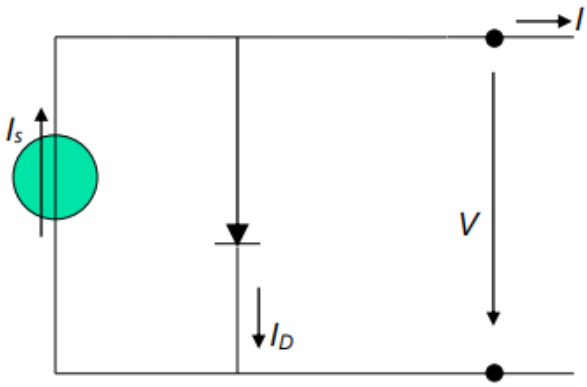

Figure 3.2 - 1 Diode and 3 Parameters equivalent circuit.

$$I_D = I_0\left(e^{\frac{V}{mV_T}} - 1\right) \tag{3.2}$$

$$V_T(T) = \frac{K}{q}T \tag{3.3}$$

In equation 3.3 q is the electron's electrical charge, T is the absolute temperature, and K the Boltzmann constant. Based on the equivalent circuit the current I can be determined using equation 3.4, and consequently, the output power can be determined, equation 3.5.

$$I = I_s - I_D = I_s - I_0\left(e^{\frac{V}{mV_T}} - 1\right) \tag{3.4}$$

$$P = VI = V[I_s - I_0(e^{\frac{V}{mV_T}} - 1)] \tag{3.5}$$

The maximum output power obtained when the module is operating in the maximum power point, implies $dP/dV = 0$, which results in the determination of the maximum power voltage, equation 3.6, and maximum power current, equation 3.7. Since equation 3.6 is a non-linear equation, an iterative process should be adopted, being necessary to establish a starting guess and to determine the three parameters of the module I_0, I_{sc} and m. These three parameters can be calculated by introducing the influence of the module temperature and irradiance in the values obtained under standard test conditions, presented in the manufacturer's datasheet. The 1D+3P model assumes that the ideality factor is constant despite variation in irradiance and temperature, the inverse saturation current varies with the temperature, according to equation 3.8, and the short-circuit current depends on the irradiance, equation 3.9. Appling equations 3.8 and 3.9, the three parameters of the model can be determined, and it is also possible to conclude that the module's output power decreases as the temperature increases and that the output power increases with the irradiance.

$$V_{MP} = mV_T \ln\left(\frac{\frac{I_{sc}}{I_0} + 1}{\frac{V_{MP}}{mV_T} + 1}\right) \tag{3.6}$$

$$I_{MP} = I_{sc} - I_0\left(e^{\frac{V_{MP}}{mV_T}} - 1\right) \tag{3.7}$$

$$I_0(T) = {I_0}^r\left(\frac{T}{T^r}\right)^3 e^{\frac{N_s\varepsilon}{m}\left(\frac{1}{{V_T}^r} - \frac{1}{V_T(T)}\right)} \tag{3.8}$$

$$I_{sc}(G) = {I_{sc}}^r\left(\frac{G}{G^r}\right) \tag{3.9}$$

A more sophisticated model than the 1D+3P could be used, the 1 Diode and 5 Parameters (1D+5P) [50]. This model complements the model previously seen by accounting for several losses existing in the PV module, namely the losses the current faces through the body of the cell, the metal electrodes and contact's resistance (R_s), and the shunt resistance (R_{sh}). The five parameters of this module (I_0, I_{sc}, R_s, R_{sh} and m) can be obtained using simultaneously the manufacturer's datasheet and the process described for the 1D+3P or by applying the process illustrated in [51]. The equivalent circuit proposed by the model can be found in figure 3.3, and the current I can be calculated using equation 3.10, which could be replaced in equation 3.5 to calculate the module DC output power.

$$I = I_s - I_D - I_{sh} = I_s - I_0\left(e^{\frac{V+R_sI}{mV_T}} - 1\right) - \frac{V + R_sI}{R_{sh}} \tag{3.10}$$

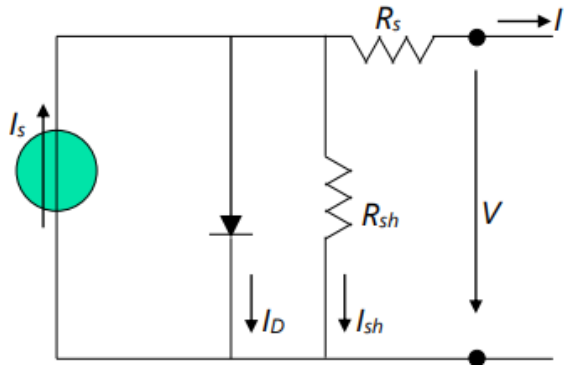

Figure 3.3 - 1 Diode and 5 Parameters equivalent circuit.

The 1D + 5P will be used to model the behavior of the PV modules and consequently the PV arrays, since this is the most complete one, and whenever it is necessary to perform calculations in order to determine the PV Array output power, namely during tests performed to the model, the Fast Estimate will be used due to its implementation ease.

3.1.2 LNEG Photovoltaic Panel Parameters

Having studied the different existing methods to model the behavior of a PV module, it is now important to determine the properties of the modules implemented in the LNEG Pilot office. The 4050 W rated power PV array is composed of 18 polycrystalline PV modules (60 cells each), displayed in two parallel strings with 9 series-connected modules per string. The module's electric characteristic at standard teste conditions (irradiance 1000 W/m^2 and Module Temperature 25ºC) can be found in table 3.1. The second PV array, with a rated power of 560 W, is composed of two polycrystalline PV modules (72 cells each) connected in series, whose electric characteristic at STC can be found in table 3.2.

Module	LDK 225P-20
Nominal Output Power [Pmax] [W]	225
Voltage at Pmax [Vmp] [V]	29.9
Current at Pmax [Imp] [A]	7.53
Open Circuit Voltage [Voc] [V]	36.5
Short Circuit Current [Isc]	8.14
Module Efficiency [%]	13.79

Table 3.1 - CS6P-225PX module electric characteristic at STC.

Module	CS6X-280P
Nominal Output Power [Pmax] [W]	280
Voltage at Pmax [Vmp] [V]	35.6
Current at Pmax [Imp] [A]	7.86
Open Circuit Voltage [Voc] [V]	44.2
Short Circuit Current [Isc]	8.42
Module Efficiency [%]	14.59

Table 3.2 - CS6X-280P module electric characteristic at STC.

3.1.3 Power Conditioning Unit

As previously stated, the output of the PV array is connected to a power conditioning unit (PCU) responsible for converting the DC power generated by the PV array into usable AC power and for guaranteeing that the PV system's output voltage and frequency meet the required standard values (frequency of 50 Hz and voltage of 230 V between phases and 400 V between phases). A typical PCU consists of a DC-DC converter and a DC-AC Inverter. The DC-DC convert, working as a boost converter, is responsible for stepping up the slightly varying output PV Array voltage to a constant higher voltage level, which will be able to guarantee a good inverter performance. By switching ON and OFF the circuit switch, presented in figure 3.4, at high frequency, the output voltage can be controlled. When the switch is in the OFF state the inductor current rises and the magnetic field in the inductor will expand, storing energy in the process, when the switch opens the current across the inductor falls, collapsing the magnetic field in the inductor, releasing the previously stored energy, and generating a large voltage, which will progressively charge the capacitor to a voltage greater than the input voltage. During this process, the capacitor voltage will progressively increase until it reaches a state of equilibrium, providing a constant output voltage, from that point on, greater than the input voltage. To size the inductor and the capacitor of a DC-DC boost convert implemented in a PV system, equations from 3.11 to 3.13 can be used, where D is the duty cycle, f_{ws} the switching frequency and P is the PV array rated power.

$$D = 1 - \frac{V_{in}}{V_{out}} \tag{3.11}$$

$$L_{Boost} = 10\frac{(1-D)^2 D {V_{in}}^2}{2 f_{ws} P} \tag{3.12}$$

$$C_{Boost} \geq \frac{DP}{0.01 f_{ws} {V_{in}}^2} \tag{3.13}$$

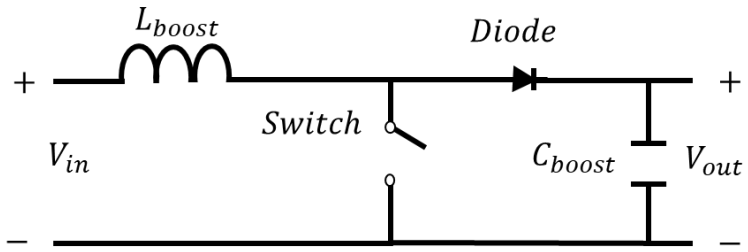

Figure 3.4 - DC-DC boost convert electric circuit.

The DC-DC converter is also used to perform the MPPT function. By controlling the duty cycle of the converter, the working point on the I-V curve can be adjusted to guarantee maximum power conditions at any instant. In the previous chapter, four MPPT techniques were presented and their advantages and disadvantages were discussed. Perturb and Observe will be the chosen technique, for this work, to perform the MPPT task. This method will make incremental changes in the voltage, changing the working point in the I-V curve, and will monitor the consequent changes in power, until the output voltage that produces the maximum output power is found (V_{MP}). In figure 3.5 the algorithm of this technique can be found, the MPPT starts by slightly changing the voltage value, if the change increases the output power, the next perturbation will be in the same direction, if the changes in voltage decrease the output power, the following perturbation will be in the opposite direction. This process will continue until a perturbation in either direction will cause a decrease in power, meaning that the V_{MP} was found.

Figure 3.5 - Perturb and Observe technique algorithm.

The DC-AC inverter, connected to the terminals of the boost converter, is responsible for converting the DC voltage into an AC three-phase voltage. By controlling the switching signal at the gates of the transistors, the voltage and frequency at the output of the inverter are modulated. A direct model predictive control (MPC), based on the one presented in [52], will be used to perform this task. The MPC will control the current at the output of the inverter by measuring the current that is being injected into the grid and comparing it with reference values. Based on the prediction of the desired behavior, the controller will create a switching pattern to minimize the error between the real and the reference values. A more detailed explanation of this procedure will be given in the following chapter. In figure 3.6 a representation of the control system can be found, in order to minimize the harmonic content of the output current and voltage, resulting from the use of switching techniques, an LCL filter will be used, whose parameters can be calculated using equation 3.14 and 3.15, where V is the filter input voltage, P the system rated power and f_{Grid} the grid frequency.

$$L_{filter} = \frac{0.1V^2}{2\pi\left(\frac{P}{3}\right)} \qquad (3.14)$$

$$C_{filter} = \frac{0.005\left(\frac{P}{3}\right)}{2\pi f_{Grid}V^2} \qquad (3.15)$$

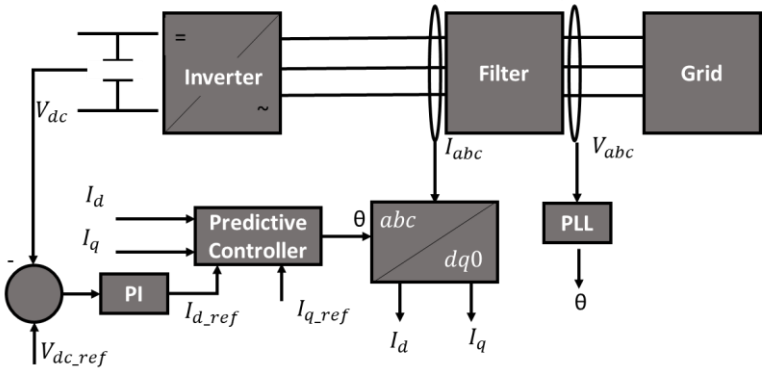

Figure 3.6 - DC-AC inverter control scheme.

3.2 Photovoltaic-Thermal System

In a combined photovoltaic-thermal system (PVT), the heat from the photovoltaic module is extracted and used separately in a thermal system, a representation of a PVT system can be found in figure 3.7. Since the focus of the present work consists in studying an electrical microgrid, this system will be approximated to an overlap between a PV module (components 1, 2, 3 and 4 of figure 3.7) and a thermal collector (components 5, 6 and 7 of figure 3.7), and only the PV module will be modeled. The influence of the heat removed will be considered when modeling the module temperature of this new system, which will have a lower maximum value than a normal PV system.

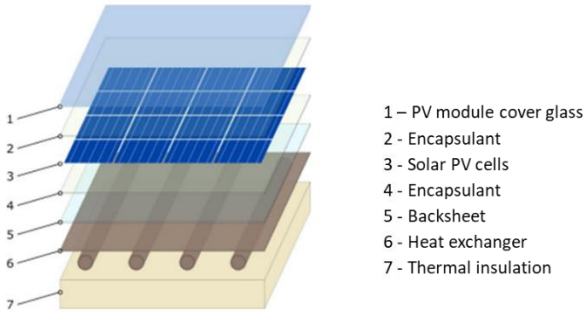

Figure 3.7 – PVT system [53].

As mentioned, the PVT system will be approximated to a PV array, composed of two polycrystalline PV modules (72 cells each) whose electric characteristic at STC can be found in table 3.3, with a module cell temperature value limited by the influence of the thermal collector component.

Module	**LDK 230P-20**
Nominal Output Power [Pmax] [W]	230
Voltage at Pmax [Vmp] [V]	29.9
Current at Pmax [Imp] [A]	7.68
Open Circuit Voltage [Voc] [V]	36.8
Short Circuit Current [Isc]	8.34
Module Efficiency [%]	14.09

Table 3.3 - CS6X-230PX module electric characteristic at STC.

3.3 Wind Power System

The last type of energy generation system implemented in the LNEG microgrid is a wind power system. This system is composed of a wind turbine, responsible for converting the wind kinetic energy into mechanical power, a generator, which converts the mechanical power into electricity, and a power conditioning unit, where the electrical signal produced by the generator is controlled and transformed using an AC-DC-AC converter which is connected to the grid, figure 3.8.

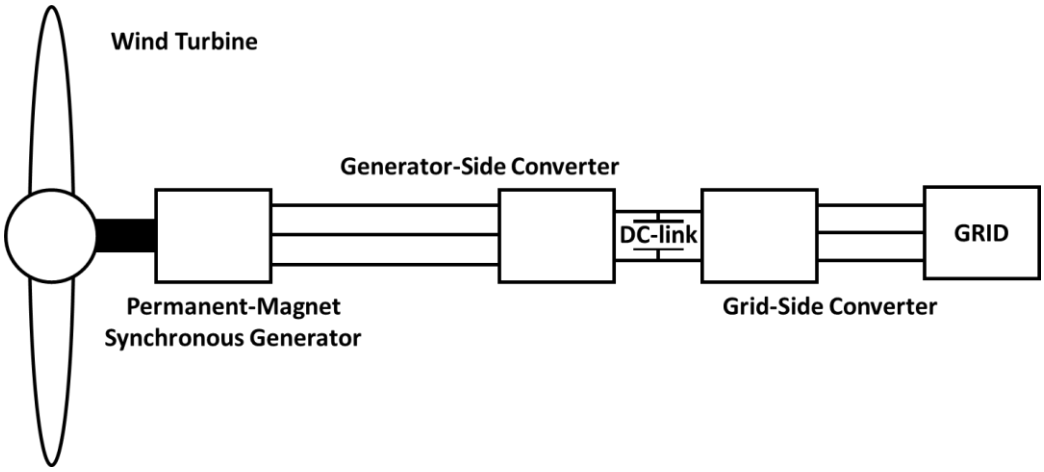

Figure 3.8 - Wind Power System Components.

3.3.1 Wind Turbine

Wind turbines can be divided into two groups, based on their shaft orientation: horizontal shaft configuration and vertical shaft configuration. The two mention groups can be individually subdivided based on the rotor blade configuration and the number of blades. In the case in hands, the wind turbine used is a horizontal shaft orientated turbine.

As mentioned, the wind turbine is responsible for converting the wind's kinetic energy into mechanical work. The mechanical output power of the turbine P_m can be calculated using equation 3.16, were ρ is the air density, A is the swept area by the wind turbine, u the wind speed and C_p is the performance coefficient, which represents the turbine's conversion efficiency.

$$P_m(u) = \frac{1}{2}\rho A u^3 C_p \tag{3.16}$$

The performance coefficient, whose maximum theoretical value was determined by Albert Betz (59,3%), depends on the tip speed ratio λ, equation 3.17, where ω_T is the angular speed of the rotor and R is the radius of the swept area by the wind turbine, and depends also on the blade pitch angle β. The C_p as a function of the tip speed ratio and for different pitch angles is depicted in figure 3.9. As it can be seen, as β increases, the wind turbine conversion efficiency decreases, and consequently, the

output power decreases. Controlling the blade pitch angle is the common way to control the mechanical output power of the turbine.

$$\lambda = \frac{\omega_T R}{u} \tag{3.17}$$

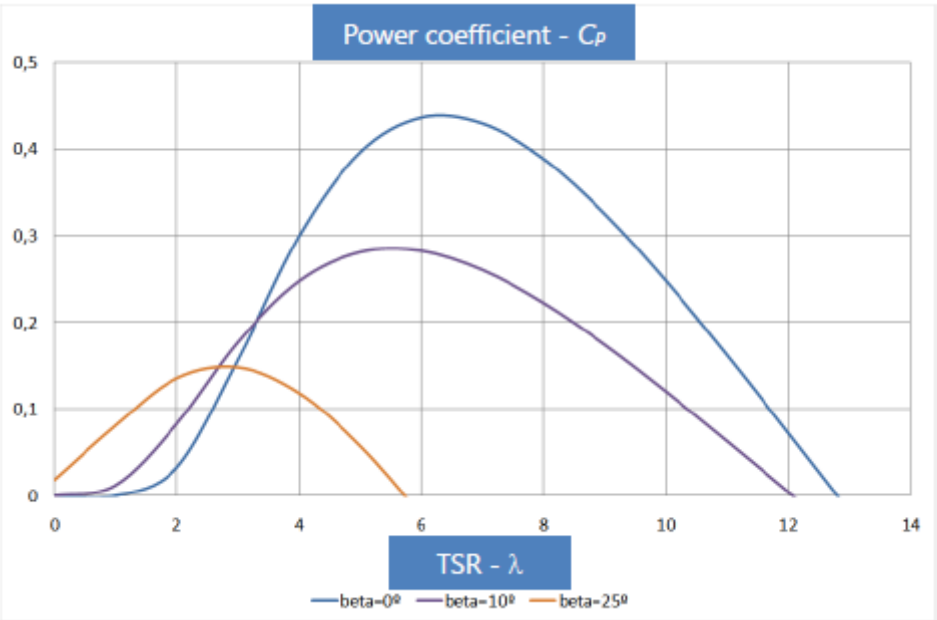

Figure 3.9 - Power coefficient as a function of blade pitch angle and tip speed ratio [50].

Equation 3.18 models the behavior illustrated in figure 3.8, where $C_1 = 0.5176$, $C_2 = 116$, $C_3 = 0.4$, $C_4 = 5$, $C_5 = 21$, $C_6 = 0.0068$ and λ_i is given by equation 3.19.

$$C_p = C_1\left(\frac{C_2}{\lambda_i} - C_3\beta - C_4\right)e^{-C_5/\lambda_i} + C_6\lambda \tag{3.18}$$

$$\lambda_i = \frac{1}{\lambda + 0.08\beta} - \frac{0.035}{\beta^3 + 1} \tag{3.19}$$

3.3.2 Generator

The generator will convert the mechanical power coming from the turbine into electric power. In the case in hands, the generator used is a Permanent Magnet Synchronous Generator (PMSG), characterized by having high efficiency and reliability. Equations 3.20 to 3.24 describe the operation of the PMSG, where d and q represent the direct and quadrant axis components, v and i the voltage and current, L_d and L_q the d and q axis inductances, s indicates stator quantities, ω_m is the angular velocity of the rotor, λ the magnitude of the flux induced by the permanent magnets of the rotor in the stator phase, and p the number of pole pairs [54].

$$\frac{d}{dt}i_d = \frac{1}{L_d}v_d - \frac{R}{L_d}i_d + \frac{L_q}{L_d}pi_q\omega_m \tag{3.20}$$

$$\frac{d}{dt}i_q = \frac{1}{L_q}v_d - \frac{R}{L_q}i_d - \frac{L_q}{L_d}pi_d\omega_m - \frac{\lambda p\omega_m}{L_q} \tag{3.21}$$

$$P_s = v_d i_d + v_q i_q \tag{3.22}$$

$$Q_s = v_d i_d - v_q i_q \tag{3.23}$$

The electromagnetic torque can be obtained by:

$$T_e = 1.5p(\lambda i_q + \left(L_d - L_q\right)i_d i_q \tag{3.24}$$

3.3.3 Power Conditioning Unit

As represented in figure 3.7, in variable speed wind turbines, the generator is connected to the grid via a power conditioning unit, which consists of a three-phase back-to-back set of inverters. The first converter, known as generator-side converter, is connected to the PMSG, and the second one, known as grid-side converter, is connected to the grid via a filter. By controlling the operation of these devices, namely the switching signal at the gates of the transistors, the performance of the wind power system can be improved.

By controlling the generator-side converter, it is possible to control the wind turbine shaft speed, which allows maximizing the output power. As seen in figure 3.8, for any value of β, there is a value of λ (λ_{opt}) that maximizes the wind turbine conversion efficiency and consequently maximizes the output power. With the variations in wind speed, equation 3.17, the rotor speed needs to be adjusted to follow these changes, guaranteeing that λ_{opt} is meet at every instant. By controlling the grid-side converter, it is possible to guarantee that the output voltage and frequency meet the required characteristics to be fed to the grid, which is similarly to what was done in the PV system's DC-AC inverter.

3.4 Energy Storage System

The energy storage system is composed of a lithium-Ion battery and a charging control unit. Batteries, in renewable energy systems, should satisfy conditions that are not present in most common battery applications, such as having the capacity of experiencing deep cycle and being left at low states of charge (SOC) for long periods of time, while steal experience a long lifetime [47]. In this sense, it is important to understand how the battery characteristics will influence their application in these types of systems and how these characteristics should be respected by the battery charging control unit.

3.4.1 Battery characteristics

There are many battery parameters, whose importance depends on the battery application. For the case in hands, Battery Capacity, State of Charge, Depth of Discharge, and Battery Voltage stand out as the most important ones.

The Battery Capacity is a measure of how much energy can be stored in the battery. This quantity can be expressed in Ampere-hour (Ah), which reflects the current value at which the battery can be discharged at a constant rate over a fixed interval, it can be expressed in reverse capacity, which reflects the time duration in minutes that a battery can produce a specified level of discharge, or it can be expressed in kWh capacity, which represents the amount of energy needed to fully charge a depleted battery. The State of Charge (SOC) measures, in percentage, the amount of energy presently stored in the battery, in relation to the nominal rate capacity. The Depth of Discharge (DOD) represents the fraction of power that can be withdrawn from the battery, without damaging or conditioning the battery life, normally deep cycle batteries can be discharged up to 15 to 20% of their capacity. The Battery Voltage, whose nominal value is calculated in equilibrium conditions, changes during the charge and discharge process. The values of the mentioned properties for the battery used in the microgrid modeled in this thesis can be found in table 3.4.

Battery	Sunlight RES OpzS
Battery Tipe	Lithium-Ion
Battery Voltage [V]	48
Battery Capacity [Ah]	660
Depth of Discharge [%]	85

Table 3.4 - Battery Properties.

3.4.2 Battery Control

The energy that can be extracted from the battery is highly dependent on the discharge process, if a battery is discharged quickly, i. e., using high discharge currents, the amount of energy extracted from the battery is lower than it would be if the battery was discharged at a slower rate. Adding to these facts, if the battery is continuously discharged beyond a certain level, the number of discharge/charge cycles that the battery would perform at rated capacity decrease. Charging at higher rates can also have negative consequences for the battery since high charging rates promote high operating temperatures, which in turn decrease the battery lifetime. Thus, it is of extreme importance to control the battery charge and discharge regimes.

The control unit, developed in this work, will be responsible for charging the battery when there is simultaneously a surplus in energy generation and the battery SOC is lower than 100%, being also

responsible for limiting the charging rate. When the demand surpasses the energy generation, the control unit will be responsible for discharging the battery until a SOC of 15% is reached, from that point on, if the demand is still higher than the generation, the control unit will stop discharging the battery to respect the DOD. It is also important to notice that when there is a surplus in energy generation and the battery SOC is equal to 100%, the left-over energy will be injected into the grid, similarly, when the demand surpasses the generation and the battery SOC is equal to 15%, the needed energy will be extracted from the grid.

3.5 Model Architecture

Having studied in more detail each of the microgrid systems, it is now possible to define the model architecture. The model will be composed of three photovoltaic systems with 4050 W, 690 W, and 560 W rated capacity. The PV arrays will be modeled using the 1D + 5P and will be connected to a DC-DC Boost Converter responsible for stepping up the PV array output voltage to a value equal to 600V while guaranteeing maximum power conditions, by implementing a Perturb and Observe scheme. The output of the DC-DC converters will be connected to an Inverter, controlled by a model predictive technique, responsible for converting the 600 V DC voltage into an AC three-phase 400 V phase-to-phase voltage with a frequency of 50 Hz. For the 2500 W rated wind power system, the wind turbine, and the generator will be modeled simultaneously in a generation unit, where the power curve, given in the manufacturer datasheet, will be implemented. The output of the wind generation unit is connected to a rectifier followed by a DC-DC converter which is connected to an inverter with the same characteristics as that of the PV systems. The output of the two types of energy generation systems, PV and Wind, will be connected to a common AC bus, where an energy storage system, composed of a 660 Ah and 48 V battery whose charging and discharging process is performed by a controlling unit, will also be found. The building consumption will be modeled implementing a load curve, where it is assumed that the loads only consume active power. The described microgrid, represented in figure 3.10, will also be connected to the grid.

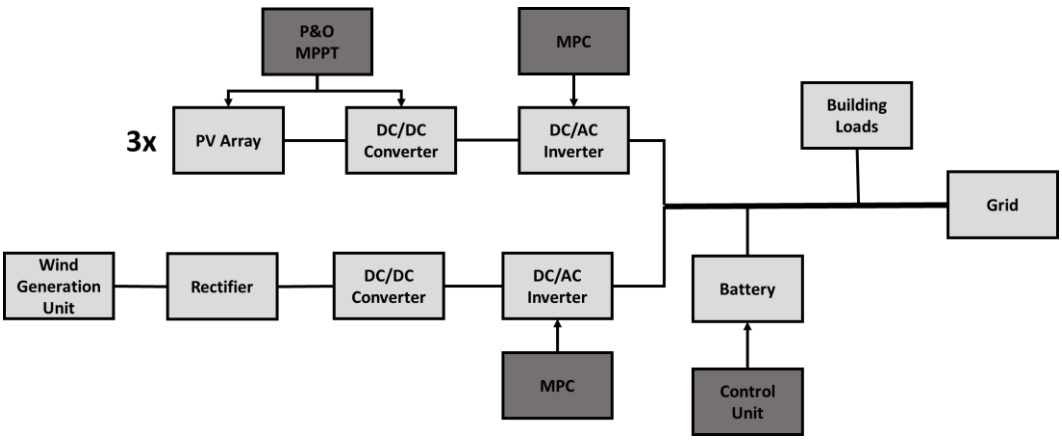

Figure 3.10 - Model Architecture.

4 Microgrid MATLAB-Simulation Model

In this chapter, the microgrid model developed in Simulink will be presented. Each one of the five systems described in the previous chapter was modeled individually and then integrated to produce the desired microgrid. During the next sections, a detailed view of the individual systems' models and an explanation of the adopted procedure will be carried out.

4.1 Photovoltaic System Model

In figure 4.1, a representation of one of the three PV system models developed can be found. Since all three systems were modeled using the same approach, for logistical reasons, only one is represented, but the information provided in the following sections applies to all of them. The present model receives as input Irradiance and Ambient Temperature data, processes this data, and calculates the values and variation in voltage, current, and power at the output of the PV Array, where the quantities are in DC, and at the output of the Power Conditioning Unit (PCU), where the quantities are in AC.

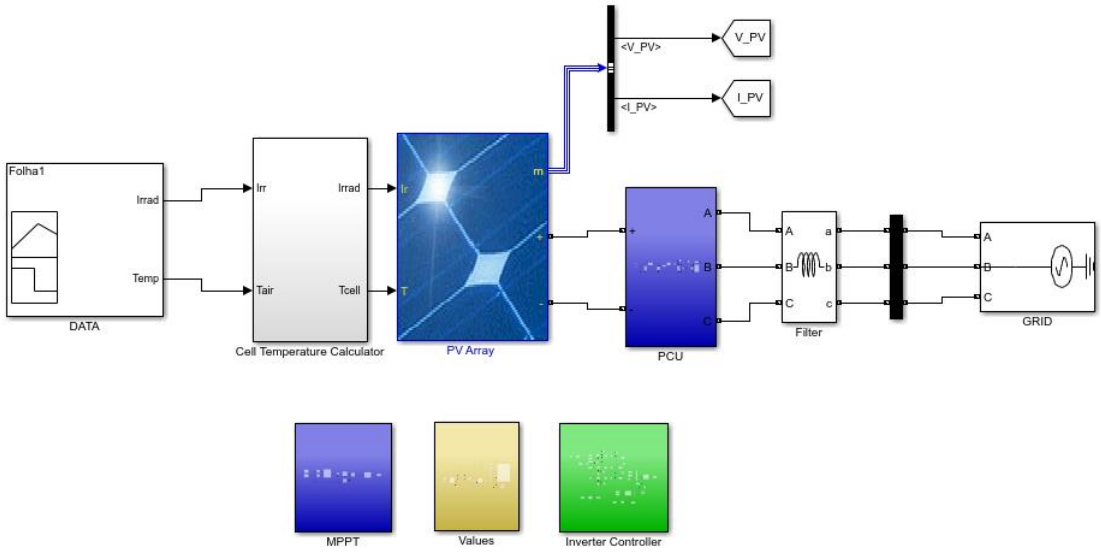

Figure 4.1 - PV System Model.

4.1.1 Photovoltaic Array

The PV Array was modeled using a MATLAB library block, represented in figure 4.2. This block implements an array of PV modules, each modeled using the 1D+5P. The user can define the number of parallel strings and the number of series-connected modules per string, the properties of the module can be chosen by selecting one of the modules presented on the block's database or by

introducing the module's datasheet properties directly on the block, figure 4.2. The presented block receives as inputs Irradiance [W/m^2] and Cell Temperature [^oC] data and gives as outputs the PV Array voltage [V], the PV Array current [A], and the diode current [A]. The cell temperature is calculated from the ambient temperature, given as input to the PV system model, by implementing equation 4.1 [50], which in the model is done in the auxiliary block Cell Temperature, represented in figure 4.1.

$$T_{cell} = T_{amb} + G\frac{45-20}{800} \tag{4.1}$$

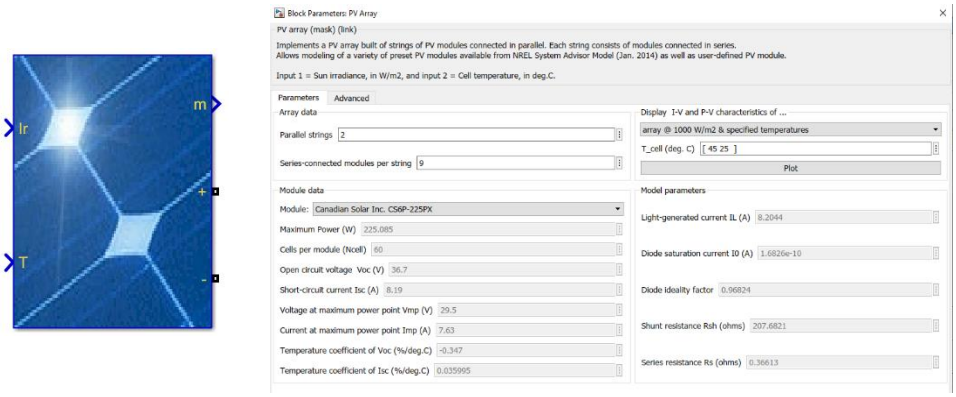

Figure 4.2 - PV Array block (left) and block's data (right).

4.1.2 Power Conditioning Unit

The PCU, represented in figure 4.3, is composed of a DC-DC boost converter and an inverter, both devices where model based on their equivalent circuit represented in section 3.1.3. The boost converter receives as inputs the voltage and current values at the output of the PV array and steps up the voltage to a value equal to 600 V. The inverter is connected to the terminals of the boost converter and converts this 600 V DC voltage into an AC three-phase 400 V phase-to-phase voltage with a frequency of 50 Hz. The calculations of the boost converter parameters were done using equations 3.11 to 3.13, whose values for the 3 PV systems are presented in table 4.1. V_{in} represents the voltage at the input of the converter, and its value is equal to the Maximum Power Voltage (V_{MP}) at STC, L the converter inductance, and C the converter capacitance. The outputs of the PV array are connected to a DC-link, composed of a capacitance and a resistance with values equal to 100 µF and 100 µΩ, respectively.

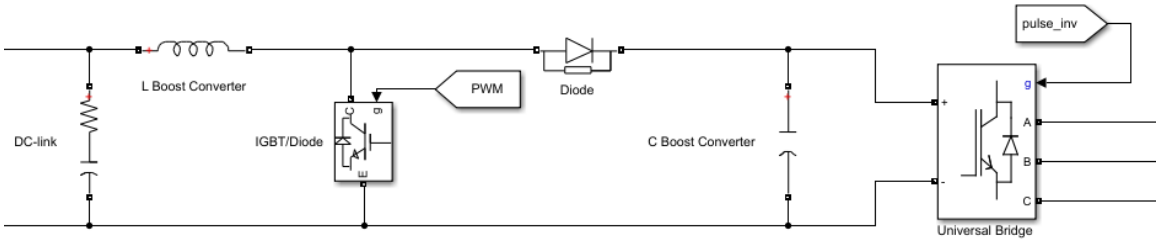

Figure 4.3 - Power Conditioning Unit electric circuit.

PV System	V_{in}	Switch freq.	L_{Boost}	C_{min}	C_{Boost}
4050 W system	270 V	5000 Hz	11.7 mH	124 µF	500 µF
690 W system	87 V	5000 Hz	9.5 mH	33 µF	100 µF
560 W system	71 V	5000 Hz	8.1 mH	27 µF	100 µF

Table 4.1 - Boost Converter parameters.

As previously mentioned, by controlling the duty cycle of the boost converter, the working point on the I-V curve can be adjusted to guarantee maximum power conditions. The MPPT block, responsible for this task is represented in figure 4.4. The output PV array voltage and current are used as inputs in a MATLAB function which implements the P&O technique explained in section 3.1.3. By implementing this technique, the MATLAB function generates a reference voltage value which is compared to the actual voltage value coming from the PV array output. The difference from the real and reference value is fed to a PI controller and compared to a repeating sequence, generating an output between zero and one, the duty cycle, which is fed to a PWM generator, responsible for controlling the circuit switch.

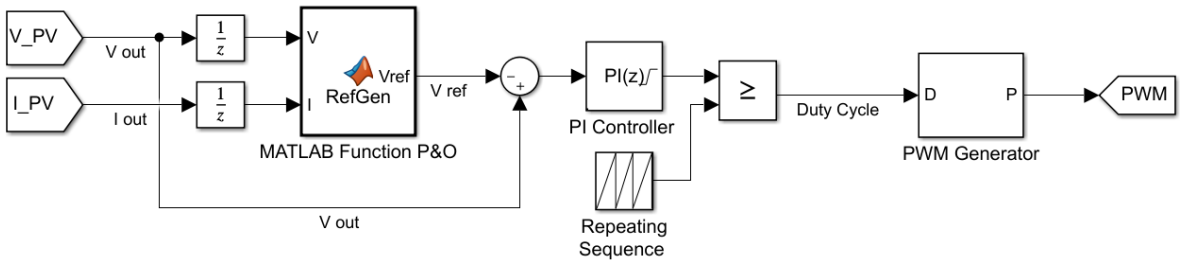

Figure 4.4 - MPPT technique implementation.

In figure 4.5 the strategy developed to control the inverter can be found, where the most important variables are highlighted. The process begins by measuring the current signal at the output of the inverter (yellow), which is a three-phase abc signal. This signal is then transformed to the dq frame, using a MATLAB library block that implements a combination of Clark's (abc to $\alpha\beta$) and Park's ($\alpha\beta$ to dq) transformation, so that the active (cyan) and reactive (red) components of the current can be controlled separately. The two components are compared with reference values. The reactive current reference value is a constant equal to zero since the goal is to only inject active power into the grid. The active current reference value (orange) is generated in the DC-link voltage control, which compares the voltage at the output of the Boost Converter with a reference value of 600V, generating the current reference and controlling the DC-link voltage to be a constant value. The differences between the two reference values and the two measured values are fed to two PI controllers, producing a transformed variable each (green and pink). These transformed variables created by the control process are then transformed into the abc reference using the same MATLAB library block as previously. The output signal of this transformation (blue) is fed to a PWM generator, which is responsible for controlling the switching pattern of the invertor's transistors.

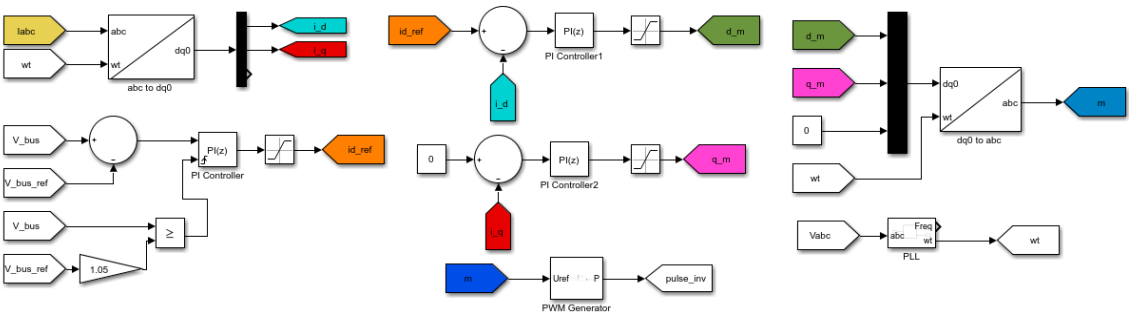

Figure 4.5 - Inverter control strategy.

The parameters of the PI controllers, determined individually by experiment and observation, for the three PV systems can be found in table 4.2. The output of the DC-AC Inverter is connected to an LCL filter, used to minimize the harmonic content of the output current and voltage, whose parameters were obtained using equations 3.14 and 3.15, and can be found in table 4.2, where L_1 represents the inverter side inductance, L_2 the grid side inductance, and C the capacitance.

	Parameter	4050 W system	690 W system	560 W system
I_d controller	**I**	1	1	1
	P	0.005	0.005	0.009
I_q controller	**I**	1	10	10
	P	0.01	0.09	0.09
DC-link controller	**I**	80	80	60
	P	0.15	0.15	0.15
Filter	**L_1**	37.7 mH	221.4 mH	272.8 mH
	C	0.13 µF	0.02 µF	0.02 µF
	L_2	37.7 mH	221.4 mH	272.8 mH

Table 4.2 - PI Controller and LCL filter parameters.

To calculate the system losses, responsible for decreasing the amount of power injected in the grid by the PV system, the procedure presented in [55] was followed. It was assumed that there are three different types of losses: losses in the cables, responsible for decreasing the injected power by 4%, losses due to soiling in the PV modules, responsible for a loss equal to 2%, and losses due to degradation of the system's components, assumed to be a linear process, resulting in a continuous decrease of power equal to 0.2%/year.

4.2 Wind Power System Model

The wind power system, represented in figure 4.6, is responsible for converting wind energy into usable electricity. To accomplish this goal, the system is divided into two units: a generation unit and a power conditioning unit. The present model receives as input wind speed data, processes this data, and calculates the values and variation in voltage, current, and power at the output of the power conditioning unit.

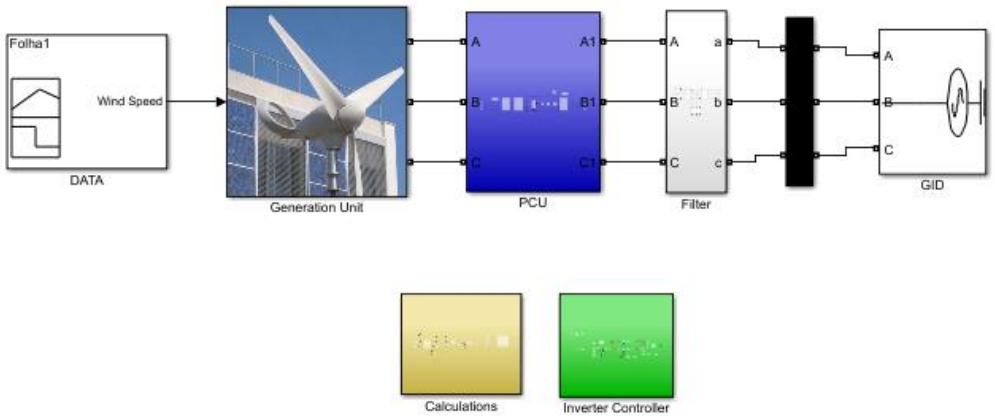

Figure 4.6 - PV Wind Power System Model.

4.2.1 Generation Unit

The generation unit, represented in figure 4.7, is composed of the wind turbine and the permanent-magnet synchronous generator. To model both components the wind turbine generator power performance curve was determined from real measured data, allowing the prediction of the electric power output based solely on the wind speed. The mathematical equation that best models the power curve can be found in equation 4.2, where 3.5 m/s is the cut-in speed, the wind speed at which the turbine starts to generate power, the 10 m/s is the rated speed, the wind speed at which the turbine reaches rated power and 25 m/s is the cut-out speed, the wind speed at which the system shuts down

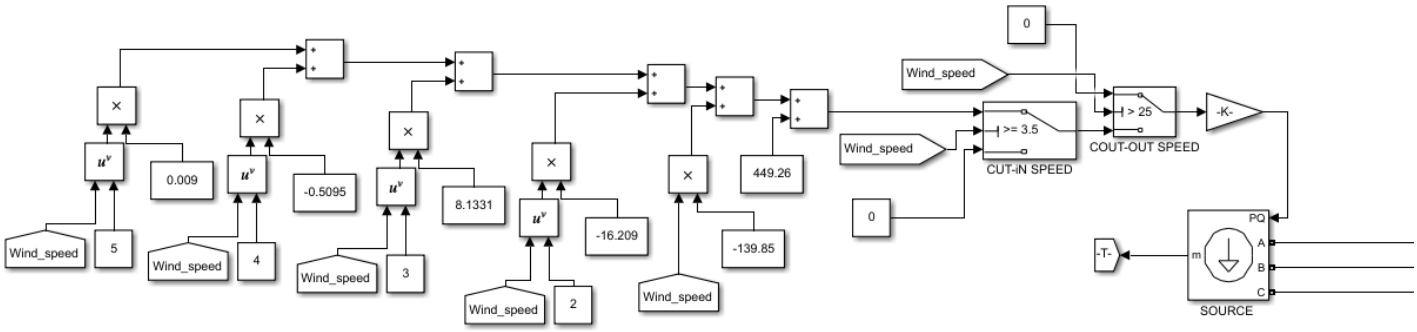

Figure 4.7 - Generation Unit block.

for safety reasons. The Simulink block developed to implement the previous equation is represented in figure 4.7, where the power value obtained from equation 4.2 is fed to a three-phase power source that is connected to the PCU.

$$\begin{cases} P_e = 0 & u < 3.5\ m/s \\ P_e = 0.009u^5 - 0.5095u^4 + 8.1331u^3 - 16.209u^2 - 139.85u + 449.26 & 3.5 < u < 25\ m/s \\ P_e = 0 & u > 25 m/s \end{cases} \quad (4.2)$$

4.2.2 Power Conditioning Unit

The power condition unit of a grid-connected wind power system is composed of an AC-DC-AC converter, figure 4.8. This unit is responsible for converting the electrical power at the output of the generator into usable power. The different components of the PCU used in this system can be found in figure 4.8. The output of the generation unit is connected to a three-phase diode rectifier, used to convert the three-phase AC output of the generation unit into DC. Since the generation unit was modeled by implementing the power curve, which predicts the electric power output without considering technical details of its components, it is not necessary to develop a control strategy for the rectifier to guarantee maximum power point conditions and pitch control, because these conditions are already being considered in the power curve. The output of the rectifier is connected to a DC-DC Boost Converter, whose parameters calculated using equations 3.11 to 3.13 are presented in table 4.3. The Boost Converter receives the slightly changing voltage and steps it up to a constant value of 600 V. This power device is then connected to a DC-AC inverter, which transforms the 600 V DC voltage into an AC three-phase 400 V phase-to-phase voltage with a frequency of 50 Hz.

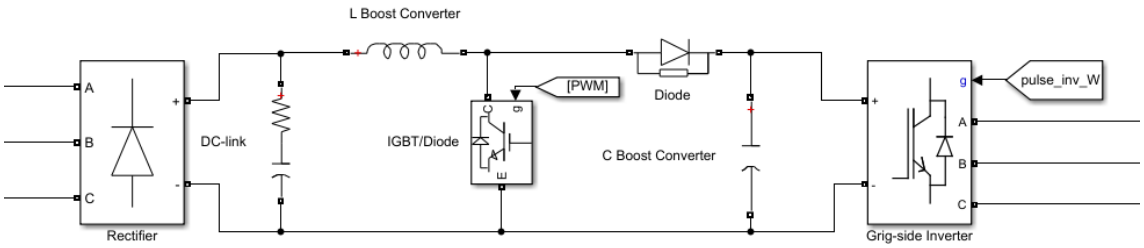

Figure 4.8 - Power Conditioning Unit electric circuit.

Wind Power System	V_{in}	Switch freq.	L_{Boost}	C_{min}	C_{Boost}
2500 W	240 V	5000 Hz	13 mH	83 µF	100 µF

Table 4.3 - Boost Converter parameters.

The strategy developed to control the grid-side inverter is the same that was used to control the PV system inverter, presented in figure 4.5. As previously described in more detail in section 4.1.2, the current signal at the output of the inverter will be measured and compared with reference values and

the differences between them will produce transformed variables used to control the switching pattern of the invertor's transistors. The parameters of the PI controllers used in the control strategy can be found in table 4.4, where there can also be found the parameters of the LCL filter connected to the terminals of the inverter and used to minimize the harmonic content of the output current and voltage. The parameters of the inverter were determined using equation equations 3.14 and 3.15, L_1 represents the inverter side inductance, L_2 the grid side inductance, and C the capacitance.

	Parameter	Wind Power System
I_d controller	**I**	1
	P	0.005
I_q controller	**I**	1
	P	0.01
DC-link controller	**I**	80
	P	0.15
Filter	**L_1**	6.1 mH
	C	0.83 µF
	L_2	6.1 mH

Table 4.4 - PI Controller and LCL filter parameters.

4.3 Energy Storage System Model

The energy storage system is composed of a lithium-Ion battery and a charging control unit. To model this system two blocks were developed, the first is responsible for determining the battery state of charge (SOC), and the second consists of the charging control unit. In figure 4.9, the first of the two blocks can be found, this block receives as inputs the battery energy capacity in kWh and the initial SOC and provides the battery SOC at every instant. To determine the SOC, this block starts by calculating the difference between the power at the output of the generation systems and the required power to satisfy the demand. To guarantee power balance, this difference needs to be compensated by charging/discharging the battery, as long as the physical limits of the equipment are respected, something that is guaranteed by implementing a saturation block that limits the maximum charging and discharging power. Having determined the available charging power or the needed discharging power, this quantity can be integrated, using an integration block, to determine the energy that is being stored in the battery. Dividing this quantity by the battery energy capacity the SOC can be determined. To guarantee that energy is being stored only when the battery is not fully charged yet, a MATLAB function was developed to produce a signal responsible for allowing the passage of energy to the battery only when the SOC is lower than 100%.

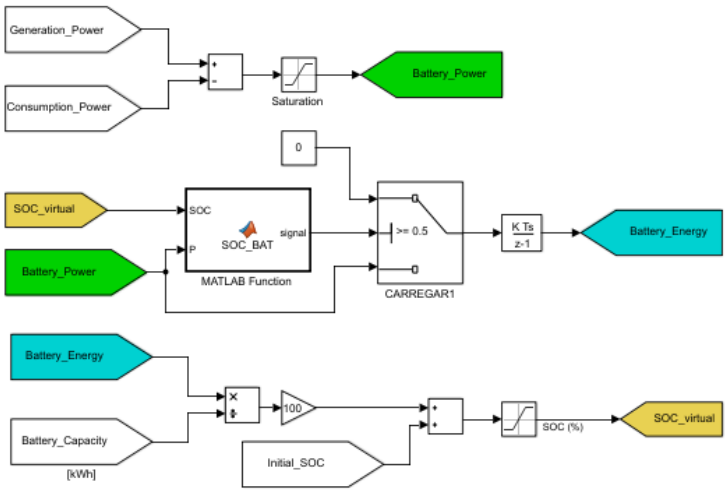

Figure 4.9 - Battery SOC block.

The charging control unit, represented in figure 4.10, receives as inputs the battery SOC and the value of the energy balance between the energy generation systems and the energy consumption. It starts by evaluating if there is a need to discharge the battery or if it is possible to charge it, charging the battery when there is a surplus in energy generation and discharging it when the demand surpasses the energy generation, a process which is controlled by the switch represented in blue. During the charging process, the control unit charges the battery until a SOC of 100% is reached, interrupting the charging of the battery from that point on. This task is performed by the switch represented in yellow which forces the power injected in the battery to be equal to zero when the battery is fully charged. During the discharging process, the control unit discharges the battery until a SOC of 15% is reached, respecting the DOD and contributing to good battery usage practices. This process is controlled by the switch represented in green, which forces the power at the output of the battery to be equal to zero after the SOC minimum value is reached. In both cases, a saturation block is used to limit the maximum power at which the battery is being charged/discharged. By implementing this control strategy, the charging control unit is capable of determining and controlling the amount of power that is being injected or removed from the battery and provide that information to a dynamic three-phase source or load, depending on if the battery is charging or discharging, which is connected to the microgrid.

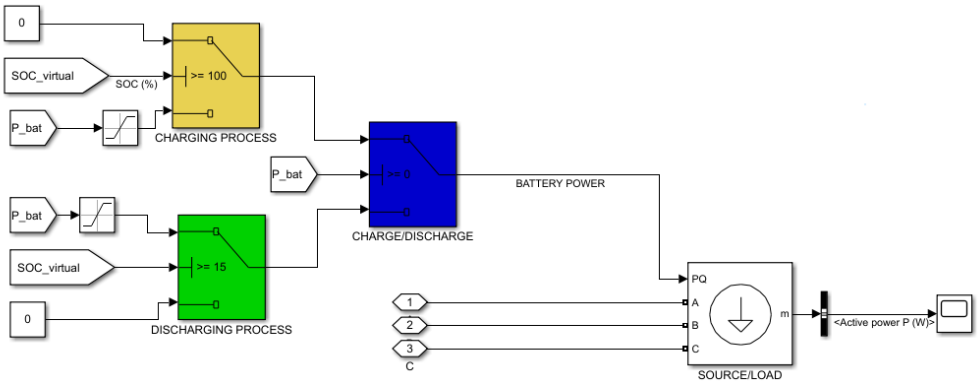

Figure 4.10 - Battery Control Unit.

4.4 Microgrid Model

Having modeled individually each one of the five systems, they can be integrated to produce the desired microgrid, presented in figure 4.11. The developed microgrid model receives as inputs weather data, such as ambient temperature, irradiance, and wind speed, it receives data about the battery properties, such as the initial SOC and the energy capacity, and it receives data about the energy consumption in the building. The model processes this data and gives information about the energy generation in each of the four generation systems, about the energy stored in the storing system, and about the amount of energy consumed or injected into the grid. The user can also define the time step and the total duration of the simulation. The building block, which has not been presented before, is a block that models the building energy demand by receiving as input the building consumption curve and converting that information into a dynamic three-phase load that is connected to the microgrid bus. A full depicture of the model previously described and of each one of its main blocks can be found in Appendix A. As a remark, it is important to recall that some of the blocks presented were fully developed from scratch, while others were adapted from information found in the literature. The block used to model the PV array, figures 4.2 and A.0.2, was extracted from MATLAB-Simulink library, the blocks used to model the PCUs used in the PV system and wind power system, figures 4.3, 4.8, A.0.3 and A.0.5, were developed based on equivalent circuits, and the block used to model the inverter controller, figures 4.5 and A.0.12, was adapted from [52]. The block used to implement the MPPT technique, figures 4.4 and A.0.12, was developed by the author based on what was found as the common practice across the literature. The blocks developed to model the wind power Generation Unit, figures 4.7 and A.0.4, the battery unit, figures and 4.9 and A.0.7, the battery control unit, figures 4.10 and A.0.8, the building consumption, figure A.0.9, all blocks used to perform auxiliary calculations, figure A.0.11, and all blocks used to collect and process input data, figure A.0.10, and to present the outputs of the program, figure A.0.13, were developed by the author.

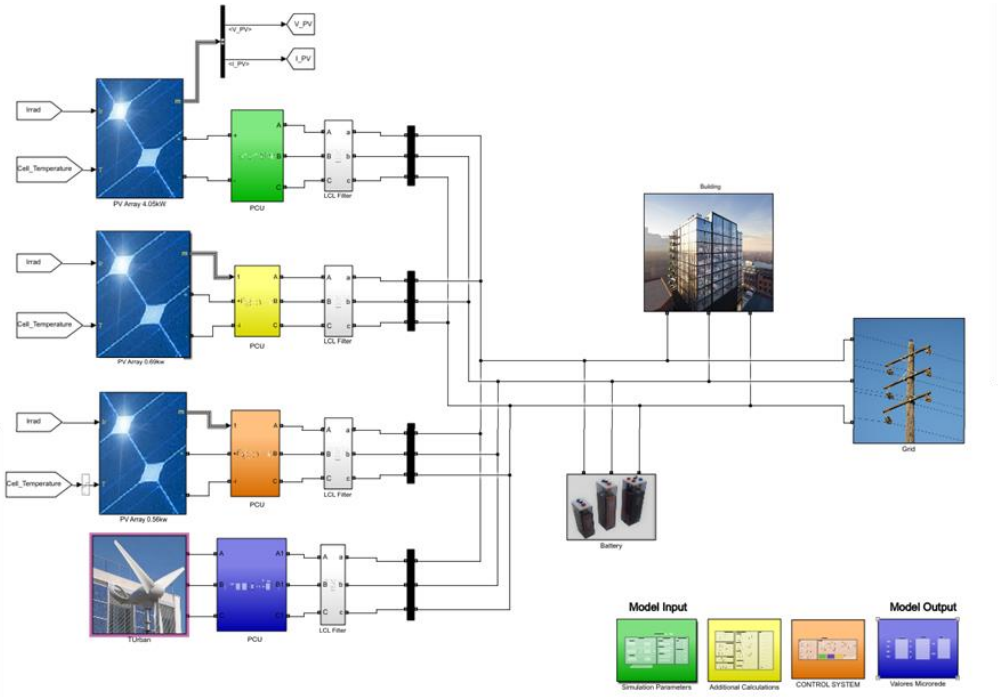

Figure 4.11 - Microgrid MATLAB-Simulation Model.

With the objective of evaluating and validating the performance of the developed system, it was decided to compare the results coming from the energy tool developed in this thesis, with the results coming from an equivalent system developed in a commercial software, this comparison is presented in chapter 6. POLYSUN, a software dedicated to the design, sizing, and optimization of energy systems for buildings, was the commercial software chosen to carry out this evaluation. An equivalent system to the one presented in figure 4.11 was developed in POLYSUN, however, it was not possible to model the wind power system, because POLYSUN database does not have any information about wind power generation technologies, the system layout is presented in figure 4.12.

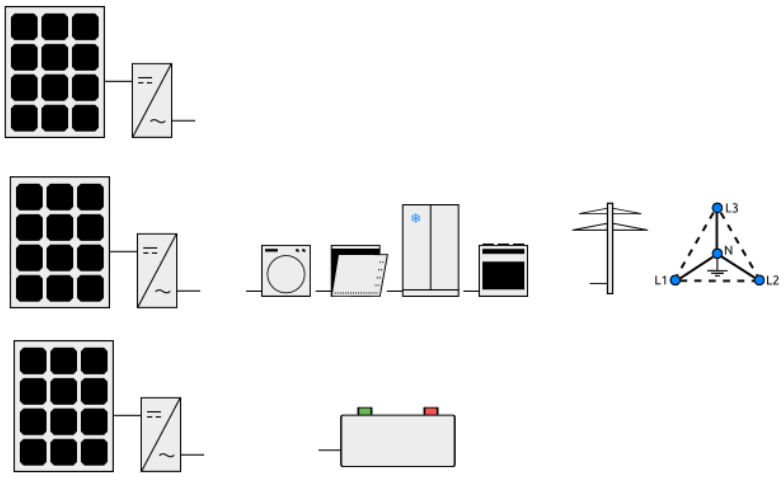

Figure 4.12 - Microgrid POLYSUN Model.

5 Demand Response

Having modeled the desired microgrid, the next logical step would be to identify the operating conditions that allow it to be used in the most efficient way. Here the concept of Demand Side Management (DSM) is introduced. As it was seen in chapter 2, DSM can be defined as a set of measurements, adopted by the consumption side, that modify the energy consumption pattern to promote better operation efficiency in electrical energy systems. According to the way the demand management is performed, DSM can be divided into three main concepts: Demand Response, Energy Efficiency, and Energy Conservation.

In the case in hands, Demand Response (DR) is the clear way to perform DSM. A price-based approach will be carried out, where the microgrid operations costs will be minimized by developing a microgrid general control, working in two dimensions, the first is related to optimizing battery energy storage schedule, where the charge and discharge processes are controlled to allow an efficient battery usage, and the second is related with load scheduling, where flexible loads are shifted to off-peak hours to maximize the economical benefit of the microgrid, and to reduce the peak load demand. This procedure results in an optimization problem.

5.1 Problem formulation

The goal is to minimize the building energy costs by performing load scheduling, according to the electricity price and the renewable energy availability, and by performing intelligent battery charging/discharging control. Equation 5.1 presents the objective function.

$$Minimize\ f = Energy\ Bill = \sum_{t=1}^{T} \left(P_{t\ grid} \times 1\ [hour] \times c_t\right) + CP \qquad (5.1)$$

The energy bill represents the costs of buying energy from the grid plus the cost associated with the contracted power (CP) on a daily basis and can be calculated using equation 5.1. $P_{t\ grid}$ represents the average hourly power value that is being supplied by the grid for a certain hour t and c_t is the electricity hourly cost for that same hour. The costs of buying energy are calculated for each hour and then are added through a predefined period of time T, which represents the total amount of hours considered in the evaluation of the energy bill, in the case of a daily analysis T is equal to 24 hours.

The average hourly power value supplied by the grid is obtained from the balance between load and generation, represented in equation 5.2. $P_{t\ Load}$ represents the average hourly load power, $P_{t\ generation}$ the average hourly generation power and $P_{t\ battery}$ represents the average hourly battery power, being lower than 0 during the discharging process and greater than 0 during the charging process.

$$P_{t\,grid} = P_{t\,Load} - P_{t\,generation} + P_{t\,battery} \quad (5.2)$$

As previously stated, loads can be divided into two groups: fixed loads, whose consumption needs must be met at every instant and cannot be rescheduled, and flexible loads, that can be rescheduled and distributed during the day to better fit the generation curve and to minimize the energy bill. Thus, the average hourly flexible load power can vary from 0, indicating that the load is switched off during that hour, to the load nominal power, indicating that the load is switched on during the entire hour. To represent the switching state of each flexible load, an hourly decision variable, varying between 0 and 1, will be used. Equation 5.3 presents the different parameters of the average hourly load power, $P_{t\,Fixed}$ is the average hourly fixed loads power, $P_{Flexible\,i}$ is the flexible load i nominal power and $x_{t,i}$ is the hourly decision variable, indicating the state of the flexible load i during hour t.

$$P_{t\,Load} = P_{t\,Fixed} + P_{Flexible\,1}\,x_{t,1} + P_{Flexible\,2}\,x_{t,2} + \cdots + P_{Flexible\,n}\,x_{t,n} \quad (5.3)$$

In a similar way, the average hourly battery power resulting from charging/discharging the battery can vary from the maximum discharging power, P_{bat_Dchg}, to the maximum charging power, P_{bat_Chg}, equation 5.4. An hourly decision variable, varying from 0 to 1, will be used to characterize each one of the two processes during a certain hour t.

$$P_{t\,battery} = P_{bat\_Chg}x_{t,chg} - P_{bat_{Dchg}}x_{t,dchg} \quad (5.4)$$

The described system is governed by some restrictions, for instance, the battery cannot be charging and discharging at the same time, this means that the summation of the two battery charging/discharging process's decision variables at a certain hour t cannot be greater than 1, equation 5.5. Still related to the battery, it is important to clarify that the battery cannot charge to a value greater than its energy capacity, ${E_{battery}}^{Capacity}$, and cannot discharge to a value lower than the DOD, which is equal to a SOC of 15%, equation 5.6 and 5.7, respectively. The flexible loads need to meet the required daily energy consumption, meaning that they cannot consume more or less than the energy necessary to perform their daily task, equation 5.8.

$$x_{t,chrg} + x_{t,dchg} \leq 1 \quad (5.5)$$

$${E_{t-1}}^{Battery} + (P_{bat\_Chg}x_{t,chg} - P_{bat_{Dchg}}x_{t,dchg})1_{[hour]} \leq {E_{battery}}^{Capacity} \quad (5.6)$$

$$0.15{E_{battery}}^{Capacity} \leq {E_{t-1}}^{Battery} + (P_{bat\_Chg}x_{t,chg} - P_{bat\_Dchg}x_{t,dchg})1_{[hour]} \quad (5.7)$$

$$\sum_{t=1}^{T} P_{Flexible\,i}\,x_{t,i} = E_{T\,Flexible\,i} \quad (5.8)$$

5.2 Particle Swarm Optimization

PSO is a random search algorithm, proposed by Kennedy and Eberhart, that is based on animals' behavior, especially birds and fishes. These animals travel in groups and use the group information to adjust their own position and velocity, reducing individuals' effort in the search of food or shelter. Following that principle, this technique associates each animal of the group to a single solution which could be viewed as a particle in the swarm. Particles can update their position and velocity according to the environment change, not having their movement limited by the swarm, but instead, continuously searching for the optimal solution in the possible solution space.

In PSO the swarm is composed of a certain number of particles, N, in a D_{space}-dimensional search space, and each particle represents a single solution in that space, having the ability to memorize the optimal position of the swarm and its own. The position and velocity vectors in a D_{space}-dimensional space, of each particle n at iteration i, are presented in equation 5.9 and 5.10, respectively.

$$\vec{x}_i{}^n = \left(x_{i,1} + x_{i,2} + \cdots + x_{i,D}\right) \tag{5.9}$$

$$\vec{v}_i{}^n = \left(v_{i,1} + v_{i,2} + \cdots + v_{i,D}\right) \tag{5.10}$$

The process starts with both previously vectors generated randomly, respecting the limits of the D_{space} variables, for each one of the N particles. At each iteration, the particle's position is updated inside the search space to find a new solution. This update is carried out by implementing equation 5.11, which calculates the new particle's position based on the current position and on the particle's velocity. The particle velocity is also updated at each iteration, using equation 5.12, which is composed of three different components, $w_i{}^n \times \vec{v}_i{}^n$ corresponding to the inertia (or previous position) component, $c1_i{}^n \times r1_i{}^n \times \left(P_{Best}{}^n - \vec{x}_i{}^n\right)$ corresponding to the cognitive learning component, and $c2_i{}^n \times r2_i{}^n \times (P_{GlobalBest} - \vec{x}_i{}^n)$ corresponding to the global learning component. A visual representation of the updating process can be found in figure 5.1.

$$\vec{x}_{i+1}{}^n = \vec{x}_i{}^n + \vec{v}_{i+1}{}^n \tag{5.11}$$

$$\vec{v}_{i+1}{}^n = w_i{}^n \times \vec{v}_i{}^n + c1_i{}^n \times r1_i{}^n \times \left(P_{Best}{}^n - \vec{x}_i{}^n\right) + c2_i{}^n \times r2_i{}^n \times \left(P_{GlobalBest} - \vec{x}_i{}^n\right) \tag{5.12}$$

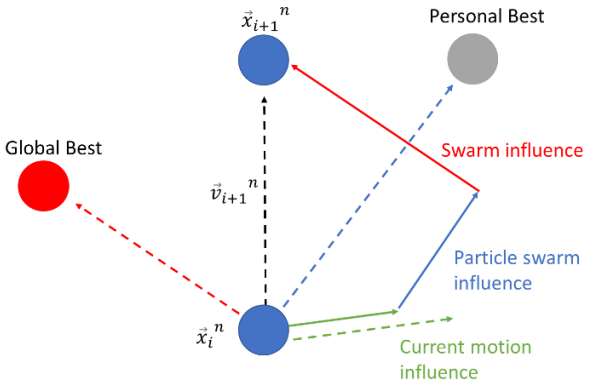

Figure 5.1 - Particle position update (adapted from [56]).

In the previous equation P_{Best} refers to the individual's optimal position, which is the position value already experienced by the particle that resulted in the best solution obtained for that same particle. $P_{GlobalBest}$ refers to the swarm's optimal position, which corresponds to the position experienced by any of the particles in the swarm that produced the best solution obtained for the entire swarm. w_i represents the inertia weight, calculated at each iteration, using equation 5.13, being the same for the whole set of particles during that iteration. As it can be seen in equation 5.13, the inertia weight decreases linearly during the search process, varying from a maximum value $w^{máx}$ to a minimum value w^{min}, this ensures strong global exploration properties in the initial phase and strong local exploitation in the final phase [57].

$$w_i{}^{n} = w^{máx} - \left(\frac{w^{máx} - w^{min}}{i^{máx}}\right) i \tag{5.13}$$

Still concerning equation 5.13, $c1_i{}^{n}$ and $c2_i{}^{n}$ are acceleration coefficients and $r1_i{}^{n}$ and $r2_i{}^{n}$ are two random numbers, varying from 0 to 1. The two acceleration coefficients can be determined using equation 5.14 and 5.15. The personal acceleration coefficient $c1_i{}^{n}$ decreases linearly during the search process, allowing a high exploration at the beginning of the process. The global acceleration coefficient $c2_i{}^{n}$, contrary to what was previously seen, increases linearly during the search process, allowing high exploitation at the end of the process. Thus, at the beginning of the search, the personal best will have a bigger impact on the definition of the new particle position than the global best, but these roles will be inverted as the process continues.

$$c1_i{}^{n} = c1^{máx} - \left(\frac{c1^{máx} - c1^{min}}{i^{máx}}\right) i \tag{5.14}$$

$$c2_i{}^{n} = c2^{min} + \left(\frac{c2^{máx} - c2^{min}}{i^{máx}}\right) i \tag{5.15}$$

To solve the problem in hands, each particle's position vector is composed of two types of decision variables: the first referring to the state of the flexible loads and the second referring to the battery charging/discharging process, both presented in the previous section. As these variables are hourly based, there will be a value for each hour comprised in the total period under analysis. Thus, the particle dimension will be equal to $2 \times T + L \times T$, where L is the total number of flexible loads and

T is the total period of time under analysis. The vector used for solving the presented optimization problem is:

$$\vec{x_i}^n = \left(x_{1,1} + \cdots + x_{T,1} + x_{1,2} \ldots + x_{T,L} + x_{1,chg} + \cdots + x_{T,chg} + x_{1,dchg} + \cdots + x_{T,dchg}\right) \quad (5.16)$$

For simplicity reasons this vector was converted into a matrix, where each column refers to the values of one decision variable, and each line refers to the decision variables' values in a certain hour, equation 5.17, having a dimension of $T \times (2 + L)$. The same approach was carried out to convert the velocity vector $\vec{v_i}^n$ into a matrix ${V_i}^n$, and a MATLAB program was developed to implement the previously describe PSO technique and solve the optimization problem presented in equation 5.1.

$${X_i}^n = \begin{bmatrix} x_{1,1} & \cdots & x_{1,dchg} \\ \vdots & \ddots & \vdots \\ x_{T,1} & \cdots & x_{T,dchg} \end{bmatrix} \quad (5.17)$$

The developed program starts by defining the number of decision variables and by setting the upper and lower bound of each variable, equal to 1 and 0, respectively. Then the number of particles is defined, and the swarm is created. The initial position of each particle is created by randomly generating numbers that fit the decision variables' bounds. Based on the generated positions, each particle is studied individually to evaluate if it respects the decision variables boundary constraints and problems constraints, presented in the previous section. In the case of not complying with those constraints, the needed corrections are performed. Then, for each particle, the optimal position is defined, and the swarm's optimal position is evaluated by comparing every particle's optimal position and selecting the one that presents the best result. After initializing the particle swarm by determining the initial position of each particle, the program starts the search cycle, updating consecutively each particle's position and velocity, respecting equations 5.11 to 5.12, and evaluating if the particle obeys the imposed restrictions, after each position update, preforming the needed corrections and updating the particles and swarm's optimal position.

As mentioned, there are two types of restrictions: boundary restrictions, and problem restrictions. The first type is concerned with the stipulated limits of the decision variables, every time that an iteration occurs a new solution will be generated, and it is necessary to evaluate if this solution respects the upper and lower bounds. If it does not, the boundary control strategy, presented in equation 5.18, is used to repair the invisible individuals, where ${X_i}^n{}_{lc}$ refers to the element in line l and column c of particle n in iteration i.

$${X_i}^n{}_{lc} = \begin{cases} máx({X_i}^n{}_{lc}, 1) \\ \min({X_i}^n{}_{lc}, 0) \end{cases} \quad (5.18)$$

The second type of restriction is concerned with the restrictions directly associated with the problem in hands, presented in the previous section. To implement these restrictions in the developed program, the penalty approach was used [58]. This technique converts the restrictions into possible penalty values that are added to the objective function, based on the number of constraints violated, creating a new function denominated as fitness function f'. Thus, if a particle does not obey the problem

restrictions, the problem solution obtained for that particle will be equal to the one coming from the objective function f plus a certain value for not complying with the requirements $penalty$, equation 5.19 and 5.20. The value of each penalty was chosen so that the fitness function for a particle that does not obey the problems restrictions, in the iteration understudy, results in a much higher value than the expected energy bill, meaning that the particle will not be considered when defining the swarm's optimal position in that iteration. The value of each penalty should be adapted for the case in hands. A flowchart of the described program can be found in figure 5.2.

$$f' = f + penalty \tag{5.19}$$

$$penalty = \begin{cases} 10 & if\ (5.5)\ and\ (5.6)\ is\ not\ met \\ 10 & if\ (5.7)\ is\ not\ met \\ 5\left|\sum_{t=1}^{T} P_{Flexible\ i}\, x_{t,i} - E_{T\ Flexible\ i}\right| & if\ (5.8)\ is\ not\ met \end{cases} \tag{5.20}$$

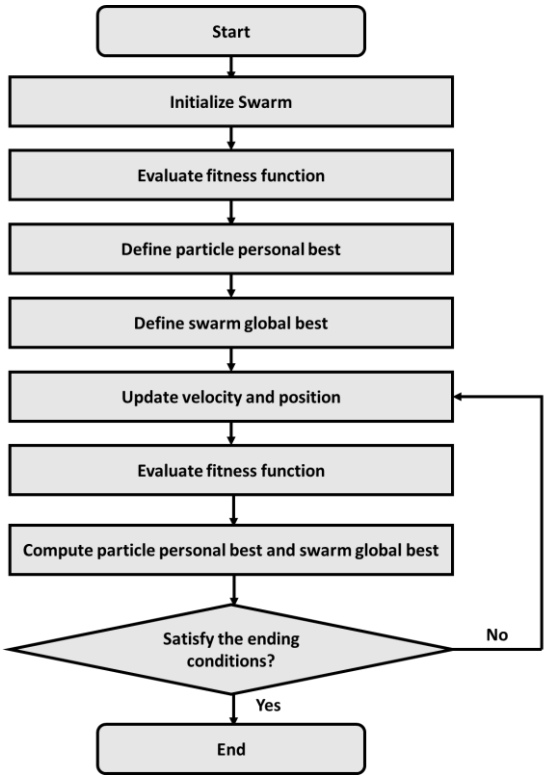

Figure 5.2 - Particle Swarm Optimization Algorithm.

6 Results and Discussion

Having modeled the entire microgrid, it is now important to evaluate the quality of the work produced. In this sense, each system was evaluated and validated separately, and then integrated into one system to produce the desired microgrid. Some parametric studies were also performed to evaluate the behavior of the microgrid.

6.1 Model Validation

6.1.1 Photovoltaic System Model

The three photovoltaic system models, developed in this thesis, were tested in two different operating scenarios. In the first one, a fictitious irradiance profile was used to evaluate if the three individual PV systems behaved as expected. In the second scenario, the integration of the three PV systems was carried out and was subjected to real irradiance profiles and the obtained results were compared to those of a commercial software. Starting with the first scenario, figure 6.1 a) shows the irradiance profile, developed by the author, used to test the MPPT and the DC-AC inverter performances at different irradiance conditions. This profile is composed of a set of constant irradiance values and the cell temperature was kept at 25 ^{o}C during the entire test, which corresponds to the temperature at STC. The time step used to perform this test was equal to $10^{-5}\ s$.

Figure 6.1 b) shows a comparison between the power generated by the model's PV Array (represented in blue) and the theoretical power that would be generated by a PV Array with the same rated power and at the same irradiance and temperature conditions as that of the model (represented in black). To calculate the theoretical value of the power generated by the PV array the Fast Estimate model, described in section 3.1.1, was used. As it can be seen, the two lines are overlapped during most part of the test, showing just a little deviation for an irradiance value of 1000 W/m^2, indicating that the power extracted from the PV array is close to the maximum available power and that the MPPT is performing as expected. In fact, in figure 6.1 c), it can be seen that the efficiency of the MPPT is close to unity during the entire test.

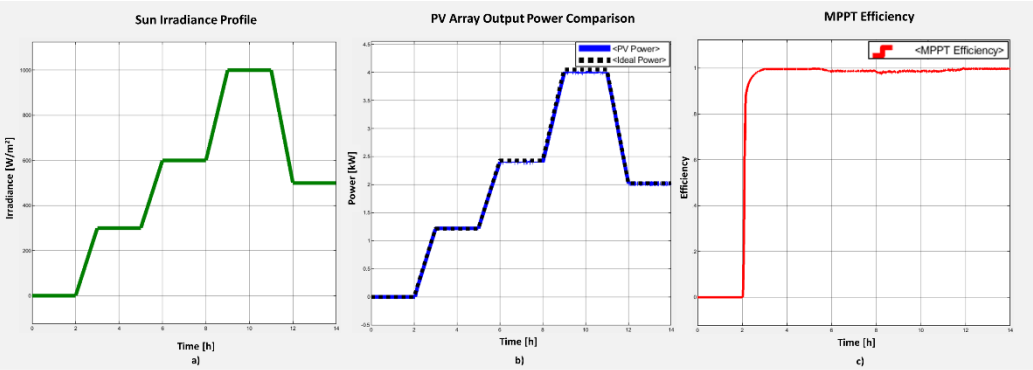

Figure 6.1 - PV system evaluation: (a) Sun irradiance profile, (b) PV array output power, (c) PV system MPPT efficiency.

Having tested the performance of the MPPT, it is now important to evaluate the performance of the DC-AC inverter. For that, the current, voltage, and power at the output of the inverter were studied. Figure 6.2 presents the voltage RMS value at the output of the inverter, as it can be seen, it has a constant value of almost 231V, which is 0.4% higher than the nominal voltage. This is a limitation of the inverter controller developed, yet a difference of 0.4% does not compromise the power quality of the system. In figure 6.2 b) the current RMS value can be found, contrary to what was seen in the output voltage behavior, this quantity varies according to the irradiance values. There is a mismatch between the RMS values of the three current phases, specialty for constant irradiance values. This limitation is introduced by two factors. The first is related to the fact that the filter is projected to work at the PV array rated power, showing better performance at irradiance values close to 1000 W/m^2 and worse for irradiance values much lower than the one referred. The second is related to the method used to perform the MPPT task since, despite being at steady state, the P&O method is constantly perturbing the system to find the maximum power point. This constant perturbation results in a power fluctuation, increasing the complexity of the inverter's controller task and producing this difference in the current RMS. Figure 6.2 c) shows the inverter output power, as it can be seen the active power behaves as expected, following the same pattern as the irradiance profile, and the reactive power is kept close to zero during the entire process. Once again, it is possible to observe the power fluctuation at steady state, resulting from the MPPT technique used.

The power factor at the output of the inverter can be found in table 6.1. By evaluating the data presented in figure 6.2 it is possible to conclude that the technique used to control the DC-AC inverter produces the desired results, yet there is a downside to it. The modeled inverter has an average conversion efficiency of 93%, which is slightly lower than that of a commercial inverter, around 97%. Although there is a 4% difference between the real and the modeled inverter efficiency, this setback can be overcome if the higher effect of losses in the inverter is offset by a lower value of losses in the cables, resulting in the same losses for the entire system.

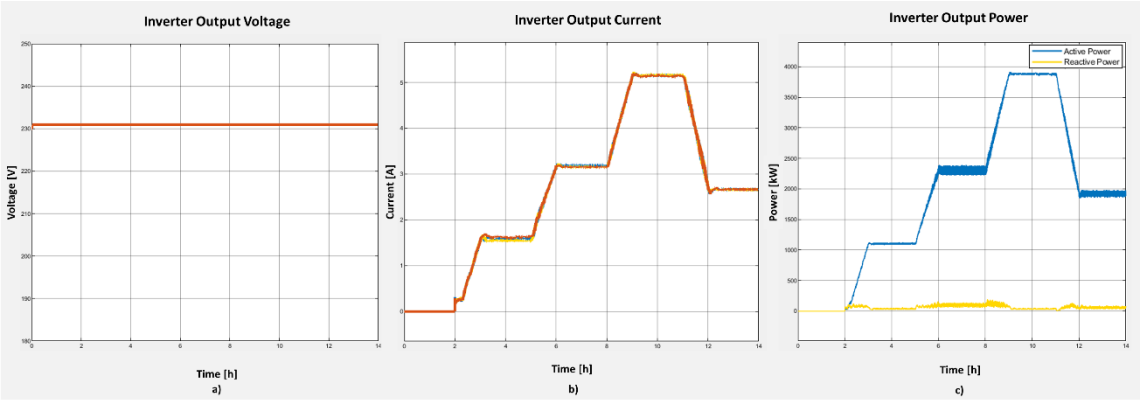

Figure 6.2 - PV system evaluation, inverter output: (a) voltage RMS value, (b) current RMS values, (c) Power.

With the objective of reducing the harmonics content to its maximum, three types of filters were tested during this experiment: an L filter, an LC filter, and an LCL filter. A conclusion was reached that the filter that produced the better results was one of the LCL type, in fact, this filter reduced the current total harmonic distribution (THD) by a value of 2% when compared with the other two types of filters. This conclusion corroborates the information found in the literature about filters. Since the LCL filter type was the one that produced the best results, it was the one chosen to integrate the PV system model, having the downside of slightly increasing the simulation time. In table 6.1 the values of current and voltage total harmonic distortion for the three systems at STC can be found. The inverter control technique implemented in this work resulted in a voltage signal without harmonic distortion, when analyzed in a computational perspective since this occurrence wouldn't be possible in physical implementation cases, and a current THD at STC equal to 2%, which is below the acceptable maximum value (5%) [59]. Although it already respects the quality standards, the value of the current THD could be reduced if a smaller time step is used, for example, for a time step of $5 * 10^{-6}\ s$ this value is equal to 1.6%. The downside of decreasing the time step is that the simulation time increases.

PV System	MPPT	Power Factor	Current THD	Voltage THD
4050 W system	99%	1	2%	0%
690 W system	97%	1	2%	0%
560 W system	96%	1	2%	0%

Table 6.1 - PV system characteristics

Having evaluated the performance of each one of the system's components, the three PV systems were integrated, as presented in figure 6.3, to form a single model. The performance of this new model was evaluated under real irradiance and temperature profiles and the results obtained during these procedures were compared to those obtained from an identical model developed in a commercial software, POLYSUN.

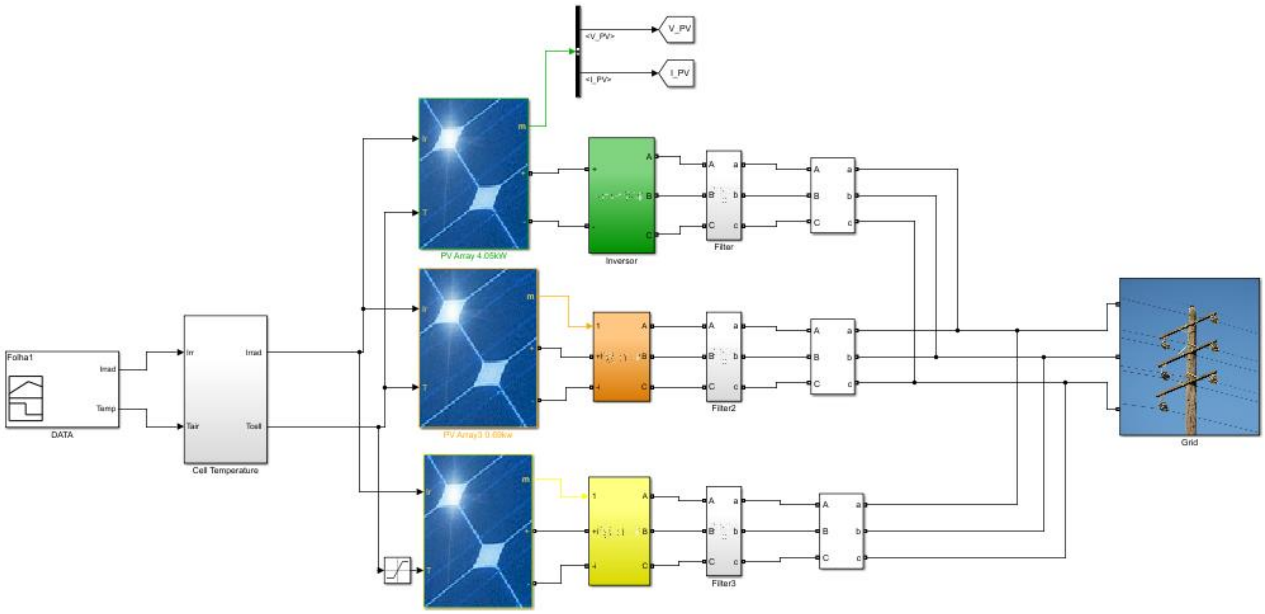

Figure 6.3 - Photovoltaic system integration.

To carry out the validation of the model, two different scenarios have been implemented. The first consists of a daily simulation, where a day at the beginning of January was chosen to represent the cold season, and the second in a weekly simulation, where a week in the middle of July was chosen to represent the hot season. Since POLYSUN only provides information about power generation, these were the quantities used to compare the two simulation tools. So, the power at the output of the PV array and at the output of the inverter was computed using the developed program and the commercial software, and the difference between them was calculated. The time step used, in the developed program, to perform both tests was equal to $10^{-5}\ s$.

In figure 6.4, the results of the first test can be seen. Figure 6.4 a) presents the power at the output of the PV array for the developed program (MATLAB) and for the commercial software (POLYSUN), and it can be seen that this value is slightly higher for the case of the developed program. Between the two sets of values, there is a mean absolute percentage error (MAPE) of 3.6%, indicating that the program developed in this thesis is producing good results. Since the same modules were used in both programs and the weather data was the same in both cases, this difference is related to the efficiency of the modules, being this efficiency higher for the developed program. From all the factors that influence the module's efficiency, there are two that can explain this difference between the simulation tools. The first is related to the difference in the calculation of the module cell temperature. Contrarily to the method chosen in this thesis, where the module cell temperature is calculated using equation 4.1, POLYSUN calculates this temperature using equation 6.1, where γ is a parameter that represents the rear ventilation.

$$T_{cell} = T_{amb} + \gamma \frac{G}{1000} \tag{6.1}$$

Despite using different methods to calculate the module cell temperature, the values obtained in both programs are very close, not varying more than 1.5°C, which according to the information in [55] can be responsible for a generation difference in the order of 0.75%. The second factor to consider is the MPPT efficiency, which might be lower for the case of POLYSUN, explaining why the PV Array output power is also lower in this case. As previously seen the developed program has an MPPT efficiency of 99%, but, unfortunately, the MPPT efficiency is not provided by POLYSUN, so it is not possible to calculate the percentage difference associated with this factor. Nonetheless, this study stands out one advantage of the developed program when compared with POLYSUN, since the last only provides data about power generation, and the first can provide this data plus a set of important parameters and characteristics of each one of the equipment used in the system.

In figure 6.4 b) a comparison between the power at the output of the inverter in the developed program and in POLYSUN can be seen. Contrary to what was seen in the previous figure, the output power is higher for POLYSUN, having a MAPE of 4.2%. This difference was already expected since, as it was discussed before, the conversion efficiency of the inverter modeled in the developed program is lower than that of a commercial inverter, resulting in a lower value of the output power.

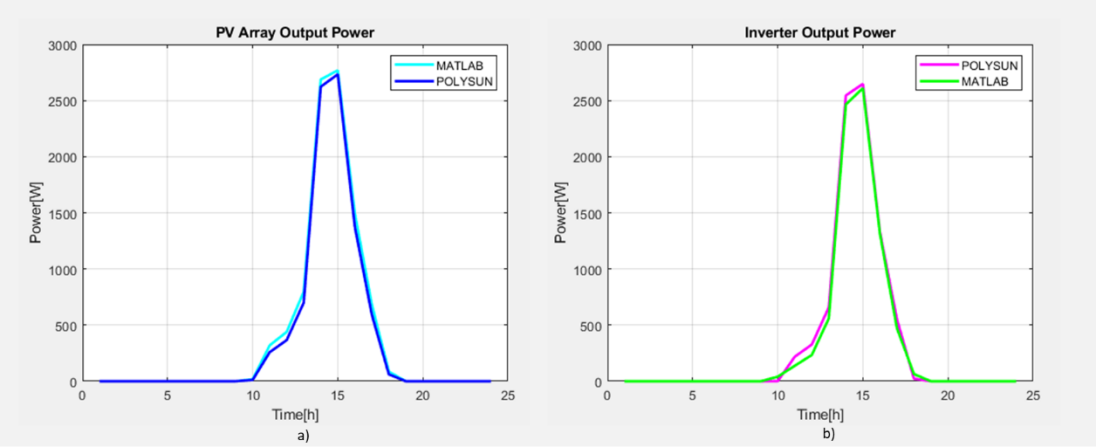

Figure 6.4 - Comparison between MATLAB-Simulink and POLYSUN for a daily simulation at (a) PV Array output (b) Inverter output.

In figure 6.5 the result for the weekly simulation can be found. As it can be seen, both the PV array and the inverter output power behave in a similar way as in the previous simulation. Figure 6.5 a) shows the comparison between the power at the output of the PV array for the developed model and for the commercial software, being this value higher for the first simulation tool. There is a MAPE between the two sets of values equal to 3.6%, indicating once again that the developed program produces good results. In figure 6.5 b) the information about the inverter output power can be found and, as it was seen for the case of the daily simulation, the output power is higher for POLYSUN, having a MAPE of 3.8%.

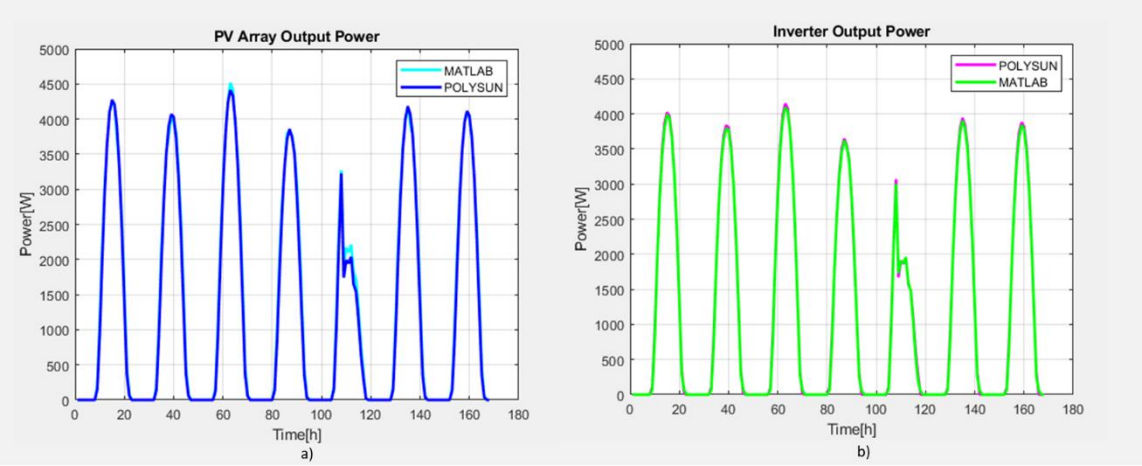

Figure 6.5 - Comparison between MATLAB-Simulink and POLYSUN for a weekly simulation at (a) PV Array output (b) Inverter output

6.1.2 Wind Power System

With the objective of evaluating the different components of the wind power system, the developed model was submitted to the wind profile presented in figure 6.6 a), where the wind speed varies linearly from 0 m/s to 30 m/s. Figure 6.6 b) represents the electric power at the output of the generation unit. As previously stated, this unit is responsible for calculating the generator output power based on the wind speed, by implementing the generator power curve. The chosen wind profile allows to study how well the developed system models the referred power curve, which is represented in figure 6.6 b). At first sight, it is possible to notice that the generated power is equal to zero for wind speeds lower than 3.5 m/s, the cut-in speed, and for a wind speed greater than 25 m/s, the cut-off speed, which proves that the developed model respects the speed limitations of the real equipment. It is possible to notice that for a wind speed of 3.5 m/s the transition from not generating power to starting to generate it, is not a smooth one, which is related to the equation used to mathematically model the power curve. Although equation 4.2 is the best equation found to model the power curve obtained from real data, it has a zero at the imaginary number with a modulus of 3.47, instead of having a zero at 3.5, originating the small discontinuity detected in figure 6.6 b). In this figure, it is also possible to notice that, contrary to what is verified in medium and large size wind turbines, the power generated by the generation unit does remain constant after the rated wind speed is reached. This

characteristic is related to the fact that for the wind turbine in hands the blade pitch control is not being applied, which, as seen in section 3.3.1, is responsible for varying the wind turbine power coefficient, allowing the generation unit to generate the same amount of power for different wind speeds. So, instead of having a constant value after the rated speed is reach, for the case in hands, there is an inflection point around this wind speed value and the power generation increases until it reaches a value of 3638 W at a wind speed equal to 18.2 m/s.

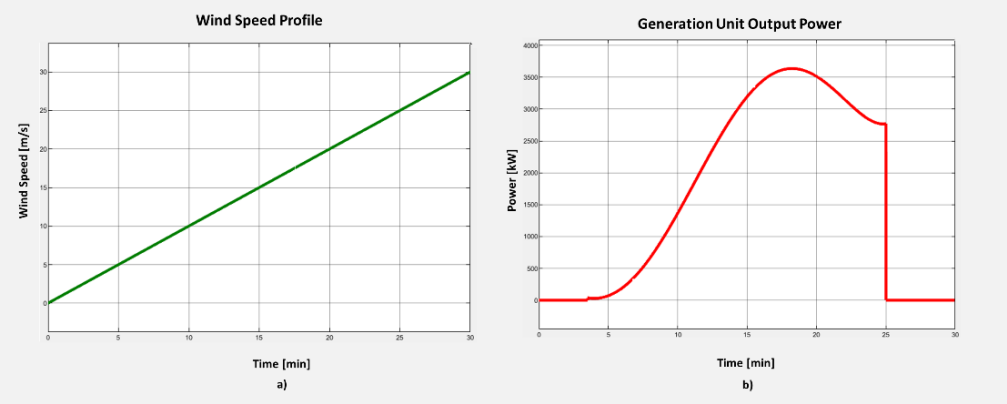

Figure 6.6 - Wind power system evaluation: (a) Wind speed profile, (b) Power curve at the output of the generation unit.

With the evaluation of the generation unit, the following objective is to study the performance of the power control unit. Figure 6.7 presents the voltage, current, and power at the output of the power conversion unit, more precisely, at the output of the inverter. As seen for the case of the PV system, the voltage RMS value is equal to 231 V, slightly above the nominal voltage, figure 6.7 a). This was already expected since the difference is a consequence of the inverter control technique, which is the same for both the PV and wind power systems. It is important to notice that the voltage THD is equal to 0%, as it was in the case of the PV system. The current RMS value, presented in figure 6.7 b), varies according to the power curve, showing a smaller mismatch between the RMS values of the three current phases than in figure 6.2 b) since, as discussed, this mismatch was originated by the PV system's MPPT technique, and in the case of the wind power system, this technique is not applied. In figure 6.7 c) the power at the output of the inverter can be found, the active power follows the power curve profile as expected and the reactive power is kept close to zero. The inverter has an efficiency of 98% and an output power coefficient equal to 1.

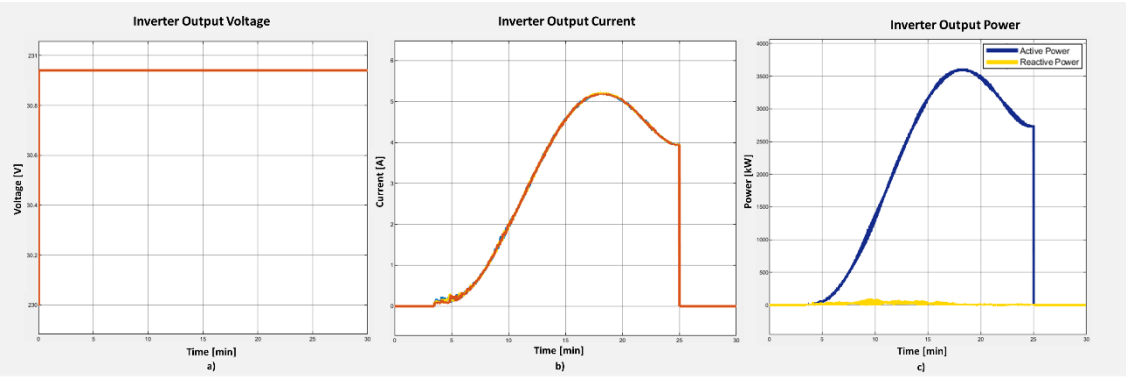

Figure 6.7 - Wind power system evaluation, inverter output (a) voltage RMS value, (b) current RMS values, (c) Power.

A closer look was given to the study of the current THD. It was noticed that if the inverter controller and the filter parameters were calculated based on the system rated power, the current THD would be low for wind speeds that generate a power value close to the nominal power, but would be very high, surpassing the acceptable limit, for wind speeds that generate a power value lower than the rated one. Since the local measured wind speed in LNEG 's Pilot is much lower than the rated speed, to guarantee power quality it is necessary to design the inverter controller and the LCL filter parameters to the most frequent wind speed instead of being projected to the rated wind speed. This new approach, although it has the downside of having a lower inverter performance when the wind speed is greater than 12 m/s, allows to lower the THD for the most common wind speed values measured at LENG.

In figure 6.8 b) a comparison between the current THD for two different PCUs can be found. In dark blue, the values refer to the unit projected based on the value of the rated power, and in light blue, the values refer to the unit projected to the power value generated by the most common wind speed, 250 W. In figure 6.8 a) the wind profile used to conduct this test can be found. By performing this evaluation, it is possible to conclude that contrarily to what is verified in the PV system, where the PCU unit is projected to the rated power, for the wind power system the PCU should be projected to the most frequent wind speed in order to guarantee power quality at every instant.

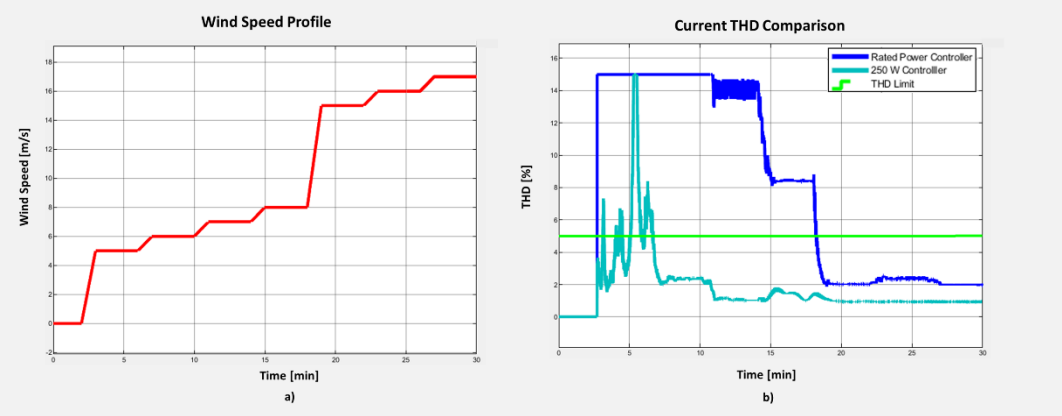

Figure 6.8 - PCU evaluation: (a) Wind Speed Profile, (b) System output current THD.

6.1.3 Energy Storage System

With the objective of evaluating the modeled energy storage system, a comparison between the developed system and one from a commercial software was carried out. Two different scenarios have been studied, first a daily simulation was performed, followed by a weekly simulation. The days used to conduct these tests were the same as the ones used in section 6.1.1 and the commercial software used was once again POLYSUN. The same load profile was used for both MATLAB and POLYSUN, as well as the same battery model, which is different from the one implemented in LNEG Microgrid since POLYSUN does not have that model available in its database. The characteristics of the battery used during this test can be found in table 6.2.

Battery Characteristics	SES-AC25
Battery Technology	Li-ion
Nominal Capacity [W]	3400
Maximum Charging Power [W]	3400
Maximum Discharging Power [W]	4080
Charging and Discharging efficiency	0.93

Table 6.2 - Battery Characteristics.

In figure 6.9 a comparison between the battery state of charge (SOC) resulting from both simulation tools can be found. It can be seen that for both simulation conditions the two sets of values behave in a similar way. This indicates not only that the amount of energy being stored in the battery for both programs is the same, but also that the battery charging and discharging processes occur at the same instant and at the same rate for both MATLAB and POLYSUN. For the daily simulation, represented in figure 6.9 a), there is a 1% MAPE between the two sets of values, and for the weekly simulation, represented in figure 6.9 b), this error is equal to 1.2%. It is important to notice that for both cases the initial state of charge was equal to 100%, and for the weekly simulation, the battery SOC remains the same during the first 48 hours, because this period corresponds to the two weekend days, where there is no consumption.

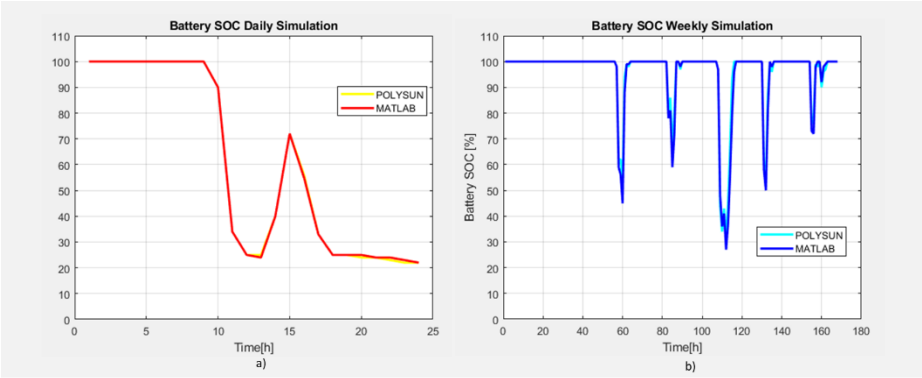

Figure 6.9 - Comparison between MATLAB-Simulink and POLYSUN battery SOC for (a) a daily simulation, (b) a weekly simulation.

6.1.4 Demand Side Management

The developed DMS program is able to perform load scheduling and battery control in order to reduce the energy consumption bill. To evaluate the optimization program a day ahead study of the daily energy bill was performed for three different situations, a day in the month of January, a day in the month of July, and a day in the month of September. To conduct this study the consumption pattern of the fixed loads was extracted from an office consumption profile, present in POLYSUN data-based, and three loads of 1 kW nominal power each were considered as the controllable loads. These three loads consume a total energy of 3 kWh/day each. It was also considered that the consumer has an energy supply tariff scheme characterized by three different periods: peak, intermediate and off-peak.

The energy prices and the hours of the day (for a winter weekday) applied for each one of these periods can be found in table 6.3, the presented values were obtained by consulting the website of the Portuguese retailer NOSSA Energia [60].

Contracted Power	**Energy Price [€/kWh]**		
17.5 kVA	Peak	Intermediate	Off-peak
0.88153 [€/day]	0.2879	0.1581	0.0999
Period	9:30 – 12:00 18:30 – 21:00	7:00 – 9:30 12 :00 – 18:30 21:00 - 24:00	24:00 – 7:00

Table 6.3 – Energy supply tariff scheme characteristics.

In table 6.4, the value of the parameters used to perform the PSO can be found. As stated in chapter 5, the time period under analysis, in this case a day, will be divided into slots of 1 hour. In each one of those slots there is one decision variable for each controllable load, indicating the state of the load, one variable referent to the battery charging process and one variable referent to the battery discharging process, resulting in a total of 120 decision variables. It was assumed that the three controllable loads are only active when the office is occupied, meaning that during the nighttime, from 8 PM to 8 AM, their energy consumption is equal to zero, reducing the number of decision variables to 84.

Particle Swarm Optimization								
Parameter	Population size	Number of iterations	$w^{máx}$	w^{min}	$c1^{máx}$	$c1^{min}$	$c2^{máx}$	$c2^{min}$
Value	100	1000	1	0.1	1.5	0.15	2	0.2

Table 6.4 - PSO parameters.

The results of the study can be found in table 6.5. The table is composed of three main columns, the first referring to battery optimization, meaning that the PSO was applied with the objective of only performing battery control, the second referring to load optimization with the objective of performing only load scheduling, and the third referring the to battery and load optimization, meaning that the PSO was applied with the objective of performing battery control and load scheduling simultaneously. Each of these three columns is then divided into three, referring to the three tests performed to the days in January (Jan), July (Jul), and September (Sep). As it can be seen, the optimization process is able to lower the daily energy bill for each one of the optimization techniques used, having a maximum standard deviation between runs, for each case, of 11 cents. Performing simultaneously battery control and load scheduling stands out as the best option to further decrease the daily costs, for the three days considered. Only performing battery control produces better results than only performing load scheduling, but this fact does not necessarily apply to every situation, if the number of loads or the nominal power of each current load was increased, the importance of load scheduling in the total process would also increase, and performing load scheduling would produce better results than only performing battery control. By performing this test, it is possible to conclude that associating DSM to

the microgrid can really help in defining the operating conditions that allow the microgrid to be used in the most efficient way.

	Battery Control			Load Scheduling			Battery Control + Load Scheduling		
	JAN	**JUL**	**SET**	**JAN**	**JUL**	**SET**	**JAN**	**JUL**	**SET**
Number of Runs	10	10	10	10	10	10	10	10	10
Original Price Value [€/day]	3.14	2.30	2.16	3.14	2.30	2.16	3.14	2.30	2.16
Optimization Average Price Value [€/day]	2.68	2.00	1.69	2.88	2.06	2.08	2.58	1.39	1.50
Standard Deviation	0.03	0.06	0.03	0.10	0.11	0.11	0.10	0.10	0.11

Table 6.5 - Results of the optimization process.

In figure 6.10 it is possible to observe a comparison between the load scheduling, figure a), and the output power of the battery, figure b), before and after the optimization process. It can be seen that the controllable loads are shifted from periods of peak power demand charges, mainly from 11 to 12 AM, to periods of intermediate peak, lowering the maximum power demand and flatten the power curve. In figure 6.10 b), the biggest difference between the battery behavior before and after the battery control is applied is that after the optimization process the battery charges during the nighttime, when the energy price is at its lowest, until a SOC of 100% is reached, blue line, instead of remaining with a SOC equal to 25%, green line. In this figure, a positive battery output power represents the charging process. Charging the battery during the night enables it to be fully charged for the period when the building demand is at its highest, between 11 and 12 AM, which also overlaps with the peak energy tariff charges, meaning that by charging the battery during the night, when energy is bought at a lower price, will enable to use this energy in a period where the energy is sold at a higher price, resulting in immediate savings. As a remark, it is important to recall that methods like the PSO do not provide the exact optimal solution to the optimization problem, giving rather good solutions for problems with a high number of decision variables.

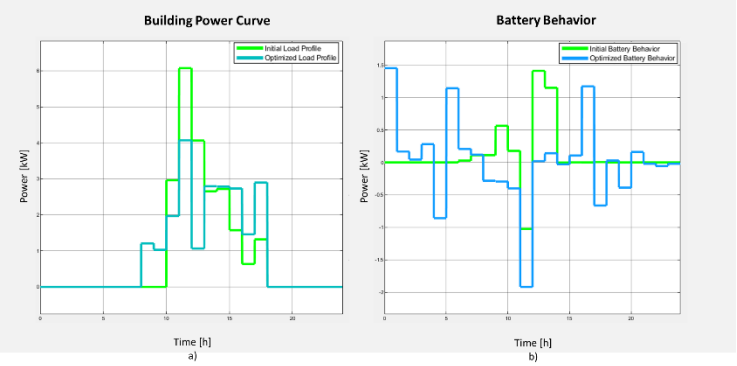

Figure 6.10 - Optimization process: (a) Power curve after load scheduling, (b) Output battery power after battery control.

6.2 Microgrid

With the objective of studying the behavior of the microgrid, an annual simulation was carried out. The weather data used to perform this test is presented in figure 6.11 and was obtained using Meteonorm, being Lisbon the chosen location for the system. The irradiance values refer to a surface with a tilt angle of 30^o.

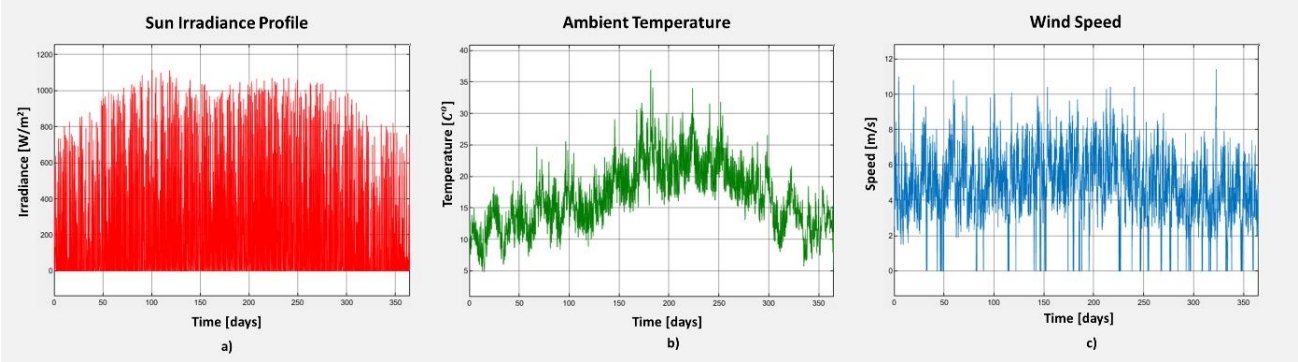

Figure 6.11 - Weather data: (a) Irradiance Profile, (b) Ambient Temperature, (c) Wind Speed Profile.

In figure 6.12 the consumption data used in this simulation can be found. This data was provided by LNEG and, although it is not the exact measured consumption, it is a realistic approximation of the pilot real consumption. In figure 6.12 a) a typical daily consumption profile is represented, as it can be seen, it is assumed that the pilot demands constant power for periods of 15 minutes. The daily demand pattern can be divided into two moments, the first referring to the period between 6:30 AM and 8:10 PM, characterized by being the working hours of the day, presenting a higher consumption than the one observed in the second moment, referring to the period between and 8:10 PM and 6:30 AM. Although the second period represents the nighttime, there is a constant power demand of 3 kW, which indicates that in the pilot there are equipment that operate all day long. In fact, this constant power demand is observed during the entire year, figure 6.12 b), indicating that the pilot has equipment with a based nominal power between 2.2 and 3 kW working all year long.

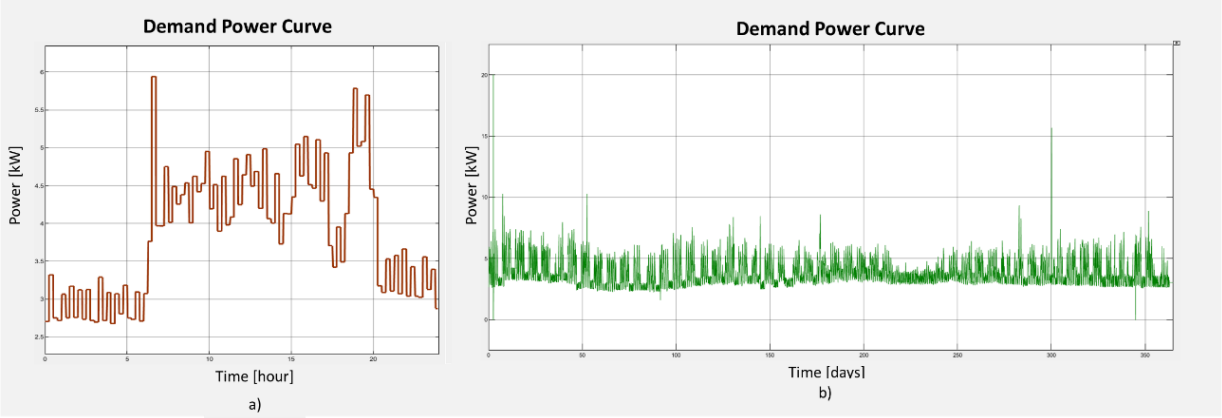

Figure 6.12 - Consumption power curve: (a) in a daily basis, (b) in a yearly basis.

To run the presented simulation a time step of $5 \times 10^{-5} s$ was chosen. In figure 6.13 the results referring to the energy generation on a monthly basis can be found. As it can be seen, the PV system's energy generation follows the irradiance pattern, producing high quantities of energy in the month of March, where the highest irradiance values of the year are reached, and in the summer months where the irradiance also reaches high values. Although the higher irradiance values are measured in March, the energy generation in the summer months is bigger because in this period the density of days with high irradiance values is higher than in the month of March. The energy generated by the wind power system also follows the wind speed pattern, not varying much during the year, having just a slight decrease in energy generation in the winter months. It is also important to notice that the energy generated by the three PV systems is much bigger than the one generated by the wind power system, producing between three to four times more in the cold season months (November to February) and between four to six times more in the hot season months (March to October). This mismatch between generation units is not only due to the difference in the installed rated power, 5.3 kW for the PV systems and 2.5 kW for the wind power system, but mainly due to the fact that the windspeed hardly ever reaches the wind power system rated speed, meaning that this system is always generating energy below its capacity. In fact, the PV systems have a utilization of peak power, calculated using equation 6.2, of 1439 hours and the wind power system has a utilization of peak power of only 695 hours. The utilization of peak power of the entire generation system is equal to 1161 hours.

$$h_a = \frac{E_{annual}}{P_{rated}} \tag{6.2}$$

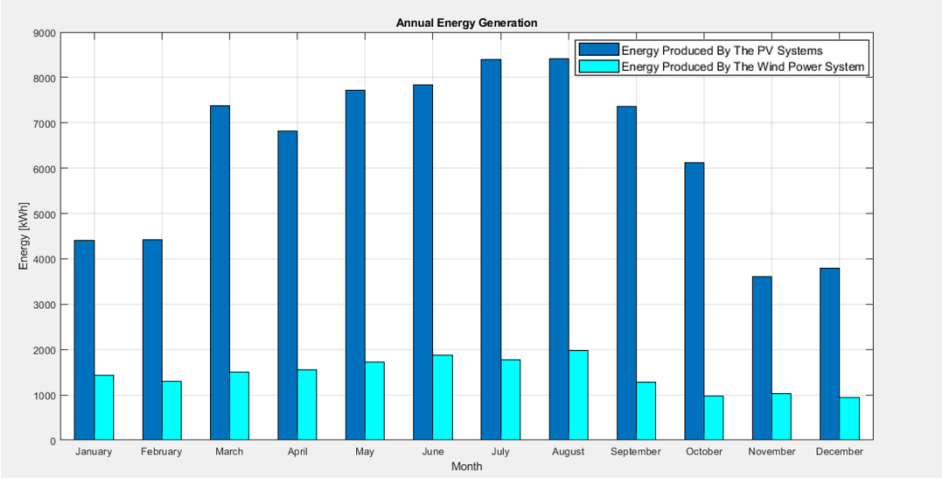

Figure 6.13 - Microgrid annual energy generation.

Using the weather and the consumption data previously discussed, it is possible to study the behavior of the microgrid throughout one year. Figure 6.14 presents the energy generation, represented in blue, the energy consumption, represented in red, and the energy extracted from the grid, represented in yellow, on a monthly basis during the period of one year. As it can be seen, the consumption surpasses the energy generation in every month. In fact, the energy generated during a year by the microgrid (9063 kWh) only accounts for 28% of the total energy consumed in the building (32228.3 kWh), the missing 72% are extracted from the grid (23165.3 kWh). This mismatch between consumption and generation was already expected, since the system nominal generation power is equal to 7.79 kW with

a utilization factor of 1163 hours and, as it was seen in figure 6.12, the building has a constant power demand between 2.2 to 3 kW during the entire year (8760 hours), this means that solely the equipment that are working all year long consume more energy than what is generated by the generation systems. Having reached the conclusion that, the microgrid does not produce enough energy to satisfy the demand, It would now be interesting to study how the energy generation and the energy extracted from the grid would vary with an increase in the nominal generation power.

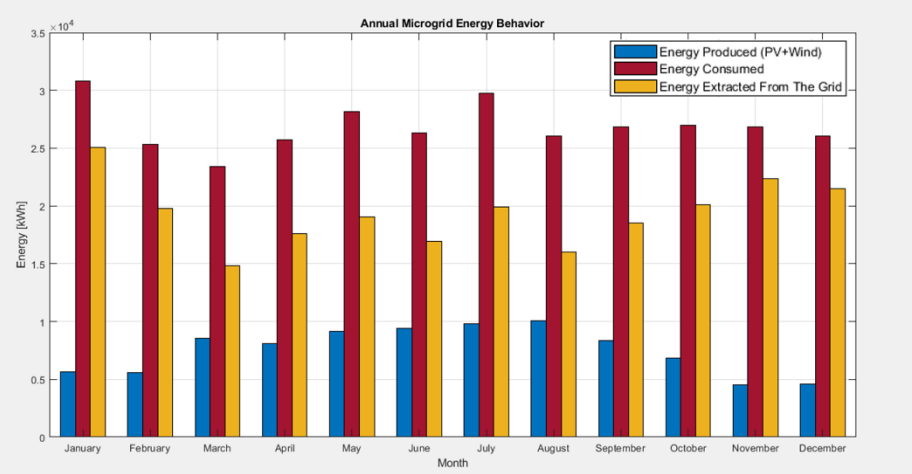

Figure 6.14 - Microgrid annual energy generation, energy consumption and energy extracted from the grid.

With the objective of reducing the energy extracted from the grid while maintaining the consumption pattern, the installed nominal generation power was increased. Since the PV systems were the ones with a higher utilization factor, it would be more productive to maintain the wind power system nominal power as it is and increase the PV systems nominal power. Figure 6.15 represents the variation in energy generation and energy extracted from the grid when the PV systems installed power is increased. As it can be seen, by increasing the installed power, the energy generation, represented in blue, increases in a linear way, and the energy extracted from the grid, represented in yellow, decreases towards a horizontal asymptote. It can be seen that the energy generation surpasses the energy extracted from the grid for an installed power 2.2 times bigger than the real system PV rated power, from that point on, the energy injected in the grid also increases in a linear way. For an installed power of 4.2 times the real system PV rated power and for an installed power of 4.6 times the real system PV rated power, the energy extracted from the grid remains almost the same, indicating that there is no more advantage in keeping increasing the PV system installed power, meaning that the limit in the total amount of power that can be installed was reached.

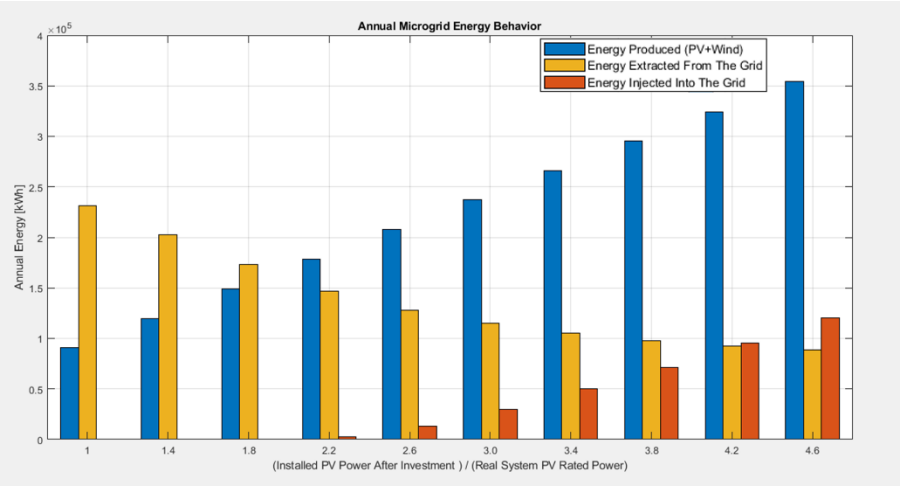

Figure 6.15 - Microgrid energy generation and energy extracted from the grid for different installed PV rated power.

Looking in more detail at the energy injected in the grid, it is possible to see that this quantity starts to have a bigger impact for an installed power of 3.4 times the real system PV rated power, surpassing the energy extracted from the grid for and installed power 4.2 times the real system PV rated power (meaning that the pilot building has reached the conditions of a nZEB). As this energy is being generated by the generation units of the microgrid but is not being used to fulfill the energy demand, it can be seen as an energy loss, and like any other loss, it would be interesting to minimize its value and convert it into useful energy, minimizing also the amount of energy extracted from the grid. This goal can be accomplished by increasing the battery energy capacity, which would allow storing more energy in periods where the energy generation surpasses the energy demand, decreasing the energy injected into the grid, and to supply more energy in periods where the energy demand surpasses the generation, decreasing the energy extracted from the grid.

In figure 6.16 the evolution of the energy extracted from the grid with the increase of the energy capacity for different configurations of the PV system rated power can be seen. As expected, the amount of energy extracted decreases with the increase of the battery capacity. For a fixed value of the PV system rated power, for example, an installed power 4.6 times greater than the one currently installed in LNEG's pilot, it is possible to notice that the energy extracted from the grid decreases towards a horizontal asymptote, meaning that there is no advantage in keeping increasing the battery capacity further than a certain value, being this limit equal to 1.8 times the installed battery capacity. By performing this study, it is possible to conclude that increasing the PV system installed rated power, associated with an increase in the battery energy capacity will have a positive impact in decreasing the amount of energy extracted from the grid. Taking as an example, the option of increasing the PV system nominal power to a value 4.6 times bigger (24.38 kW) than the rated power of the system implemented in the pilot (5.30 kW), and increasing the battery capacity 1.8 times (57 024Wh) than the current battery energy capacity (31 680Wh) the percentage of energy generated by the microgrid generation units would account for 86% of the total energy consumption, instead of the initial 28%, and the energy extracted from the grid would decrease from 23165.3 kWh to 4669.5 kWh.

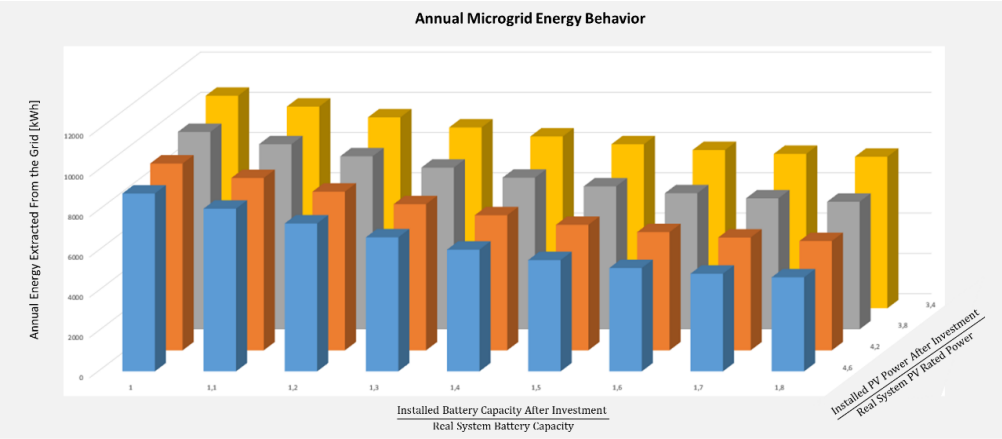

Figure 6.16 - Microgrid energy extracted from the grid for different battery energy capacities.

As a final remark, the simple payback period of the investment related to increasing the installed PV rated power and the battery energy capacity will be calculated, equation 6.3. To do so, two parameters need to be computed: the first is the investment cost, which is the upfront cost related to installing the necessary equipment, and the second is the value of the annual savings, resulting from the decrease in the energy extracted from the grid.

$$Payback = \frac{Investment}{Annual\ Savings} \tag{6.3}$$

The investment is divided into three categories, the cost of buying PV modules, the cost of buying DC-AC inverters, and the cost of buying battery cells. It was assumed that if the investment were carried out, the equipment bough would be the same as the one which is already installed in LNEG's pilot. In [61] the LDK 225P-20 modules are sold for a price of 0.56€ /Wp, the SMA Sunny Boy inverter is priced at a maximum value of 0.42€ /W [62], and a battery Sunlight RES OPzS 660Ah 2 V cell costs 227.30€ at [63], which represents a cost of 0.172€ /Wh. So, to calculate the total value of the investment, equation 6.4 can be used, where I_{nv} represents the investment, P the total PV rated power in W to be installed, and EC represents the increase in the battery energy capacity calculated in Wh.

$$I_{nv} = P \times (0.56 + 0.42) + EC \times 0.172 \tag{6.4}$$

To calculate the annual savings the yearly energy costs before and after the investment were computed. It was assumed that the annual consumption remains the same thought out the years. Thus, the annual savings can be calculated by applying equation 6.5, where S represents the savings.

$$S = \Delta Cost \tag{6.5}$$

To determine the energy tariff used to calculate the energy bill two scenarios were considered: the first corresponds to the energy bill with current installed conditions and the second corresponds to the energy bill after increasing the PV system nominal power to a value 4.6 times bigger than the rated power of the system implemented in the pilot. For each of these scenarios, the yearly energy bill was calculated using three different tariffs, a one period (simple tariff), a two different periods tariff (dual-tariff), and a three different periods tariff (triple-tariff), the three tariffs can be found in the website of

the portuguese retailer NOSSA Energia [60]. The results of the study are presented in table 6.6, since the difference between the results obtained with the simple tariff and the other two tariffs, especially the triple-tariff which is the one that results in a lower energy bill, is not significant, for simplicity reasons a simple tariff of 0.146 €/kWh was chosen to proceed with the payback period evaluation. The energy bill is directly calculated by the program that receives the energy tariff as an input, being this one of the advantages when comparing the developed program with POLYSUN.

	Simple Tariff	Dual-Tariff	Triple-tariff
Current Conditions	3766	3827	3745
After Investment	1060	1066	1039

Table 6.6 - Energy bill for different electricity tariffs.

In table 6.7, the payback period for the different installation conditions can be found. At a first glance, it can be seen that this quantity ranges from 5.16 years to 9.48 years, depending on the configuration chosen. As a remark, the payback period for battery capacities bigger than the one currently installed in LNEG's pilot was not computed for an installed PV power lower than 2.6 times the real PV system rated power because, as it was seen in figure 6.15, for those installation conditions the energy injected into the grid is negligible so there wouldn't be any advantage in increasing the battery capacity. Looking first at the evolution of the payback period with the increase of the installed PV system power, maintaining the battery with the same capacity as the one currently installed in the microgrid, the first column, it is possible to see that the payback period increases from a minimum of 5.15 years, for an installation 1.4 times bigger than the real PV system rated power, and this value remains under 5.5 years until an installation power equal to 2.6 times the actual installed rated power is reached. From that point on the payback period increases linearly with the increase of the PV system installed power, reaching a maximum value of 9.5 years for an installed power 4.6 times bigger than the one currently installed in the microgrid. Now looking at the evolution of the payback period caused by the increase in the battery capacity for a fixed PV installed Power, it is possible to see that, for a fixed installed PV power bigger than 3 times the real PV system rated power, the payback period has a minimum for an installed battery capacity between 1.2 to 1.5 times greater than the one currently installed in LNEG's microgrid, meaning that, at first sight, increasing the battery capacity is a good investment opportunity.

	Investment Payback Period [years]									
	Installed Battery Capacity After Investment to Real System Battery Capacity									
Installed PV Power After Investment to Real PV System Rated Power		1.0	1.1	1.2	1.3	1.4	1.5	1.6	1.7	1.8
	1.4	5.16	-	-	-	-	-	-	-	-
	1.8	5.17	-	-	-	-	-	-	-	-
	2.2	5.34	-	-	-	-	-	-	-	-
	2.6	5.82	6.30	6.16	6.37	6.62	6.89	7.18	7.47	7.78
	3.0	6.49	6.81	6.61	6.68	6.80	6.94	7.11	7.32	7.54
	3.4	7.19	7.43	7.17	7.18	7.21	7.28	7.38	7.53	7.70
	3.8	7.91	8.08	7.77	7.72	7.72	7.74	7.81	7.91	8.06
	4.2	8.70	8.76	8.39	8.30	8.25	8.24	8.28	8.37	8.49
	4.6	9.48	9.48	9.06	8.91	8.81	8.76	8.78	8.85	8.96

Table 6.7 - Investment Payback Period,

One thing that was not considered in the previous calculation of the payback period, the equipment limitations. To calculate the investment, it was assumed that each equipment needed to be bought only one time, but if the lifetime of the equipment is lower than the payback period this is not the case, because the equipment would need maintenance or to be replaced during the initial calculated payback period, which would increase the investment and consequently increase the payback period. A PV module has a service life of at least 20 years and the inverter has a service life of up to 15 years, since the maximum payback period is inferior to 15 years, there won't be any additional costs concerning the PV system than the initial investment. In the case of the battery cell, according to the information presented in [63], it has an expected number of cycles for a DoD of 50% equal to 2800 and equal to 2300 for a DoD of 60%. In the developed program the maximum battery DoD is equal to 85% but the average DoD, determined after running the yearly simulation, is slightly lower than 60%, and since the battery is operating during the entire year, going through a cycle a day, it is possible to consider that the battery cells have an expected service life of 6.30 years, meaning that, for installations with a payback period superior to the battery service life, the costs of buying a second unit should be considered as an investment. Table 6.8 presents the payback periods for the different installation configurations after the service life of the equipment have been considered. This time the payback period has a minimum equal 5.16 years, for an installed power equal to 1.4 times the real PV system rated power, that allows an annual energy savings of 427.56€ with an investment of 2201€, and has a maximum of 10.58 years, that allows an annual energy savings of 2700.43€ with an investment of 28562€. The main difference between table 6.8 and table 6.7 is that after considering the equipment life service, the payback period for each fixed installed PV power does not decrease if the battery installed capacity is bigger than the one currently installed in LNEG's microgrid.

		Investment Payback Period [years]								
		Installed Battery Capacity After Investment to Real System Battery Capacity								
		1.0	1.1	1.2	1.3	1.4	1.5	1.6	1.7	1.8
Installed PV Power After Investment to Real PV System Rated Power	1.4	5.16	-	-	-	-	-	-	-	-
	1.8	5.17	-	-	-	-	-	-	-	-
	2.2	5.34	-	-	-	-	-	-	-	-
	2.6	5.82	6.96	6.84	7.37	7.93	8.52	9.12	9.73	10.35
	3.0	6.49	7.40	6.47	7.54	7.92	8.31	8.74	9.20	9.68
	3.4	7.19	7.98	7.71	7.97	8.23	8.52	8.85	9.22	9.61
	3.8	7.91	8.59	8.28	8.46	8.67	8.90	9.17	9.48	9.83
	4.2	8.70	9.25	8.88	9.00	9.16	9.34	9.57	9.85	10.18
	4.6	9.48	9.95	9.54	9.59	9.68	9.82	10.02	10.27	10.58

Table 6.8 - Investment Payback Period after considering the service life of the equipment.

To complement this financial analysis, the Net Present Value (NPV) of each one of the investments options was calculated to determine the best economical option. In equation 6.6 I_{nv_0} represents the initial investment, Cf_j the savings in year j, T the period under analysis and i the discount rate.

$$NPV = -I_{nv_0} + \sum_{j=1}^{T} \frac{Cf_j}{(1+i)^j} \tag{6.6}$$

The NPV was calculated for a period of 15 years, the lifetime of the PV system, and with a discount rate equal to 0.95, representing a risk-free rate [64]. It was assumed that the battery cells were replaced after 5 years of utilization, meaning that for the cash flows of years 5 and 10 the cost of replacing the battery was subtracted from the yearly energy savings. In table 6.9 the results of this economical assessment can be found. The NPV ranges from 2.29k€ to 12.60k€, for an installation power 3 times bigger than the real PV system rated power, and it is possible to see that increasing the battery capacity has no economic advantage. By performing these analyses, it is possible to conclude that there is a good investment possibility in redesigning the technologies capacities installed in the microgrid under study, and that there are two paths that can be flowed. If the objective is to enhance the economical performance of the microgrid, the installed PV system show be increased to a value 3 times the current installed condition, since this is the configuration that results in the highest NPV. If the objective is to lower the amount of energy extracted from the grid and increase the percentage of energy demand satisfied by renewable energy generated in the microgrid, enhancing the environmental performance of the microgrid, the installed PV system should be increased to a value 4.6 times the current installed condition and the battery capacity should also be increased to a value 1.8 times the current installed capacity.

		Net Present Value [k€]								
		Installed Battery Capacity After Investment to Real System Battery Capacity								
		1.0	1.1	1.2	1.3	1.4	1.5	1.6	1.7	1.8
Installed PV Power After Investment to Real PV System Rated Power	1.4	3.75	-	-	-	-	-	-	-	-
	1.8	7.46	-	-	-	-	-	-	-	-
	2.2	10.63	-	-	-	-	-	-	-	-
	2.6	12.27	10.00	10.45	9.33	8.07	6.70	5.25	3.78	2.29
	3.0	12.60	10.64	11.36	10.67	9.77	8.77	7.60	6.28	4.89
	3.4	12.39	10.51	11.45	10.91	10.26	9.49	8.51	7.34	6.07
	3.8	11.72	9.98	11.06	10.64	10.10	9.42	8.55	7.50	6.28
	4.2	10.58	9.06	10.30	10.00	9.56	8.97	8.15	7.13	5.92
	4.6	9.28	7.83	9.18	9.02	8.71	8.20	7.39	6.45	5.26

Table 6.9 - Net Present Value of the different investments.

7 Conclusions

7.1 Main Conclusions

The proposed goal for this work was to develop an energy model tool capable of modeling the interaction between energy demand and energy generation in services and mom-residential buildings, with a special focus on studying a microgrid implemented on a pilot office owned and managed by LNEG.

To accomplish this objective, a microgrid model, that best represents the electric microgrid understudy, was developed using MATLAB-Simulink. This model is composed of one energy storage system and four generation systems, three photovoltaic systems and one wind power system. Each one of these systems was modeled individually and went through an evaluation and validation process before being integrated into the microgrid. The developed model presented good results under different operating conditions and when compared to commercially available software, such as POLYSUN. During the development of this thesis, a conclusion was reached that to fully take advantage of the microgrid capabilities, a microgrid general controller based on demand-side management (DSM) could be developed. So, although this was not the core of the present thesis, a DSM program capable of performing load scheduling and battery control was developed in MATLAB, using particle swarm optimization.

After evaluating and validating the model, a yearly simulation, to studying the behavior of the microgrid throughout one year, was carried out. With this simulation, it was possible to conclude that for the system in hands, the PV systems have a much bigger utilization of peak power than the wind power system. Meaning that in the case of LNEG's pilot, it is more advantageous to invest in increasing the installed PV rated power and to correctly size the battery, so that energy could be available during the nighttime, instead of investing in increasing the wind rated power. It was also possible to conclude that, for the consumption needs of the pilot, the microgrid energy generation only accounts for a small fraction of the total energy consumed in the building, indicating that there is an investment potential in increasing the currently installed generation rated power. To explore this investment opportunity, different installation designs were considered and studied, and it was concluded that increasing the PV system rated power to a value equal to 24.3 kW and the battery energy capacity to a value equal to 47.5 kWh would be the energetically most interesting option and increasing the PV system rated capacity to a value equal to 15.9 kW while maintaining the battery energy capacity, would be the economically most advantageous option.

During the evaluation and validation phase of the energy model tool developed, it was possible to conclude that the model is capable of performing at a similar level as other commercially available tools, such as the case of POLYSUN. It was observed that for the same test conditions both programs would generate identical results, but the developed energy model tool has the advantage of providing information about energy generation and consumption on any time basis, something that is not

possible using POLYSUN, also having the advantage of providing additional information about power quality, about the performance indicators of the different technologies, and providing financial information to the user, namely allowing a comparison between energy contracts to select the best energy tariff, all this information is not available in POLYSUN. These advantages allow the usage of this model as a tool to design, size, and optimize energy systems for buildings.

As a final remark, it is important to notice that, although the presented program was developed to model a specific microgrid, the developed tool is modular, scalable, and easily adapted to other microgrid configurations, including different number and types of energy generation systems.

7.2 Future work

Using the developed model for future work, two main paths could be pursued. The first is related to testing different approaches to the control techniques used in this work, and the second is related to building upon the developed tool.

Looking at more detail at the first path, it would be interesting to explore different maximum power point tracking techniques, namely Fuzzy Logic, and Neural Network, and compare its performances with the Perturb & Observe method used in this thesis. Different inverter control techniques could also be implemented with the objective of increasing the inverter conversion efficiency to a value closer to those of commercial inverters. Additionally, testing different MATLAB-Simulink solver options could be an intriguing way to decrease the computational effort of the model, its main disadvantage when compared to commercially available tools. It would also be interesting to compare the results obtained in the developed program with measured generation data, in order to best fit the tool with the real microgrid system installed in LNEG.

Following the second path, a central energy management system, more complex than the one developed in this thesis, could be integrated in the microgrid model to convert it into a day ahead operation prediction program. The program would receive the prediction of the irradiance, temperature, and wind speed data, the prediction of the market energy prices, and a prediction of the energy consumption, for the day ahead, and based on this data it would schedule the operation of the different microgrid components in order to maximize the exploitation of renewable energy potential and reduce utilization costs.

REFERENCES

[1] E. Commission, “2030 climate & energy framework | Climate Action.” https://ec.europa.eu/clima/policies/strategies/2030_en#tab-0-0 (accessed Feb. 15, 2021).

[2] Matthias Buck, Andreas Graf, Dr. Patrick Graichen, “European Energy Transition 2030: The Big Picture,” pp. 11–21, 2019, [Online]. Available: https://www.agora-energiewende.de/fileadmin2/Projekte/2019/EU_Big_Picture/153_EU-Big-Pic_WEB.pdf.

[3] B. G. Alhogbi, “A Renovation Wave for Europe - greening our buildings, creating jobs, improving lives,” *Commun. FROM Comm. TO Eur. Parliam. Counc. Eur. Econ. Soc. Comm. Comm. Reg.*, 2020, [Online]. Available: https://eur-lex.europa.eu/legal-content/PT/TXT/PDF/?uri=CELEX:52020DC0562&from=EN.

[4] A. V. Roscini, O. Rapf, and D. J. Kockat, “On the way to a climate-neutral Europe – Contributions from the building sector to a strengthened 2030 climate target", Buildings Performance Institute Europe (BPIE), December 2020, [Online]. Available: https://www.bpie.eu/wp-content/uploads/2020/12/On-the-way-to-a-climate-neutral-Europe-_Final.pdf.

[5] E. Commission, “From where do we import energy and how dependent are we?” https://ec.europa.eu/eurostat/cache/infographs/energy/bloc-2c.html (accessed Feb. 15, 2021).

[6] “SUDOE IMPROVEMENT project (SOE3/P3/E0901), Interreg SUDOE Program and the European Regional Development Fund (ERDF), European Commission.” http://in3.dem.ist.utl.pt/projects/IMPROVEMENT (accessed Feb. 15, 2021).

[7] D. E. Olivares *et al.*, “Trends in microgrid control,” *IEEE Trans. Smart Grid*, vol. 5, no. 4, pp. 1905–1919, 2014, doi: 10.1109/TSG.2013.2295514.

[8] “So, What is a Microgrid, Exactly? : HOMER Microgrid News.” https://microgridnews.com/what-is-a-microgrid/ (accessed Feb. 19, 2021).

[9] Dan T.TonMerrill A.Smith, "The U.S. Department of Energy's Microgrid Initiative", The Electricity Journal Volume 25, Issue 8, October 2012, Pages 84-94, 2012. Available: http://dx.doi.org/10.1016/j.tej.2012.09.013.

[10] Open Course Ware (TU Delft), “1.2.1 Definition of a Microgrid”, https://ocw.tudelft.nl/course-lectures/1-2-1-definition-microgrid/ (accessed Feb. 19, 2021).

[11] S. Parhizi, H. Lotfi, A. Khodaei, and S. Bahramirad, “State of the art in research on microgrids: A review,” *IEEE Access*, vol. 3, no. July, pp. 890–925, 2015, doi: 10.1109/ACCESS.2015.2443119.

[12] A. Hirsch, Y. Parag, and J. Guerrero, “Microgrids: A review of technologies, key drivers, and outstanding issues,” *Renew. Sustain. Energy Rev.*, vol. 90, no. March, pp. 402–411, 2018, doi: 10.1016/j.rser.2018.03.040.

[13] A. B. Lovins, "*Small is profitable: The Hidden economic benefits of making electrical resources the right size*", 2003, doi: 10.1016/s1471-0846(03)80111-7

[14] J. J. Iannucci, L. Cibulka, J. M. Eyer, and R. L. Pupp, “DER Benefit Analysis Studies: Final report,” *Natl. Renew. Energy Lab.*, no. September, p., 2003, [Online]. Available:

https://www.nrel.gov/docs/fy03osti/34636.pdf.

[15] “Large scale integration of micro-generation to low voltage grids (MICROGRIDS) | MICROGRIDS Project | FP5 | CORDIS | European Commission.” https://cordis.europa.eu/project/id/ENK5-CT-2002-00610 (accessed Feb. 22, 2021).

[16] P. Singh, D. P. Kothari, and M. Singh, “CERTS REPOURT,” *Res. J. Appl. Sci. Eng. Technol.*, vol. 7, no. 1, pp. 91–96, 2014, doi: 10.19026/rjaset.7.225.

[17] “Microgrids – Benefits, Models, Barriers and Suggested Policy Initiatives for the Commonwealth of Massachusetts Prepared by | Janmejaya Mishra - Academia.edu.” https://www.academia.edu/33439590/Microgrids_Benefits_Models_Barriers_and_Suggested_Policy_Initiatives_for_the_Commonwealth_of_Massachusetts_Prepared_by (accessed Feb. 22, 2021).

[18] B. S. Hartono, Budiyanto, and R. Setiabudy, “Review of microgrid technology,” *2013 Int. Conf. Qual. Res. QiR 2013 - Conjunction with ICCS 2013 2nd Int. Conf. Civ. Sp.*, no. June, pp. 127–132, 2013, doi: 10.1109/QiR.2013.6632550.

[19] M. F. Akorede, H. Hizam, and E. Pouresmaeil, “Distributed energy resources and benefits to the environment,” *Renew. Sustain. Energy Rev.*, vol. 14, no. 2, pp. 724–734, 2010, doi: 10.1016/j.rser.2009.10.025.

[20] E. Konečná, S. Y. Teng, and V. Máša, “New insights into the potential of the gas microturbine in microgrids and industrial applications,” *Renew. Sustain. Energy Rev.*, vol. 134, no. July, 2020, doi: 10.1016/j.rser.2020.110078.

[21] A. A. Moghaddam, A. Seifi, T. Niknam, and M. R. Alizadeh Pahlavani, “Multi-objective operation management of a renewable MG (micro-grid) with back-up micro-turbine/fuel cell/battery hybrid power source.,” *Energy*, vol. 36, no. 11, pp. 6490–6507, 2011, doi: 10.1016/j.energy.2011.09.017.

[22] M. Zachar and P. Daoutidis, “Energy management and load shaping for commercial microgrids coupled with flexible building environment control.,” *J. Energy Storage*, vol. 16, pp. 61–75, 2018, doi: 10.1016/j.est.2017.12.017.

[23] L. Mariam, M. Basu, and M. F. Conlon, “Microgrid: Architecture, policy and future trends Lubna,” *Renew. Sustain. Energy Rev.*, vol. 64, pp. 477–489, 2016, doi: 10.1016/j.rser.2016.06.037.

[24] N. M. Kumar *et al.*, “Distributed Energy Resources and the Application of AI, IoT, and Blockchain in Smart Grids,” *Energies*, vol. 13, no. 21, p. 5739, 2020, doi: 10.3390/en13215739.

[25] H. Fontenot and B. Dong, “Modeling and control of building-integrated microgrids for optimal energy management – A review,” *Appl. Energy*, vol. 254, no. April, p. 113689, 2019, doi: 10.1016/j.apenergy.2019.113689.

[26] D. Quiggin, S. Cornell, M. Tierney, and R. Buswell, “A simulation and optimisation study: Towards a decentralised microgrid, using real world fluctuation data,” *Energy*, vol. 41, no. 1, pp. 549–559, 2012, doi: 10.1016/j.energy.2012.02.007.

[27] “Energy Storage | Department of Energy , USA.” https://www.energy.gov/oe/energy-storage (accessed Feb. 23, 2021).

[28] H. Nazaripouya, Y.-W. Chung, and A. Akhil, “Energy Storage in Microgrids: Challenges,

Applications and Research Need," *Int. J. Energy Smart Grid*, vol. 3, no. 2, pp. 60–70, 2019, doi: 10.23884/ijesg.2018.3.2.02.

[29] X. Tan, Q. Li, and H. Wang, "Advances and trends of energy storage technology in Microgrid," *Int. J. Electr. Power Energy Syst.*, vol. 44, no. 1, pp. 179–191, 2013, doi: 10.1016/j.ijepes.2012.07.015.

[30] A. A. Khodadoost Arani, G. B. Gharehpetian, and M. Abedi, "Energy Storage 1," *Int. J. Electr. Power Energy Syst.*, vol. 107, no. December 2018, pp. 745–757, 2019, doi: 10.1016/j.ijepes.2018.12.040.

[31] M. Faisal, M. A. Hannan, P. J. Ker, A. Hussain, M. Bin Mansor, and F. Blaabjerg, "Review of Energy Storage System Technologies in Microgrid Applications: Issues and Challenges," *IEEE Access*, vol. 6, pp. 35143–35164, 2018, doi: 10.1109/ACCESS.2018.2841407.

[32] A. A. K. Arani, G. B. Gharehpetian, and M. Abedi, "Review on Energy Storage Systems Control Methods in Microgrids," *Electr. Power Energy Syst.*, vol. 107, no. August 2018, pp. 745–757, 2019, doi: 10.1016/j.ijepes.2018.12.040.

[33] D. Akinyele, J. Belikov, and Y. Levron, "Battery Storage Technologies for Electrical Applications: Impact in Stand-Alone Photovoltaic Systems," *Energies*, vol. 10, no. 11, pp. 1–39, 2017, doi: 10.3390/en10111760.

[34] G. J. May, A. Davidson, and B. Monahov, "Lead batteries for utility energy storage: A review," *J. Energy Storage*, vol. 15, pp. 145–157, 2018, doi: 10.1016/j.est.2017.11.008.

[35] H. C. Hesse, M. Schimpe, D. Kucevic, and A. Jossen, "Lithium-ion battery advantages," *Energies*, vol. 10, no. 12, 2017, doi: 10.3390/en10122107.

[36] H. K. Ringkjøb, P. M. Haugan, and I. M. Solbrekke, "A review of modelling tools for energy and electricity systems with large shares of variable renewables," *Renew. Sustain. Energy Rev.*, vol. 96, no. April 2017, pp. 440–459, 2018, doi: 10.1016/j.rser.2018.08.002.

[37] "HOMER - Hybrid Renewable and Distributed Generation System Design Software." https://www.homerenergy.com/ (accessed Mar. 03, 2021).

[38] W. Feng *et al.*, "A review of microgrid development in the United States – A decade of progress on policies, demonstrations, controls, and software tools," *Appl. Energy*, vol. 228, no. July, pp. 1656–1668, 2018, doi: 10.1016/j.apenergy.2018.06.096.

[39] S. Sharma and Y. R. Sood, "Microgrids: A Review of Status, Technologies, Software Tools, and Issues in Indian Power Market", IETE Technical Review, 2020, doi: 10.1080/02564602.2020.1850367.

[40] "DER-CAM | Grid Integration Group." https://gridintegration.lbl.gov/der-cam (accessed Mar. 05, 2021).

[41] J. Huang and R. J. Davy, "Predicting intra-hour variability of solar irradiance using hourly local weather forecasts," *Sol. Energy*, Volume 139, 1 December 2016, Pages 633-639, doi: 10.1016/j.solener.2016.10.036. Solar Energy

[42] S. S. Dihrab and K. Sopian, "Electricity generation of hybrid PV/wind systems in Iraq," *Renew. Energy*, vol. 35, no. 6, pp. 1303–1307, 2010, doi: 10.1016/j.renene.2009.12.010.

[43] V. S. Bugade and P. K. Katti, "Dynamic modelling of microgrid with distributed generation for

grid integration," *Int. Conf. Energy Syst. Appl. ICESA 2015*, no. Icesa, pp. 103–107, 2016, doi: 10.1109/ICESA.2015.7503321.

[44] A. Muhtadi, "Solar PV & DFIG based Wind Energy Conversion System for St . Martin ' s Island," *2017 IEEE 3rd Int. Conf. Eng. Technol. Soc. Sci.*, 2017, doi: 10.1109/ICETSS.2017.8324152.

[45] M. Puianu, R. O. Flangea, N. Arghira, and S. S. Iliescu, "Microgrid simulation for smart city," *Proc. 2017 IEEE 9th Int. Conf. Intell. Data Acquis. Adv. Comput. Syst. Technol. Appl. IDAACS 2017*, vol. 2, pp. 607–611, 2017, doi: 10.1109/IDAACS.2017.8095164.

[46] A. Shaqour, H. Farzaneh, Y. Yoshida, and T. Hinokuma, "Power control and simulation of a building integrated stand-alone hybrid PV-wind-battery system in Kasuga City, Japan," *Energy Reports*, vol. 6, pp. 1528–1544, 2020, doi: 10.1016/j.egyr.2020.06.003.

[47] A. Tomaszewska *et al.*, "Lithium-ion battery fast charging: A review," *eTransportation*, vol. 1, p. 100011, 2019, doi: 10.1016/j.etran.2019.100011.

[48] A. F. Meyabadi and M. H. Deihimi, "A review of demand-side management: Reconsidering theoretical framework," *Renew. Sustain. Energy Rev.*, vol. 80, no. March, pp. 367–379, 2017, doi: 10.1016/j.rser.2017.05.207.

[49] L. Gelazanskas and K. A. A. Gamage, "Demand side management in smart grid: A review and proposals for future direction," *Sustain. Cities Soc.*, vol. 11, pp. 22–30, 2014, doi: 10.1016/j.scs.2013.11.001.

[50] R. Castro, "Renewable Energy Sources and Dispersed Power Generation, Support text for Renewable Energy Course, IST," no. September. 2018, [Online]. Available: https://fenix.tecnico.ulisboa.pt/disciplinas/ERPD36451113264/2019-2020/2-semestre.

[51] S. Shongwe and M. Hanif, "Comparative Analysis of Different Single-Diode PV Modeling Methods," *IEEE J. Photovoltaics*, vol. 5, no. 3, pp. 938–946, 2015, doi: 10.1109/JPHOTOV.2015.2395137.

[52] A. I. M. Ali, E. E. M. Mohamed, and A. R. Youssef, "MPPT algorithm for grid-connected photovoltaic generation systems via model predictive controller," *2017 19th Int. Middle-East Power Syst. Conf. MEPCON 2017 - Proc.*, vol. 2018-Febru, no. December, pp. 895–900, 2018, doi: 10.1109/MEPCON.2017.8301286.

[53] M. Lämmle, M. Herrando, and G. Ryan, "Basic concepts of PVT collector technologies, applications and markets", Solar Heating and Cooling Technology Collaboration Programme (SHC), International Energy Agency (IEA), 2020, doi: 10.18777/ieashc-task60-2020-0002.

[54] S. D. P. Paul C. Krause, Oleg Wasynczuk, Scott D. Sudhoff," *Analysis of Electric Machinery and Drive Systems*", 3rd Edition, ISBN: 978-1-118-52432-9 May 2013 Wiley-IEEE Press .

[55] V. S. AG, "© 2019 Vela Solaris AG | www.velasolaris.com," 2019.

[56] D. Wang, D. Tan, · Lei Liu, and L. Liu, "Particle swarm optimization algorithm: an overview," Soft Computing volume 22, pages 387–408 (2018), doi: 10.1007/s00500-016-2474-6.

[57] R. Faia, T. Pinto, Z. Vale, and J. M. Corchado, "Strategic Particle Swarm Inertia Selection for Electricity Markets Participation Portfolio Optimization," *Appl. Artif. Intell.*, vol. 32, no. 7–8, pp. 745–767, 2018, doi: 10.1080/08839514.2018.1506971.

[58] A. R. Jordehi, "A review on constraint handling strategies in particle swarm optimisation,"

Neural Comput. Appl., vol. 26, no. 6, pp. 1265–1275, 2015, doi: 10.1007/s00521-014-1808-5.

[59] IEEE Std 519, “IEEE Std 519-2014 (Revision of IEEE Std 519-1992), IEEE Recommended Practice and Requirements for Harmonic Control in Electric Power Systems,” *IEEE Std 519-2014 (Revision IEEE Std 519-1992)*, vol. 2014, pp. 1–29, 2014, [Online]. Available: http://ieeexplore.ieee.org/servlet/opac?punumber=6826457.

[60] NOSSA Energia, " “NOSSA Energia - Homepage", https://nossaenergia.pt/ (accessed Aug. 11, 2021).

[61] Secondsol, “Solar Panel - LDK Solar - 225P-20 - 225Wp - Poly - Secondsol.” https://www.secondsol.com/en/anzeige/2559/photovoltaic-modules/polycrystalline-modules/ldk-solar/225p-20 (accessed Jul. 13, 2021).

[62] UNBOUND SOLAR, “SMA Sunny Boy Review: Pricing, Specs, Pros and Cons (2021 Edition).” https://unboundsolar.com/blog/sma-sunny-boy-review (accessed Jul. 13, 2021).

[63] SOLARSHOP , “Sunlight RES OPzS 660Ah 12/24/48v batteries.” https://www.solarshop.pt/index.php?route=product/product&product_id=88 (accessed Jul. 13, 2021).

[64] Banco Portugal, "Taxa de juro", https://www.bportugal.pt/sites/default/files/anexos/10-taxas_juro_bancarias.pdf (accessed Jul. 16, 2021).

APPENDICES

Appendix A – Model and model's subsystems presentation

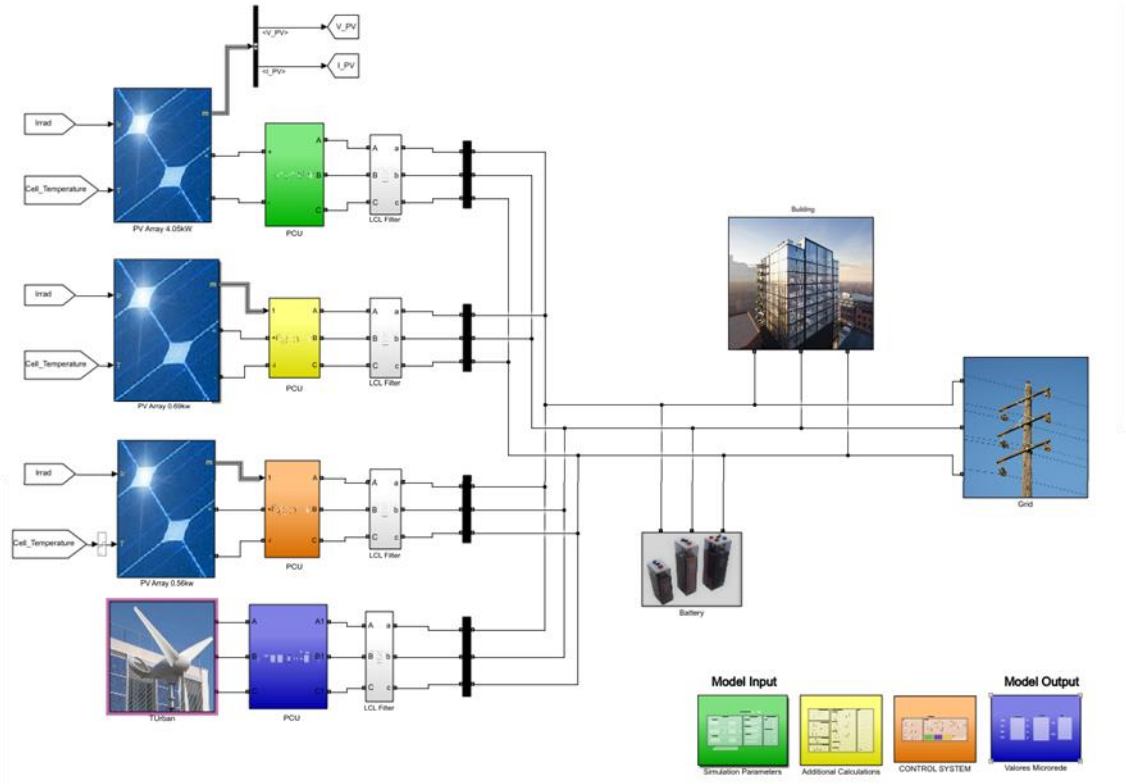

Figure A.0.1 - Developed Model Layout

A.1 – Model subsystems

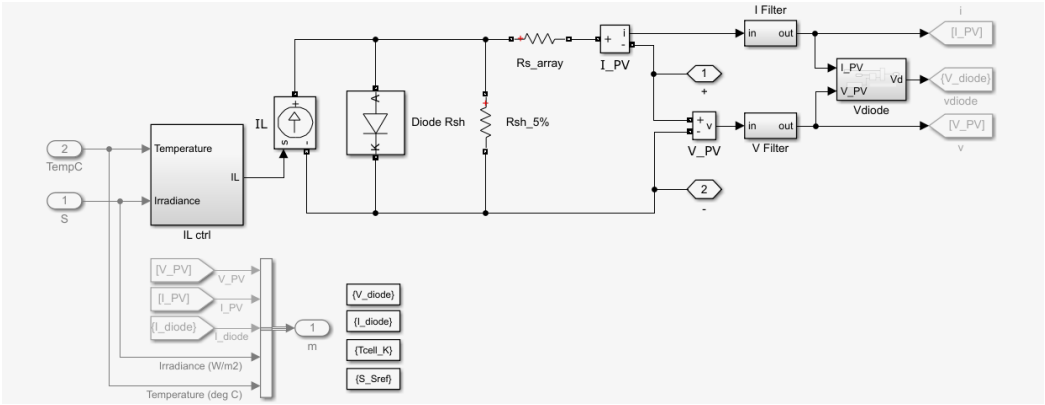

Figure A.0.2 - Simulink library photovoltaic module block.

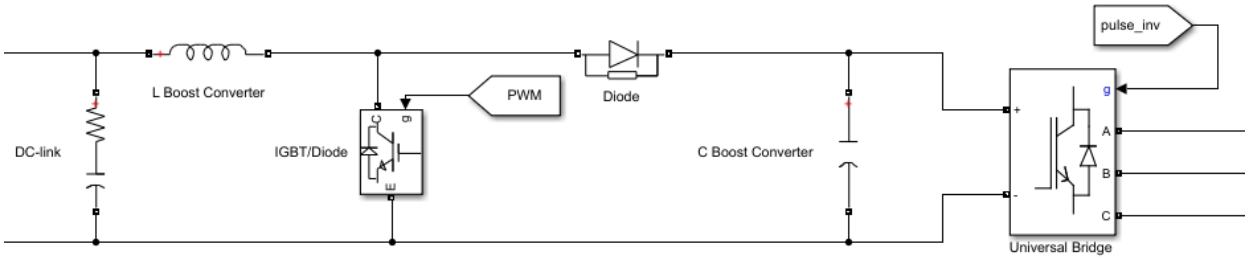

Figure A.0.3 - Photovoltaic system power condition unit block.

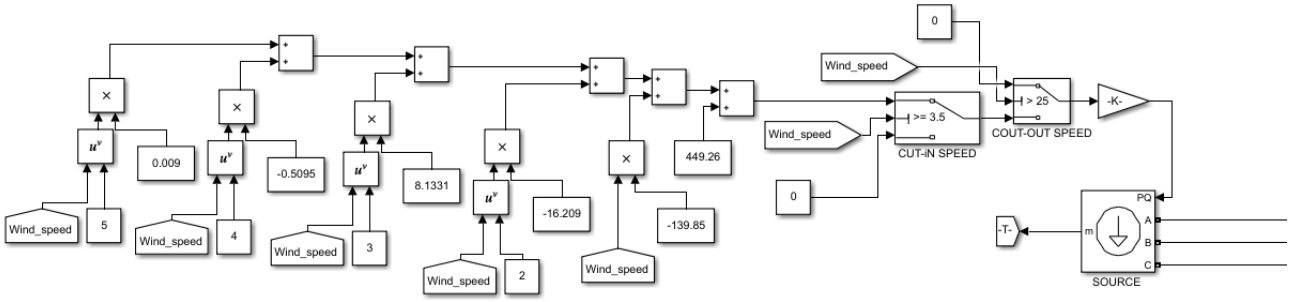

Figure A.0.4 - Wind power system generation unit block.

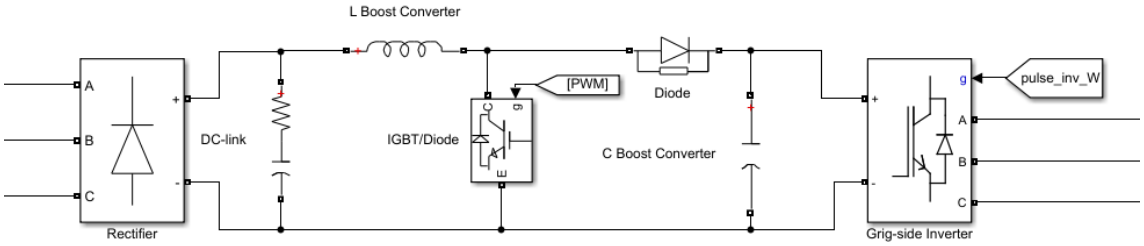

Figure A.0.5 - Wind power system power condition unit block.

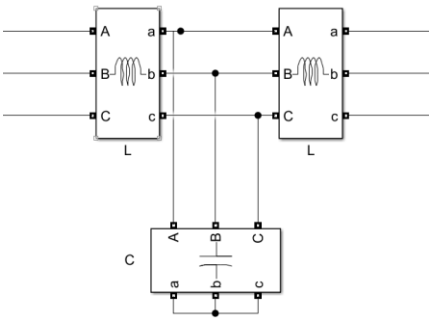

Figure A.0.6 - LCL Filter

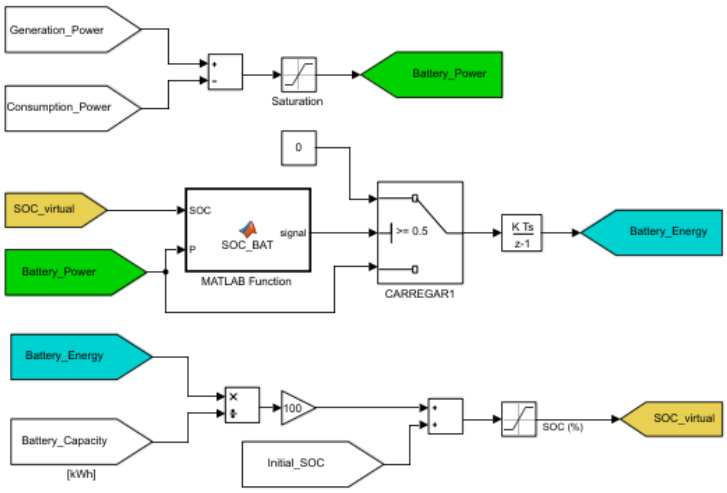

Figure A.0.7 - Battery SOC block.

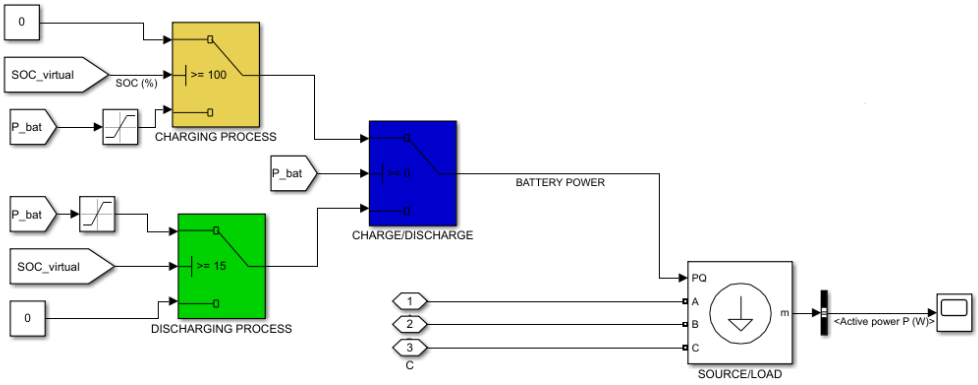

Figure A.0.8 - Battery control unit block.

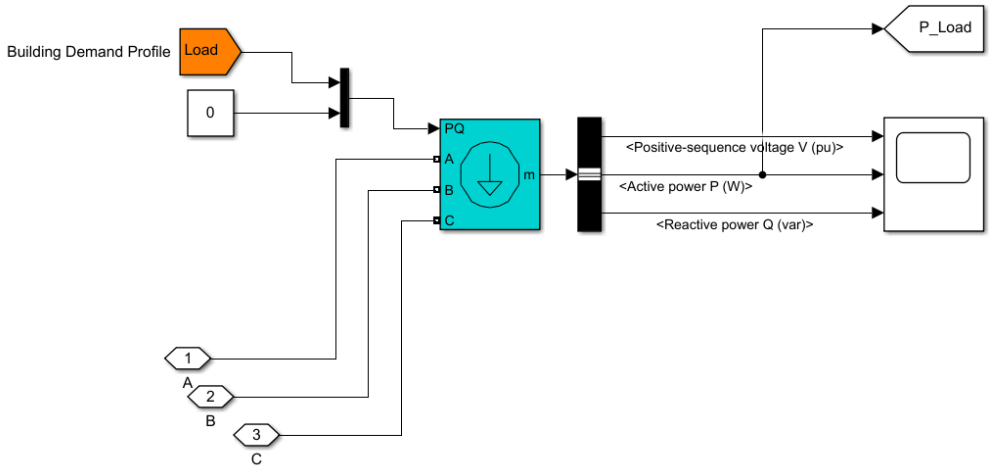

Figure A.0.9 - Building demand profile block

A.2 – Model operational blocks

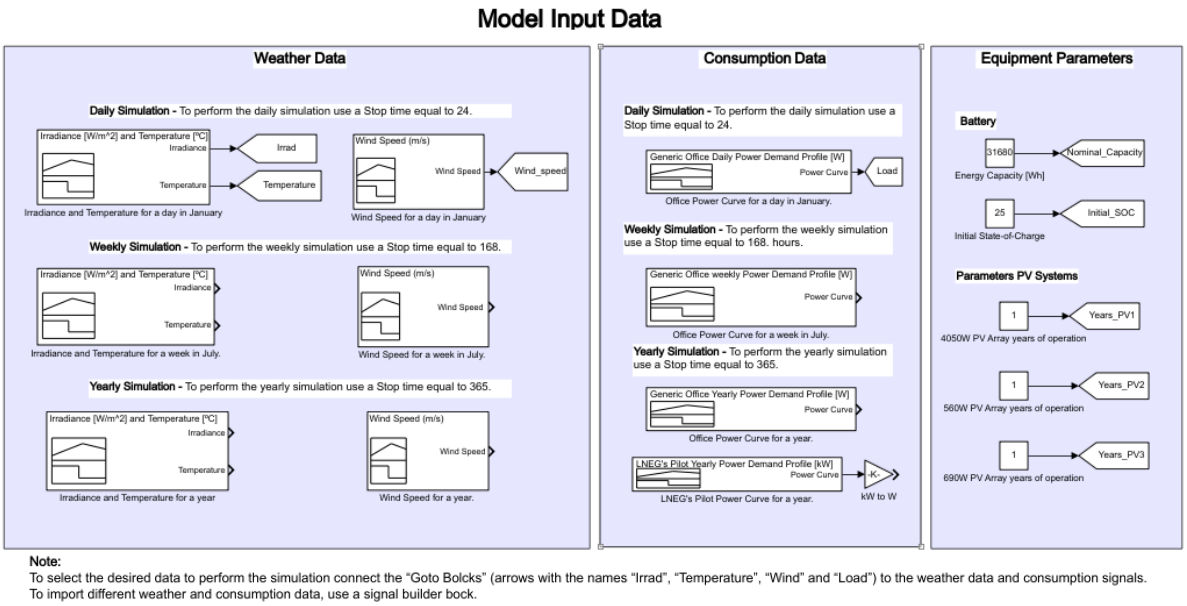

Figure A.0.10 - Model input data block (represented in green in figure A.1).

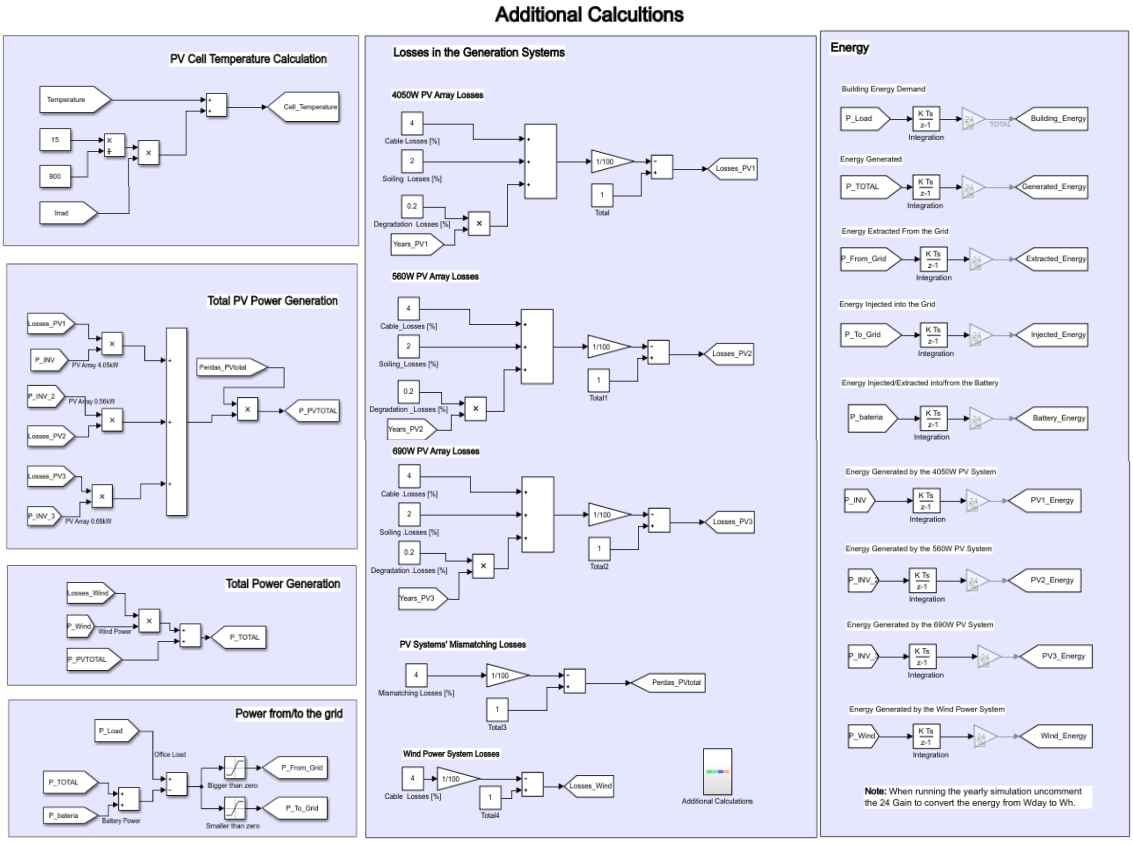

Figure A.0.11 – Additional Calculations block (represented in yellow in figure A.1).

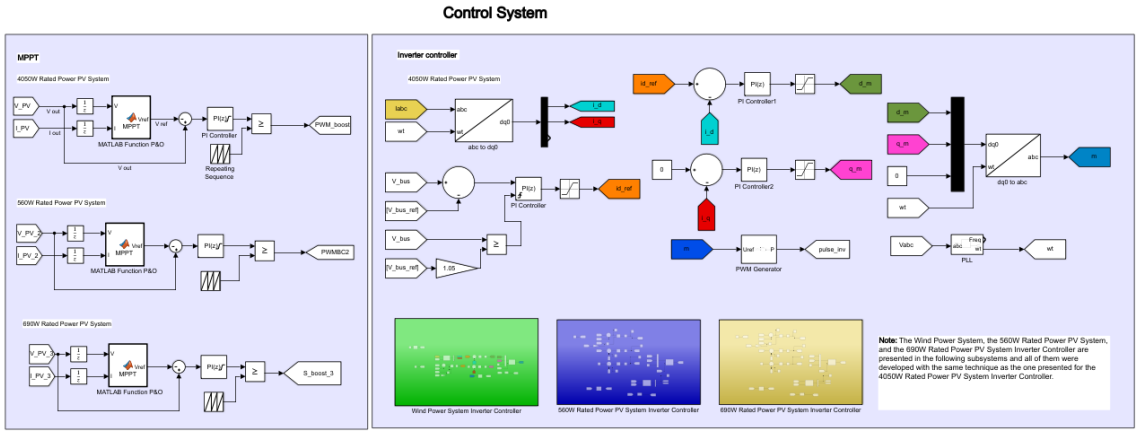

Figure A.0.12 – Control System block (represented in orange in figure A.1).

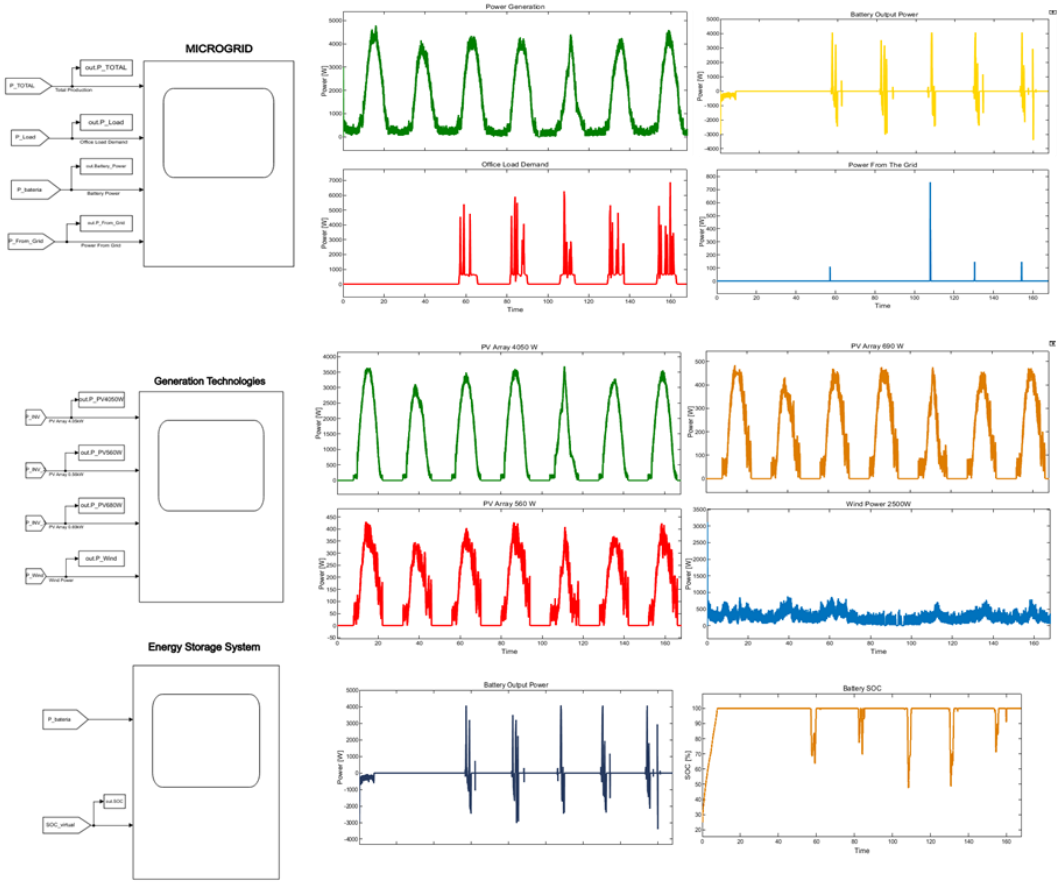

Figure A.0.13 - Model Output block (represented in blue in figure A.1).